IMPACT OF EQUIVALENT AXLE LOADING FREQUENCIES ON CRITICAL STRAINS AND DISTRESS PREDICTIONS IN ASPHALT CONCRETE PAVEMENTS

By

Peng Chen

A DISSERTATION

Submitted to
Michigan State University
in partial fulfillment of the requirements
for the degree of

Civil Engineering – Doctor of Philosophy

2024

ABSTRACT

Accurately predicting strain responses under axle loadings is crucial for the design of flexible pavements using the mechanistic-empirical approach, especially within the prevalent Pavement ME methodology. These strains are directly used in pavement damage calculation and predicting distresses. The stiffness of the top layer of flexible pavement, asphalt concrete (AC), is influenced by both loading frequency and temperature due to its viscoelastic nature. Typically, the mechanistic behavior of AC is characterized by the dynamic modulus (E*) master curve, derived from laboratory tests under uniaxial sinusoidal loadings. While a full dynamic viscoelastic analysis can precisely predict critical strains, it is computationally demanding. Consequently, Pavement ME employs a layered linear-elastic analysis, relying on the concept of "equivalent loading frequency" to determine the elastic modulus of the AC layer under specific axle loadings. However, this method has limitations in accurately predicting critical strains within the AC layer.

This thesis introduces two novel frequency calculation methods: the "centroid of PSD" and the "equivalent frequency." The former computes frequency based on the weighted center of Power Spectral Density (PSD) of vertical stress pulses induced by axle loadings, while the latter iteratively adjusts frequency until it matches strains computed by dynamic viscoelastic analysis under moving loads. The accuracy of these methods, alongside the Pavement ME method, is evaluated against dynamic viscoelastic analysis results under moving loads.

Findings reveal that while Pavement ME underestimates surface strains, it provides reasonable predictions with increasing depth for single and multiple axle configurations. Differences in loading frequencies between axle configurations are highlighted, and a correction method based on pulse width and equivalent frequency is proposed. Finally, both the original and corrected frequencies are implemented in MEAPA software to predict long-term pavement distress for real projects in Michigan. The results show that the difference between bottom-up fatigue cracking predicted by the original and corrected Pavement ME frequencies is negligible. The corrected frequency yields higher rutting predictions compared to the original Pavement ME method, ranging from approximately 15% to over 20% for AC rutting and 5% to 10% for total rutting, depending on pavement structures and traffic volumes.

TABLE OF CONTENTS

INTRODUCTION

1.1 Research Motivation

The objective of the Mechanistic-Empirical pavement design methodology is accomplished through a two-part process. First, it involves calculations of the pavement's physical response due to various loadings. Then, the performance of the pavement is predicted by employing empirical models that establish correlations between the physical response and pavement distress. The major advantage of the mechanistic-empirical procedures over the traditional 1993 AASHTO Guide equation is that it enables pavement engineers to consider a variety of pavement materials, loading conditions, and corresponding responses more fundamentally rather than primarily relying on the observation of the pavement performance and ride quality. The accuracy of the mechanistic calculation of the pavement response under vehicle loadings will greatly affect the design results, which has a profound influence on the long-term performance and life-cycle cost of the pavement system.

The uppermost layer of the flexible pavement structure is composed of asphalt concrete (AC), whose modulus is dependent on both frequency (time) and temperature due to the material's viscoelastic properties. A full dynamic-viscoelastic analysis can yield very accurate predictions of the strain and stress responses within pavement structures subjected to axle loadings. However, due to its time-intensive nature, it is not practical for implementation into mechanistic-empirical design methods. The widely adopted AASHTOWare Pavement ME Design software (Pavement ME) employs a static layered linear elastic analysis program to calculate the pavement responses to axle loadings, which relies on the concept of "equivalent or predominant loading frequency" to determine the representative elastic modulus of the AC layer as demonstrated in Figure 1.1.

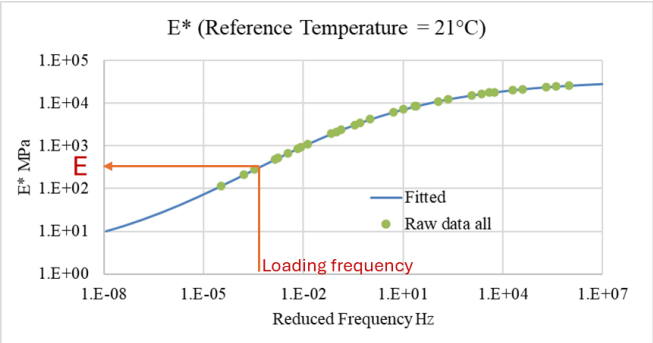

Figure 1.1 Dynamic modulus master curve.

The determination of the loading frequency is complicated and is affected by multiple factors including vehicle speed, the geometry of the tire footprint, and the stiffness and thickness of the AC layer (Losa and Di Natale 2012). Furthermore, some researchers claim that distinct sets of loading frequencies should be applied in the calculation of various strain and stress components (Losa and Di Natale 2012; Ulloa et al. 2013). The Pavement ME has a simplified procedure to calculate the loading frequency for all types of responses under axle loadings. The method first divides the AC layer into sublayers and transforms this multi-layered system into a single-layered system based on Odemark's method, and then assumes the influence zone of the vertical stress induced by tire loadings is distributed at 45 degrees along the depth. The loading frequency is calculated as the reciprocal of the loading time, which equals the width of vertical stress divided by vehicle speed. Despite Odemark's method accounting for the modulus of the AC layer, Pavement ME employs fixed AC layer moduli for calculating loading frequency. Consequently, this results in the frequency being a function solely of vehicle speed and the depth of interest.

Concerns have been raised about the accuracy of the pavement ME method in calculating loading frequencies due to the simplicity and some incorrect assumptions being used by its procedure. Many studies claim that the Pavement ME overestimates the loading frequency, especially at shallow depth and near the surface of the AC layer (Al-Qadi et al. 2008a and 2008b; Losa and Di Natale, 2012). A major consequence of this error is that it renders a higher elastic modulus of the AC layer and consequently underestimates the vertical strains throughout the AC layer and horizontal tensile strains at the bottom of the layer. These two types of strain components are directly related to the prediction of rutting and bottom-up fatigue cracking of the pavement, which are the two main distress modes associated with flexible pavement. Even though

various researchers have developed approaches to calculate axle loading frequencies and some have suggested expedient adjustments for the Pavement ME frequency method, including the use of correction factors (Al-Qadi et al. 2008a; Losa and Di Natale, 2012), most of these modifications concentrate solely on the frequency calculation phase and very few have conducted a comprehensive evaluation of the Pavement ME method, particularly in relation to the strains induced by actual axle loadings and the subsequent predictions of rutting and fatigue cracking.

Top-down cracking is another distress mode being considered by mechanistic-empirical pavement design approaches. Despite the absence of a consensus in the academic community regarding the underlying causes and mechanisms of top-down cracking, this phenomenon is widely acknowledged to be influenced by a variety of factors including climate, traffic loadings, pavement structures, and the properties of the AC materials (Wu and Muhunthan, 2019). The Pavement ME methodology utilizes the principal tensile strains near the surface of the AC layer as the critical parameter for predicting top-down cracking. Wu and Muhunthan (2019), on the other hand, introduced a model that predicts top-down cracking by including shear strain at the edge of the tire as a critical response. It is evident that principal strain and shear strain also play an important role in the distress predictions for flexible pavement design. The Pavement ME frequency is derived based on the vertical stress pulse only; however, some literature indicates that loading frequency values tend to vary when calculating different types of strain responses (Losa and Di Natale, 2012). In addition, in contrast to vertical and horizontal tensile strains, which typically reach their peak values beneath the tire, the precise positions and orientations of maximum principal and shear strains remain indeterminate due to the complex interactions among the dual tires and multiple axles. Consequently, the reliability of the Pavement ME frequency in estimating the peak values of principal and shear strains is questionable.

The Pavement ME design software uses the same loading frequency for both single axle and multiple configurations. Nevertheless, the representative elastic modulus of the AC layer under multi-axle loadings may diverge from that under single-axle loadings, particularly when the layer is stiff and thick, owing to the complex interaction between axles. Hence, it is crucial to comprehend the characteristics of the loading frequency and its accuracy and validity in calculating various strain responses subjected to different axle

loadings for flexible pavements.

1.2 Research Objectives

The primary objective of the research is summarized as follows:

1. Understand the characteristics and physical significance of loading frequency obtained by different methods.
2. Comprehensively evaluate the accuracy and validity of the Pavement ME frequency in terms of:
   - Frequency itself,
   - Representative elastic modulus,
   - Critical strains predicted by the frequency, and
   - Ultimate pavement distresses predicted using the loading frequency.
3. Propose an improvement strategy for the Pavement ME methodology for calculating an equivalent frequency that can be integrated into the Pavement ME design software.

LITERATURE REVIEW

The Pavement ME design methodology incorporates the dynamic modulus |E*| sweep data, which is measured in the laboratory at different temperatures under a uniaxial sinusoidal load, as a key input for defining the properties of the AC material and the method relies on the concept of "equivalent loading frequency" to represent the loading rate and select |E*| from the frequency domain.

One of the most straightforward and commonly adopted methods for calculating the equivalent axle load frequency, including the Pavement ME methodology, involves a two-step process. Initially, one must determine the duration of the loading time (or duration of the loading stress pulse). Subsequently, this loading duration is translated into an equivalent frequency through the application of mathematical operations. Both steps can be sources of errors.

As presented in Appendix CC-3 of the NCHRP report (ARA, 2001), the Pavement ME methodology calculates the loading time as the vertical stress pulse durations at different depths of the AC layer. This method divides the AC layer into sublayers and transforms this multi-layered system into a single-layered system based on a revised Odemark's method, and then assumes the influence zone of the vertical stress induced by tire loadings is distributed at 45 degrees along the depth.

Barksdale (1971) Studied the shape and duration of the vertical stress pulse induced by vehicle loading at different depths beneath the flexible pavement surface using the finite element method without considering viscous effects and inertia forces. The results of the study showed that the shape of the compressive stress pulse varies from approximately a sinusoidal at the surface to more nearly a triangular shape at depths below approximately the middle of the base and the compressive pulse time is negatively correlated with the vehicle speed. The author also claimed that pavement geometry and layer stiffness have insignificant impacts on the pulse time. Figure 2.1 shows the relationship between vertical stress pulse time and vehicle speed and depth beneath the pavement surface developed by the author of this study.

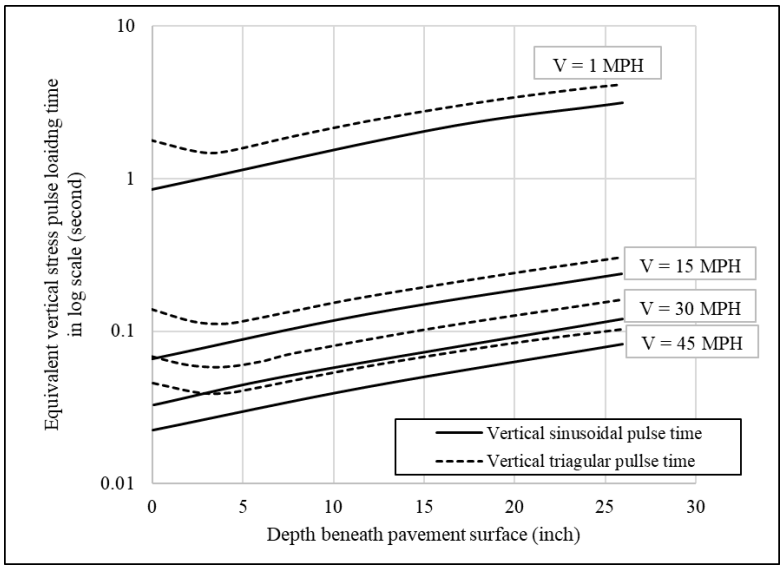

Figure 2.1 Variation of equivalent vertical stress pulse time with vehicle velocity and depth (adopted from Barksdale 1971).

Brown (1973) derived an equation for the determination of the representative loading time as a function of vehicle speed and thickness of the AC layer based on the average of the pulse times of stresses in the vertical and horizontal directions obtained from layered elastic theory as shown in Equation 2.1:

$$\log(t) = 0.5d - 0.2 - 0.94\log(v) \tag{2.1}$$

where t is time in (s), d is depth in (m), and v is the speed in (km/h). Ullidtz (2005) proposed another equation for calculating the loading time as shown in Equation 2.2:

$$t_p = \frac{2(a+Z)}{V} \tag{2.2}$$

where t_p is the time of loading, a is the radius of the loading area, Z is the thickness of the asphalt layer, and V is the vehicle speed.

Loulizi et al. (2002) measured the compressive stress pulse induced by a moving truck and falling weight deflectometer (FWD) at Virginia Smart Road using instruments to investigate the influence of vehicle speed, pavement temperature, and depth in the layer on the pulse duration. The test was carried out at the target speed of 8 km/h, 24 km/h, 40 km/h, and 72 km/h while considering depths ranging from 40 mm to 597 mm beneath the pavement surface. The research found that a haversine or a normalized bell-shaped equation could effectively characterize the measured normalized compressive stress pulse associated with the moving load as demonstrated in Figure 2.2. The measured pulse durations exhibited a

negative correlation with the target speeds and a positive correlation with the depth beneath the surface. Higher temperature will increase the peak of the stress pulse but has no significant influence on the normalized stress pulse. The research by Loulizi et al. (2002) also simulated the vertical stress pulses by elastic layered theory using Kenlayer software (Huang 1993). The pulse was obtained by plotting the calculated vertical stresses versus time, which equals the radial distance from the load center divided by speed. Results showed that there is no significant difference between the measured stress pulse and those simulated by the elastic layered theory except that simulated pulses are symmetrical and do not predict residual stresses occurring during the unloading phase.

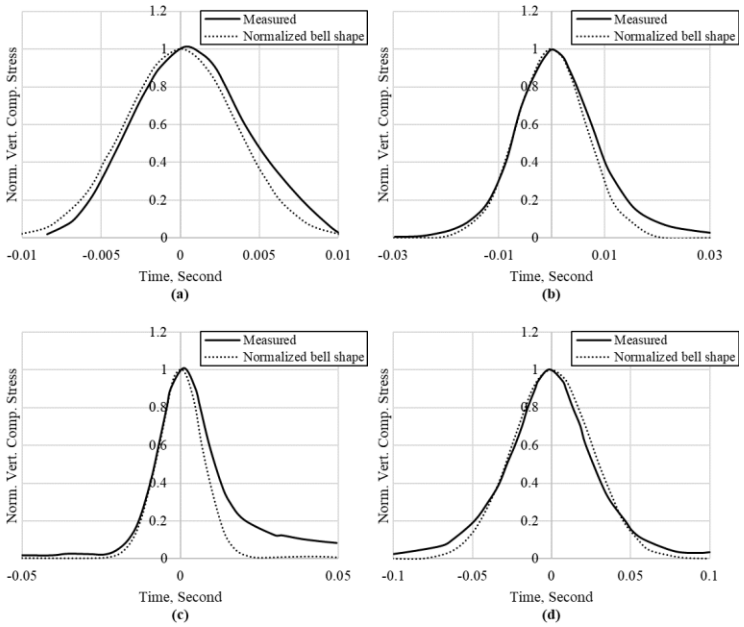

Figure 2.2 Measured normalized compressive stress pulse and its normalized bell representation for the 72 km/h test at (a) 40 mm, (b) 190 mm, (c) 267 mm, and (d) 597 mm (adopted from Loulizi et al. 2002).

Al-Qadi et al. (2008a) simulated vertical stress pulses with a 3-D finite element model using the Abaqus software to evaluate the accuracy of the Pavement ME method in the calculation of loading time. The pulses were induced by a moving wheel at speeds of 13 km/h and 80 km/h on the pavement with varying thicknesses at different temperatures. The model considered the actual tire ribs and the contact stress between tire ribs and the pavement surface. The viscoelastic properties of the AC material measured from the laboratory were also incorporated into the model. This method assumes that the genuine loading and unloading of the pavement correspond to a shift in the wave's slope direction. Thus, the span of the

loading can be defined by locating the instances when the slope shifts from negative to positive at both the start and end of the wave (Figure 2.3). The authors concluded that, in comparison with their proposed method, the Pavement ME method overestimates the loading frequency by up to 300% near the surface of the pavement layer, and then both frequencies converge gradually as the depth increases. A limitation of the study is that the slope at the beginning and end of the pulse is sensitive to numerical analysis. As a result, the loading time tends to be overestimated as a significant segment of the stress signal with a very small magnitude is included as shown in Figure 2.3.

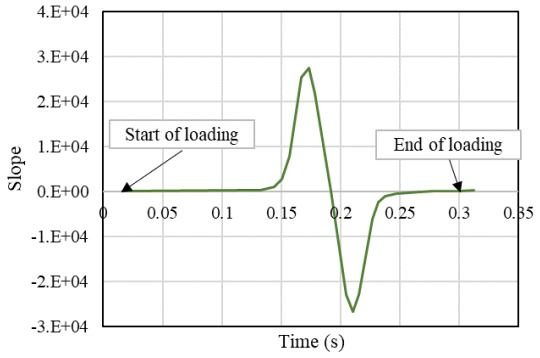

Figure 2.3 loading time calculation based on the results of the FE model (adopted from Al-Qadi et al. 2008a).

Hu et al. (2010) simulated the vertical stress pulse based on the layered elastic theory and found that the loading time (duration) is not only a function of the vehicle speed and depth below the pavement surface but also a function of the moduli ratio between the layer of interest and the directly underlying layer. The authors calculated the vertical stress pulses for two scenarios with the moduli ratios equal to 50 and 0.5 respectively at different depths. The results showed that the moduli ratio has a great influence on the pulse width especially near the bottom of the AC layer. When the ratio is large, the duration of the pulse near the bottom of the layer is much longer than the condition where the ratio is small (Figure 2.4). The study also proposed equations for loading time calculations that consider the effect of the moduli ratio. These equations were verified by field-measured data from the Virginia Smart Road project (Al-Qadi et al. 2004; Al-Qadi et al. 2005) and can be implemented by the Pavement ME design methodology. The authors compared loading times calculated from their study with those from the Pavement ME method. The findings indicated that the Pavement ME method overestimates loading time, implying an underestimation of the

asphalt concrete (AC) layer's elastic modulus. Consequently, the Pavement ME method resulted in a considerably more conservative design, yielding approximately 21.8% thicker pavement than those equations proposed by the study.

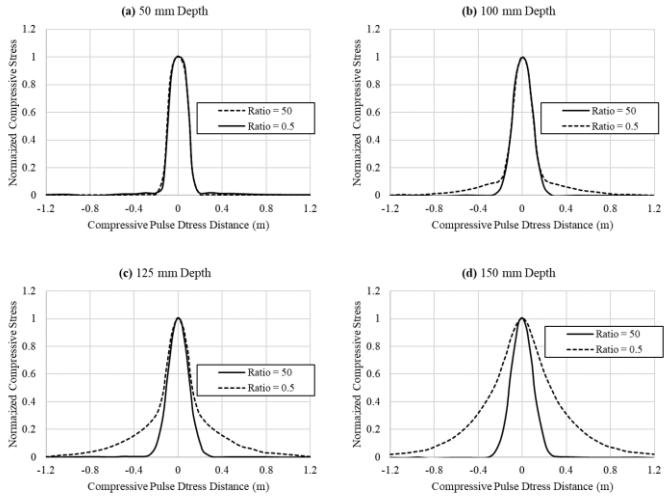

Figure 2.4 Normalized compressive stress pulse at different depths beneath the pavement surface with varied moduli ratio (adopted from Hu et al. 2010).

The aforementioned literature concentrates on determining vehicle axle loading time, by either finding the loading stress pulses or using a direct math equation, which is the first step in finding the equivalent axle loading frequency. The loading frequency can be obtained by using some relationship between the loading in the time domain and frequency domain. One of the simplest ways to convert the loading time into frequency is the assumption that frequency equals the reciprocal of the loading time, "$f = 1/t$" (the one used by Pavement ME), or some variants of this equation. For example, in Ferry's book "Viscoelastic Properties of Polymers" (1980), the loading time can be computed using the formula "$t = 1/\omega$". Correspondingly, the frequency in hertz (Hz) is determined by the formula "$f = 1/(2\pi t)$". A summarization of various relationships for time-frequency conversion is listed in Table 2.1.

Table 2.1 Various Relations for Time-Frequency Conversion (Dongré and D'Angelo 2006; Al-Qadi et al. 2008b).

Source	Author	Relation
Book: Viscoelastic Properties of Polymers	Ferry	$t = 1/\omega$
Personal Comment	Schapery	$t = 0.1/f$
TRB Journal	Kim and Daniels	$t = 0.08/f$
Personal Comment	Sharma	$t = 1/\omega$
NCHRP 9-29 Report	Bonaquist	$t = 1/f$

In addition to the straightforward formula, a more sophisticated approach to determine the equivalent loading frequency involves transforming the loading stress pulse from the time domain to the frequency domain using Fourier Transform analysis. For example, Al-Qadi (2008b) proposed a method to obtain the vehicular loading frequency using FFT (Fast Fourier Transform). The authors calculated the frequency spectra of haversine and bell-shaped curves, which are two typical fitting functions for the vertical stress pulse. Even though the two curves have similar durations, their frequency spectra are different (Figure 2.5). For flexible pavement, the shapes of the loading pulses vary with the depth beneath the layer surface (Barksdale 1971; Loulizi et al. 2002), and neither the haversine nor bell-shaped curve can fit the stress pulses at various depths. This implies that using the time-frequency conversion formula of "$f = 1/t$" and its variants form (such as "$f = 1/(2\pi t)$") for the determination of loading frequency for general loading and pavement conditions is inaccurate. The authors of this study then performed FFT for stress pulses measured from the field testing and took the frequency values that corresponded to the weighted center of the frequency spectra as the dominant frequency of the pulses. The dominant frequencies obtained by FFT were also compared with those calculated by the Pavement ME method ($f = 1/t$) and the angular frequency "$f = 1/(2\pi t)$"; results showed that the Pavement ME method exhibits errors from 40% to 140% depending on vehicle speed and pavement depth.

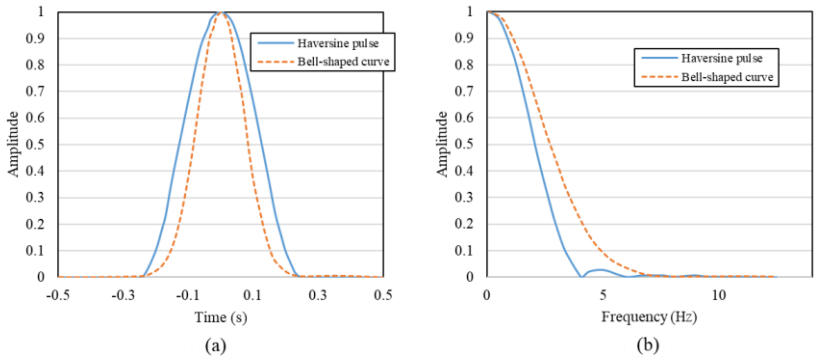

Figure 2.5 Time Domain and Frequency Spectrum of Haversine and Bellshaped Functions (a) Pulse in Time Domain (b) Frequency Spectrum (adopted from Al-Qadi et al. 2008b).

Ghanizadeh and Fakhri (2018) proposed a similar approach using FFT to determine the axle loading frequencies in flexible pavement. The study analyzed 1200 pavement sections and the equivalent loading frequencies were calculated using the FFT method at various depths of the AC layer. The vertical stress pules were simulated by the NoNPAS program based on the layered elastic theory and the weighted center of the Fourier spectra of these pulses is used as the equivalent loading frequency. A nonlinear regression equation (Equation 2.3) and a feed-forward Artificial Neural Network (ANN) were also developed by the authors for the prediction of loading frequency. The regression equation is shown below:

$$f_{FFT} = 0.126 \times V \times \exp\left(-0.6398 \ln(R) - 0.3122 \times \ln(d) + 2.6780\right)(R^2 = 0.985) \qquad (2.3)$$

where f_{FFT} is frequency based on the FFT method (Hz), V is vehicle speed (km/h), R is the contact radius of the wheel (cm) and d is the depth (cm). The validity of the regression equation and the ANN model was verified by comparing the predicted frequencies with field measurements from Virginia Smart Road (Al-Qadi et al. 2008b). Critical pavement responses calculated through quasi-static analysis based on layered elastic theory using frequencies acquired via the FFT method are also found to be comparable to those obtained from dynamic analysis. The Parametric analysis conducted by this research concluded that only three factors, vehicle speed, tire contact radius, and depth of the layer, are the most effective factors that influence the equivalent loading frequency.

Ulloa et al (2013) attempted to calculate the predominant frequencies under a tandem-axle load for flexible pavement by the FFT method and investigate whether the predominant or equivalent loading frequencies can predict critical strain responses induced by axle loadings within the AC layer. Different from other literature in which the frequency of the vertical stress pulse is used for all types of pavement

response prediction, this study also used pulses of various types of strains: vertical, horizontal longitudinal, and horizontal transverse, and calculated their frequencies respectively for the prediction of those responses. The loading pulses were simulated by dynamic viscoelastic analysis and then transformed the strain amplitudes into the frequency domain by FFT. Rather than employing the weighted center of frequency spectra, frequencies corresponding to the maximum peak—excluding the peak in the very low frequency (near zero), which the authors associate with the static component of the strain pulse—are regarded as the predominant frequency (Figure 2.6). The researchers then developed linear regression equations as a function of only vehicle speed for critical strains in the three directions and found that using two loading frequency values (one for the top 2-inch of the AC layer and one for the rest of the layer) for a pavement structure is adequate to predict critical strains within the AC layer. In their study, Ulloa et al. (2013) also used strains predicted by the Pavement ME frequency, the frequency proposed by the authors, and dynamic viscoelastic analysis as inputs into the empirical model equations of the Pavement ME method to forecast the amount of rutting and bottom-up fatigue cracking. Results showed that the Pavement ME frequency underestimates rutting depth by up to 50% compared with dynamic viscoelastic analysis, but it estimates bottom-up cracking reasonably with an error within 10%.

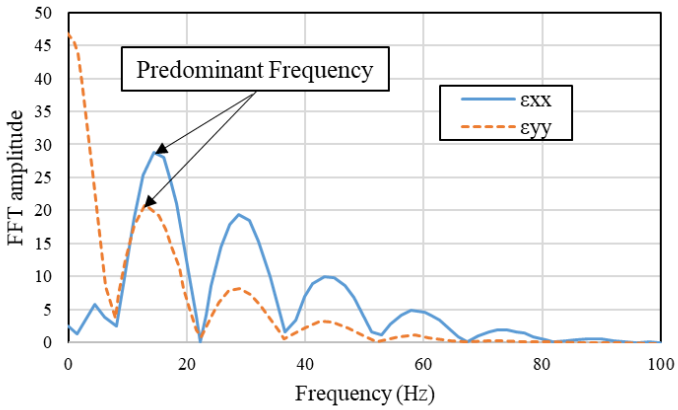

Figure 2.6 FFT amplitudes of the normal strain histories under the center of the tire at the bottom of the 10-cm HMA layer (adopted from Ulloa et al. 2013).

In addition to the previously discussed literature, another approach to determining loading frequency relies on iteration. The fundamental rationale of this method involves continuously adjusting the equivalent frequency value until the pavement responses, as predicted by linear elastic analysis using this frequency,

match those derived from comprehensive dynamic viscoelastic analysis or field measurements. The loading frequency determined through iteration is the most accurate for predicting pavement responses. Nevertheless, this method is computationally intensive, and the equivalent frequency obtained is only valid within the range used in the iterative procedure.

Losa and Di Natale (2012) determined the equivalent loading frequency using the iteration method, conducting the iterative process for strain response in three directions: vertical (z), longitudinal (x), and transverse (y). A flowchart detailing the steps of this iterative procedure is presented in Figure 2.7. A statistical analysis was conducted on various parameter combinations relevant to determining the equivalent loading frequency. It was discovered that the critical parameters include footprint dimension, asphalt concrete (AC) layer temperature, depth beneath the pavement surface, vehicle speed, and the specific direction of interest (x, y, z). The authors of this study developed regression equations to calculate loading frequencies (Hz) in three directions (Equations 2.4 to 2.8):

$$f_x = 0.027V\left(\frac{1}{2a} + \frac{1}{2b}\right)e^{-3.14z+\alpha(T)} \tag{2.4}$$

$$f_y = 0.042\frac{V}{2a}e^{-3.34z+\beta(T)} \tag{2.5}$$

$$f_z = 0.043\frac{V}{2a}e^{-2.65z+\beta(T)} \tag{2.6}$$

$$\alpha(T) = 2.12 * 10^{-5} * T^3 - 2.6 * 10^{-3} * T^2 + 12.8 * 10^{-2} * T \tag{2.7}$$

$$\beta(T) = 1.25 * 10^{-5} * T^3 - 1.6 * 10^{-3} * T^2 + 9.20 * 10^{-2} * T \tag{2.8}$$

where V is the vehicle speed in m/s, a and b are half the length of the rectangular footprint in longitudinal and transverse directions, respectively, in meters, and T is the AC temperature in ℃. It can be found by applying these equations that the equivalent loading frequency is highest in the longitudinal direction, followed by the vertical direction, and lowest in the transverse direction. Ultimately, the authors compared the frequencies calculated using their proposed equations with those from the Pavement ME method and frequencies presented by Al-Qadi et al. (2008a). It was found that while the Pavement ME method tends to overestimate the frequencies, Al-Qadi's approach underestimates them. One limitation of this study is that the AC layer was not subdivided, and strains were only considered at the bottom of the layer.

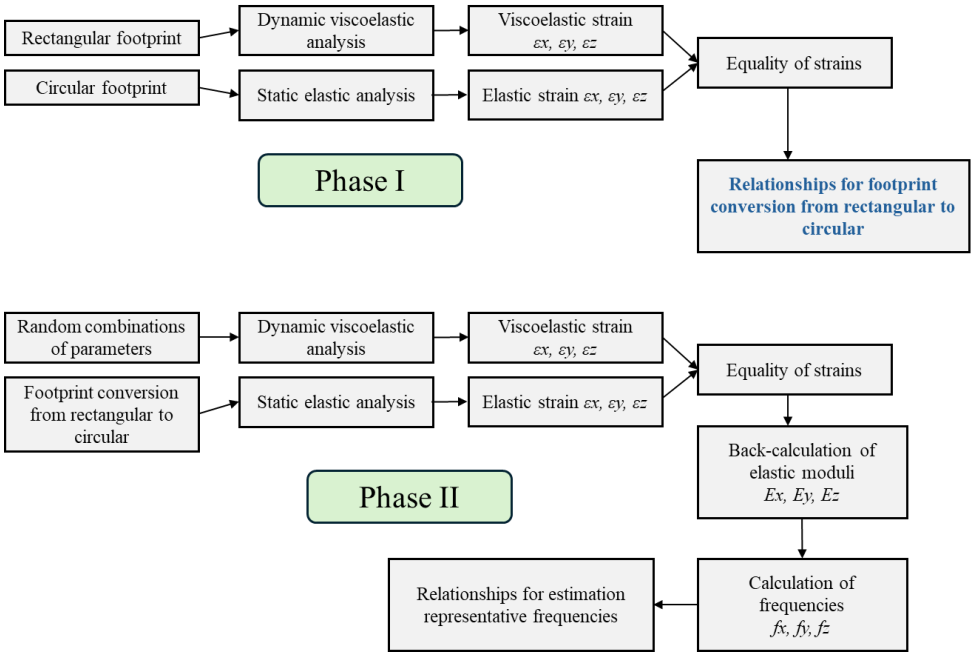

Figure 2.7 Method adopted in defining relationships for estimation of representative frequency (adopted from Losa and Di Natale 2012).

Bodin et al. (2017) examined the relationship between vehicle speed and the equivalent asphalt modulus (EAM), as well as the equivalent loading frequency using an iteration method similar to the one employed by Losa and Di Natale (2012). The author simulated a single-axle dual tire loading moving on the pavement at speeds ranging from 30 km/h to 110 km/h and at the AC temperature of 5°C and 40°C with the Viscoroute software. The maximum tensile strains (longitudinal direction) at the bottom of the AC layer were calculated by both the viscoelastic and linear elastic analyses to search for the EAM that ensured identical strain output from both analyses. The iteration approach is illustrated schematically in Figure 2.8. After the EAM was obtained, the equivalent loading frequency can be determined from the inverted function of the complex modulus master curve.

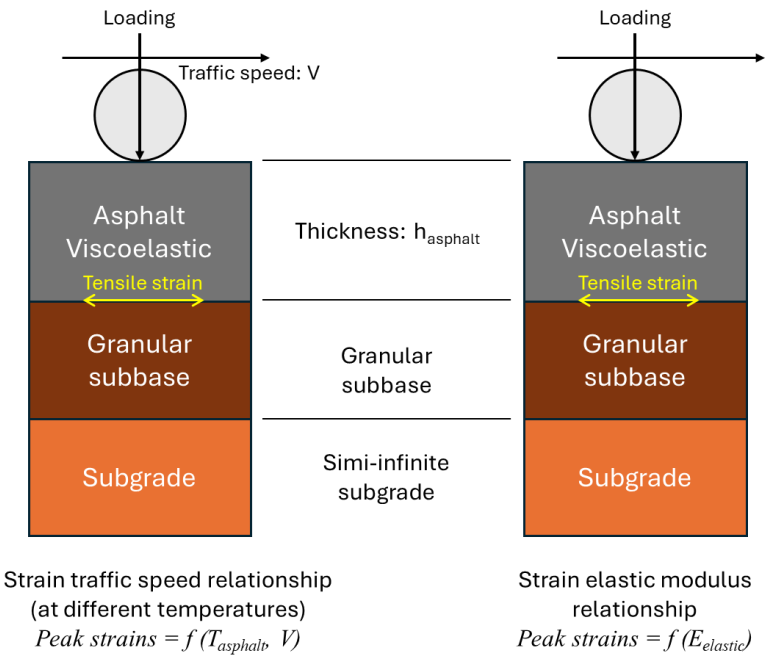

Figure 2.8 Schematic view of the process used for determining the EAM of the asphalt material with temperature and speed (adopted from Bodin et al. 2017).

Underwood and Kim (2009) evaluated several approximation methods including the Pavement ME method, for the calculation of stresses and strains in linear viscoelastic materials by comparing analysis results from the exact linear viscoelastic solutions. The concept of "equivalent loading frequency" was not involved in the study; instead, the one-dimensional strain responses induced by a haversine stress pulse were calculated for different methods using analytical equations. Strains calculated by the exact viscoelastic solutions were used as the datum as shown in Equation 2.9:

$$\varepsilon_0 = \max\left[\int_0^t D(t-\tau)\frac{d(\frac{\sigma_0}{2}\sin\left(\omega\tau-\frac{\pi}{2}\right)+\frac{\sigma_0}{2})}{d\tau}dt\right] \quad (2.9)$$

where D is the creep compliance of the material. The first approximation method being evaluated is called quasi-static analysis, which assumes that the maximum strain amplitude occurs when the stress is a maximum, as shown in Equation 2.10:

$$\varepsilon_0 = \mathrm{D}(\frac{t_p}{2}) \times \sigma_0 \quad (2.10)$$

where t_p is the duration of the loading pulse. The second approximation method is named steady-state analysis, which is taken by the Pavement ME methodology. The amplitude of the strain response is given

by Equation 2.11:

$$\varepsilon_0 = |D^*|_{f=1/t_p} \times \sigma_0 \tag{2.11}$$

where D* is the complex compliance of the material. Equation 2.11 is equivalent to the Pavement ME because it calculates strains by stress devised by |E*| at *f=1/t* and |D*| is the reciprocal of the |E*|. The last approximation method is the hybrid (superposition) analysis, in which the haversine loading pulse is separated into a sinusoidal portion and a constant loading portion as shown in Figure 2.9, and the strain amplitude is given by Equation 2.12:

$$\varepsilon_0 = \frac{|D^*|_{f=1/t_p} + D\left(\frac{t_p}{2}\right)}{2} \times \sigma_0 \tag{2.12}$$

The comparison of strains calculated by these methods and the results from the exact solutions indicated that the hybrid analysis is the most accurate in terms of strain prediction. The Pavement ME method underestimates strains in general with errors of up to 31%. It should be noted that all solutions involved in this research are one-dimensional, while the actual pavement responses are three-dimensional. In addition, the axle loading pulse used by the Pavement ME is not necessarily the same as the haversine that was assumed by the study.

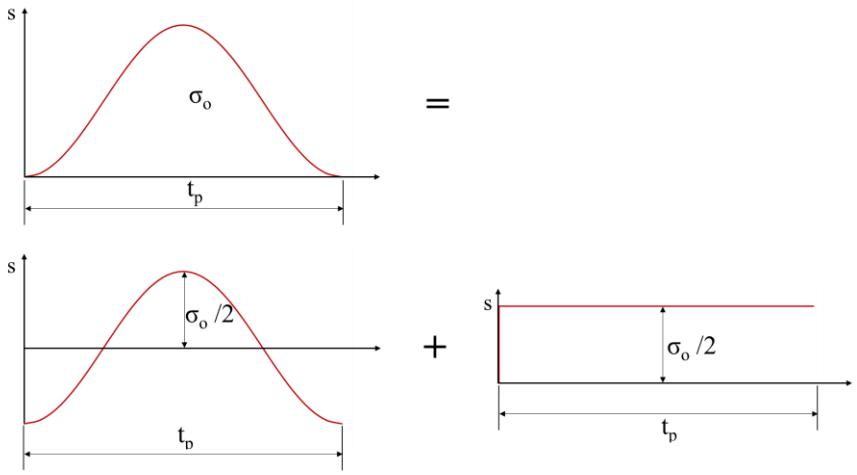

Figure 2.9 Decomposition of the haversine stress history (adopted from Underwood and Kim 2009).

Researchers have developed different methods to calculate axle loading frequencies, most of them only focus on the frequency calculation stage and very few of them evaluated the Pavement ME method systematically in terms of strains induced by real axle loadings as well as the ultimate distress prediction.

In the evaluations concerning the Pavement ME model's loading frequency, the majority (Al-Qadi et al. 2008a and 2008b; Underwood and Kim 2009; Losa and Di Natale 2012; Ulloa et al. 2013) assert that the model tends to overestimate the loading frequency. However, there is at least one study (Hu et al. 2010) that counters this view, claiming that the Pavement ME model underestimates the loading frequency. Furthermore, research efforts have predominantly concentrated on single-axle scenarios. Studies investigating the characteristics of multiple-axle loading frequencies and the validity of applying single-axle loading frequencies to multiple-axle scenarios are notably absent. Additionally, there is a notable lack of literature addressing the impact of loading frequencies on shear strain, principal strain, and the prediction of top-down cracking.

EVALUATION OF THE ACCURACY OF PAVEMENT ME METHODOLOGY IN CALCULATING EQUIVALENT LOADING FREQUENCY AND ITS EFFECT ON STRAIN RESPONSE PREDICTIONS IN FLEXIBLE PAVEMENTS

3.1 Objectives

The main goal of this chapter is to evaluate the accuracy of axle loading frequency calculated by the Pavement ME method. The first half of this chapter introduces the concepts of predominant and equivalent frequencies, provides a brief explanation of the difference between them, and introduces three predominant frequency calculation methods borrowed from earthquake engineering. In the second half of the paper, the Pavement ME methodology is compared with other methods in terms of frequency and modulus. Finally, the normal strain responses in vertical and horizontal (longitudinal and transverse) directions are compared with results from the full dynamic viscoelastic analysis.

3.2 Overview of Pavement ME Methodology

The Pavement ME method calculates the loading frequency as the inverse of the loading time, as described in the following steps:

Step 1: Divide the AC layer into sub-layers and calculate the effective thicknesses of the AC layer using Odemark's method, as shown in Figure 3.1, and Equations. 3.3 to 3.4:

$$h_{ie} = h_i \sqrt[3]{\frac{E_i}{E_{SG}}} \tag{3.3}$$

$$Z_{eff} = \sum_{i=1}^{n} h_{ie} \tag{3.4}$$

where h_i is the real layer thickness, E_i is the layer modulus, E_{SG} is the subgrade modulus, h_{ie} is the effective layer thickness, and Z_{eff} is the effective depth from the pavement surface to the point of interest. If the depth of interest is not on a layer interface, h_{ne} should be equal to the distance between that point to the nearest layer interface on its top, instead of the whole layer thickness.

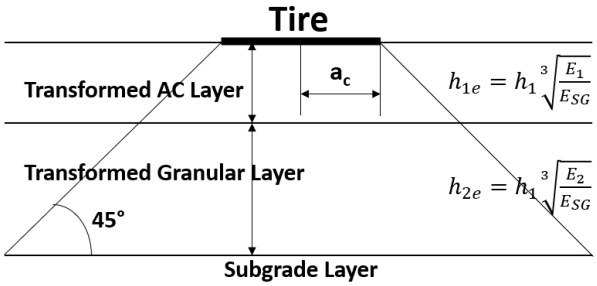

Figure 3.1 Effective thickness calculation based on Odemark's method (adapted from ARA 2001).

Step 2: After the multi-layered AC has been transformed to a single-layered system, assume the vertical stress induced by the tire loading distributes at 45 degrees along the depth, as shown in Figure 3.2, and calculate the effective length and time duration of the loading by Equations. 3.5 to 3.6:

$$L_{eff} = 2(a_c + Z_{eff}) \tag{3.5}$$

$$t = \frac{L_{eff}}{17.6\, v_s} \tag{3.6}$$

where a_c is the radius of the circular load, v_s is the vehicle speed in mph, L_{eff} is the effective length, in inches, at the effective depth Z_{eff}, and t is the time duration of the tire loading.

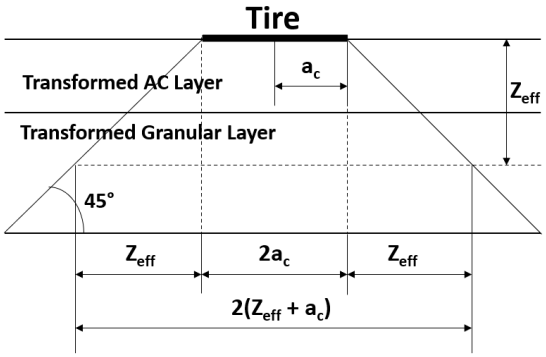

Figure 3.2 Effective length computation for single axle load configuration (adapted from ARA 2001).

Step 3: Calculate the axle loading frequency by Equation. 3.7:

$$f = \frac{1}{t} \tag{3.7}$$

3.3 Predominant Frequency and Equivalent Frequency

The predominant frequency refers to the frequency that carries the most significant energy of the axle loading pulse. This is a fundamental physical property of the signal, and it can be calculated using either the loading time or actual loading pulses. On the other hand, the equivalent frequency is not a physical property of the signal and has no direct relationship with the loading time or loading pulses. Therefore, it's

important to distinguish between these two concepts to accurately analyze the behavior of the signal and its impact on the system. The purpose of equivalent frequency is to make responses from linear-elastic analysis match those from the viscoelastic analysis.

There are three common methods to determine the predominant frequency of a pulse (Lei 2011, Chen et al. 2023) using: (1) Fourier Transform to convert the pulse from the time domain into the frequency domain and calculating the centroid of the area formed by the Fourier Spectrum as the dominant frequency (Centroid of Fourier); (2) the centroid of the area that is formed by the power spectral density (PSD) in the frequency domain as the dominant frequency (Centroid of PSD); and (3) the Central Frequency, which is also based on PSD, but involves additional mathematical operations (Kramer 1996) as shown in Equations. 3.8 to 3.10:

$$f = \frac{1}{2\pi}\sqrt{\frac{\lambda_2}{\lambda_0}} \tag{3.8}$$

$$\lambda_n = \int_0^{\omega_N} \omega^n G(\omega) d\omega \tag{3.9}$$

$$G(\omega) = \frac{1}{\pi T_d} c_n^2 \tag{3.10}$$

where f is the central frequency (Hz), λ_n is the spectra moment,ω is the angular frequency (rad/sec), ω_N is the Nyquist (highest) frequency (rad/sec) in the Fourier series, c_n is the amplitude of the Fourier series, and T_d is the time duration of the entire pulse.

Properties of the predominant frequency obtained from the three methods are demonstrated using four typical pulse signals, which are rectangular, triangular, half-sine, and haversine pulses. Figure 3.3 shows an example of these pulses in both the time and frequency domains. Predominant frequencies of different pulse shapes obtained by different methods are compared in Table 3.1 and Figure 3.4. For each method, the frequencies are calculated with both the full range of the amplitude in the frequency domain and only the dominant portion of the amplitude (the portion before the amplitude first reaches zero), respectively. All pulses are normalized and have a duration of 1 second. Thus, the frequencies calculated by "$f = 1/t$" and "$f = 1/(2t)$" are equal to 1 Hz and 0.5 Hz, respectively. As can be seen from Figure 3.4, the differences between dominant frequencies calculated by these methods are significant when considering the entire frequency domain. On the other hand, frequencies obtained by these methods are lower and relatively concentrated

when only taking the dominant portion of the amplitude in the frequency domain. As shown in Figure 3.3, there are secondary frequency components for those pulses with sharp discontinuities, especially for the rectangular pulse. The disagreement among different methods for the rectangular pulse is the highest and the difference between frequencies calculated by considering the full range and only the dominant portion of the amplitude in the frequency domain is the largest as well. On the contrary, the secondary frequency components are insignificant for the haversine pulse, which is very smooth. It is well known that this high-frequency portion of the amplitudes in the frequency domain is there to account for the sharpness of the pulse in the Fourier Transform, and does not represent the dominant energy of the loading pulse. Thus, considering only the dominant portion of the amplitude in the frequency domain is more reasonable when calculating the predominant frequency. Even if considering the full range of the frequency domain, frequency values calculated by the Centroid of PSD and the central frequency methods are much more stable among different pulses than the centroid of Fourier method because PSD represents the dominant energy of the pulse and is less sensitive to the shape of the pulse. So, the Centroid of PSD and the central frequency methods are more reasonable than the centroid of the Fourier spectrum when calculating predominant frequencies. Another important point is that when only considering the dominant portion of the amplitude in the frequency domain, dominant frequencies obtained by all three methods are closer to 0.5 Hz than 1 Hz. This implies that the frequency-time relationship of "$f = 1/(2t)$" is more reasonable than "$f = 1/t$" if the pulse duration is accurate.

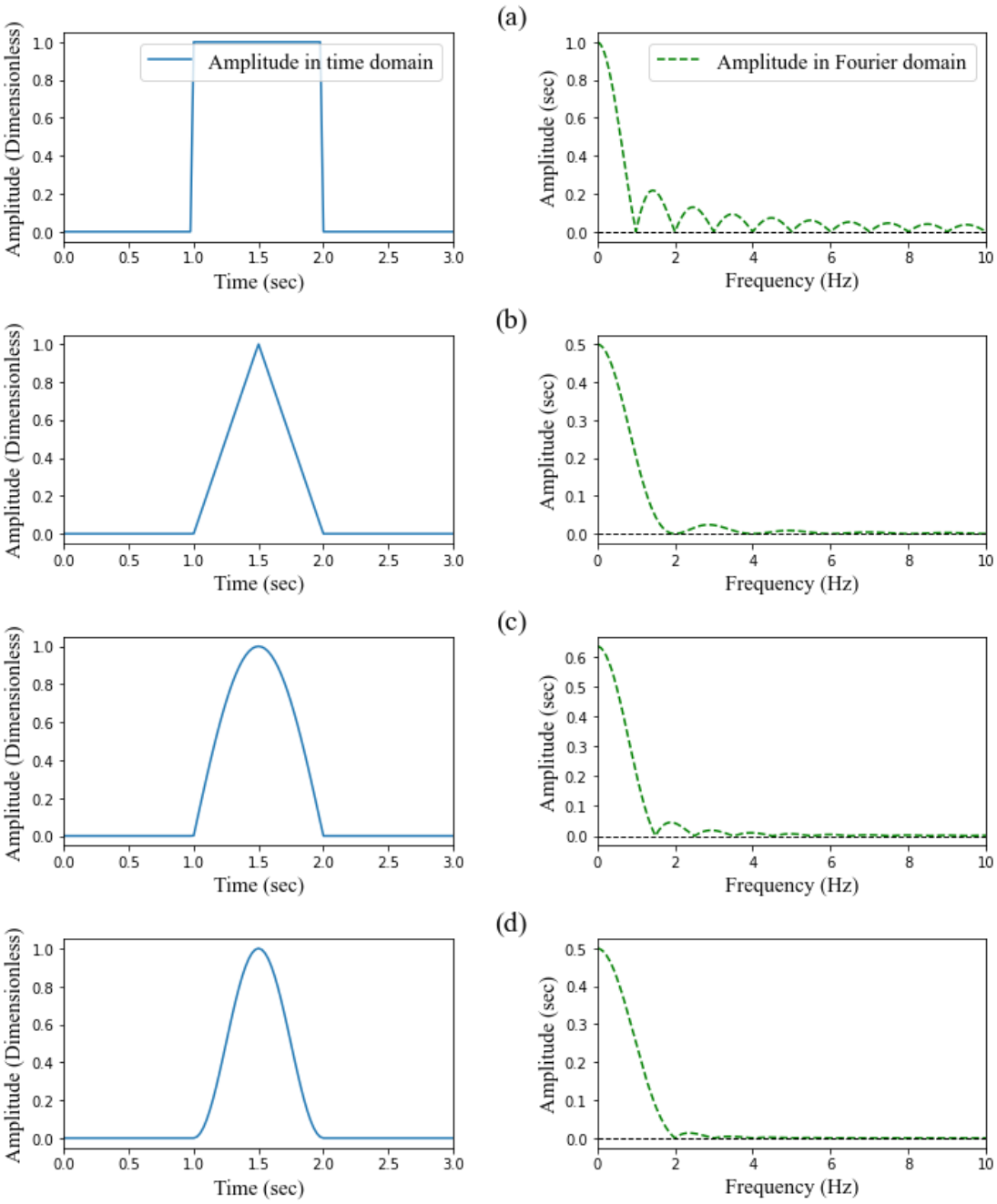

Figure 3.3 Simplified loading pulses in the time and frequency domain. (a) Rectangular pulse; (b) Triangular pulse; (c) Half-sine pulse; (d) haversine pulse.

Table 3.1 Dominant frequencies for different example pulses.

Pulse with 1-sec duration	Centroid of Fourier (Hz)		Centroid of PSD (Hz)		Central Frequency (Hz)	
	Full Range	Dominant	Full Range	Dominant	Full Range	Dominant
Rectangular	3.80	0.34	0.60	0.27	1.68	0.34
Triangular	1.05	0.55	0.42	0.41	0.56	0.51
Half-sine	0.97	0.49	0.39	0.38	0.50	0.46
Haversine	0.69	0.61	0.47	0.46	0.58	0.57

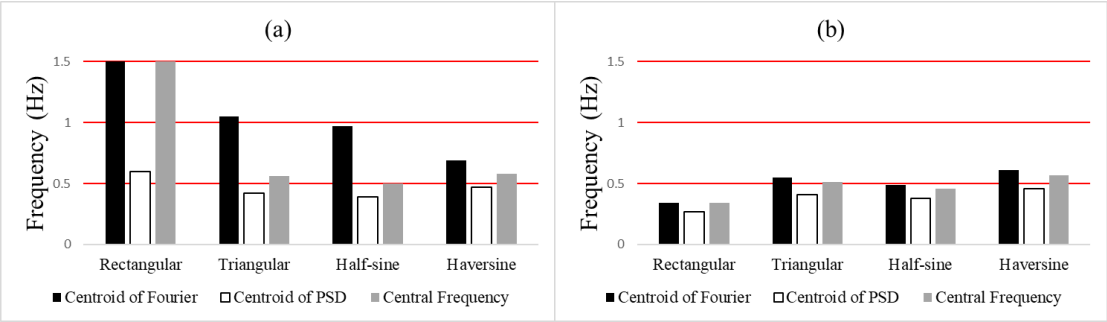

Figure 3.4 Dominant frequencies compared with "f = 1/t" and "f = 1/(2t)". (a) using the entire frequency domain, (b) using only the dominant portion in the frequency domain.

3.4 Evaluation of The Pavement ME Method

In this section, the Pavement ME is evaluated in terms of pulse width, frequency, and strain. Eight cases from Al-Qadi et al. (2008a) and four cases added by the authors (to include mid temperatures) with combinations of different AC temperatures, AC thickness, vehicle speed, and binder stiffness are selected for the analysis. Details of the twelve cases are summarized in Table 3.2 and Figure 3.5. For all twelve cases, the AC layers are evenly divided into 6 sub-layers. Frequencies are calculated at different depths within the AC layer by the Pavement ME method, the Centroid of PSD method, and the equivalent frequency. The equivalent frequencies are obtained by iteration such that vertical strains predicted by the equivalent frequencies using linear elastic analysis equal those simulated by the viscoelastic analysis. Vertical and horizontal strains at the middle of each sub-layer are also calculated by linear elastic analysis using different loading frequencies and are compared with the results of the viscoelastic analysis. Both linear elastic and viscoelastic analysis are performed by the "3D-Move" software (version 2.1) (2013) to simulate the pavement responses under a single tire load. As one of the input data for 3D-Move software,

the phase angle is estimated as a function of frequency by taking the derivative of the E* function (Rowe 2009, Oshone et al. 2017).

Table 3.2 Summary of simulation conditions.

Case No.	Pavement Temperature (°C)	HMA Thickness (mm)	Pavement Thickness (mm)	Target Speed (km/h)	Binder
1	46	152	660	13	Soft
2	46	304	813	13	Soft
3	10	152	660	80	Soft
4	10	304	813	80	Soft
5	46	152	660	13	Stiff
6	46	304	813	13	Stiff
7	10	152	660	80	Stiff
8	10	304	813	80	Stiff
9	25	152	660	80	Soft
10	25	304	813	80	Soft
11	25	152	660	80	Stiff
12	25	304	813	80	Stiff

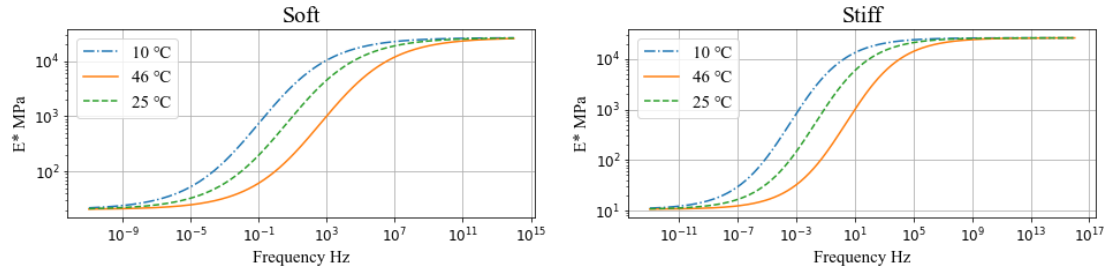

Figure 3.5 Dynamic modulus master curves at different temperatures.

Pulse Width

The pulse width calculated by the Pavement ME method is compared with one of the predominant frequency methods, the Centroid of PSD, the method proposed by Al-Qadi et al (2008a), and the equivalent pulse obtained using the equivalent frequency in Figure 3.6 and Figure 3.7. Al-Qadi's method is not shown in cases 9 to 12 since it only has data for cases 1 to 8. Pulse width can be calculated as the pulse duration multiplied by vehicle speed. Since Pavement ME and Al-Qadi et al. (2008a) define frequency as the inverse of pulse duration, the pulse duration of these two methods is simply equal to 1 divided by frequency. However, the Centroid of PSD method and the equivalent frequency do not calculate loading

time explicitly. Instead, the loading time of these methods can be obtained as $t = 1/(2f)$, which comes from the relationship $f = 1/(2t)$ as discussed in the previous section.

Since the loading frequency is related to the vertical stress pulse, the change of pulse width along the depth can be approximately considered as the vertical stress distribution. Three main findings can be drawn from this analysis. First, Figure 3.6 and Figure 3.7 show that the PSD method agrees well with the equivalent frequency method in shapes and values, except near the AC surface. Second, Figure 3.6 and Figure 3.7 indicate that the slope of the stress distribution is dependent on the layer stiffness. The pulse width by the Centroid of PSD and the equivalent frequency is much wider in stiff layers (e.g., cases 7 and 8) than in soft layers (e.g., cases 1 and 2). The stress distribution slope of the Pavement ME method does not change among cases; it always uses fixed moduli for simplification purposes. Third, the shape of the stress distribution is dependent on the relative stiffness between the AC and base layers. The vertical stress distribution along the depth obtained by the Centroid of PSD method and the equivalent frequency varies among cases (nearly linear in cases 1 and 2 except for the equivalent frequency near the AC surface, concave in all other cases). This is because when the AC layer is very soft (e.g., cases 1 and 2), the combined AC and base/subbase layers behave more like a uniform half-space. In this case, the stress distribution slope does not change much with increasing depth. When the AC layer is much stiffer than the base/subbase layer (e.g., cases 7 and 8), it behaves more like a beam. Consequently, the stress influence zone will be much larger near the bottom of the AC layer because the deformation range of the AC layer at this depth is much wider than at the top. This leads to a concave stress distribution.

Another finding is that the procedure by Al-Qadi et al. (2008a) tends to overestimate the pulse width. The reason is that this method defines the start and end of the pulse as where the slope of the stress changes from negative to positive and positive to negative. However, the location where the slope starts to change is sensitive to numerical analysis and can be far away from the main pulse. Thus, a long period where stress is very small and contains negligible energy is included as part of the pulse. Consequently, the loading time and loading distance predicted by Al-Qadi et al. (2008a) are large in general, and the stress distributions tend to be irregular. Adjusting the definition of starting and ending the loading function can make the estimated loading time more accurate. This would provide a more accurate estimate of the pulse time

duration, and if the frequency-time relationship of f = 1/(2t) is used, one would be able to obtain a better estimate of the predominant frequency.

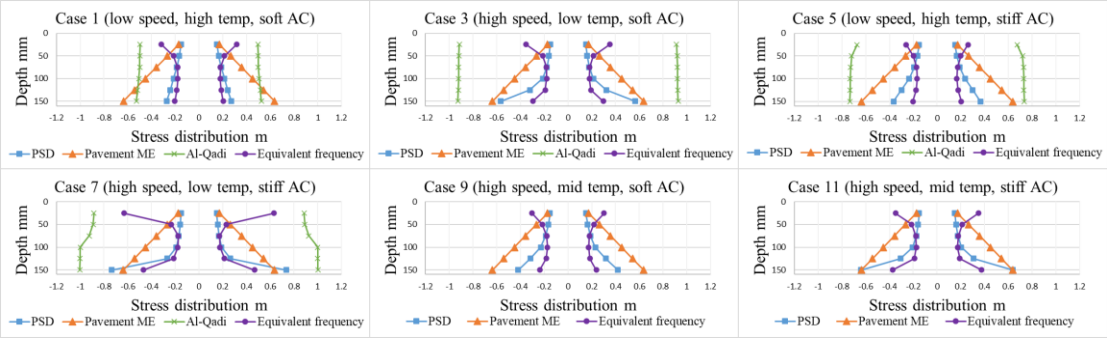

Figure 3.6 Comparison of pulse width from various methods – Thin AC layer.

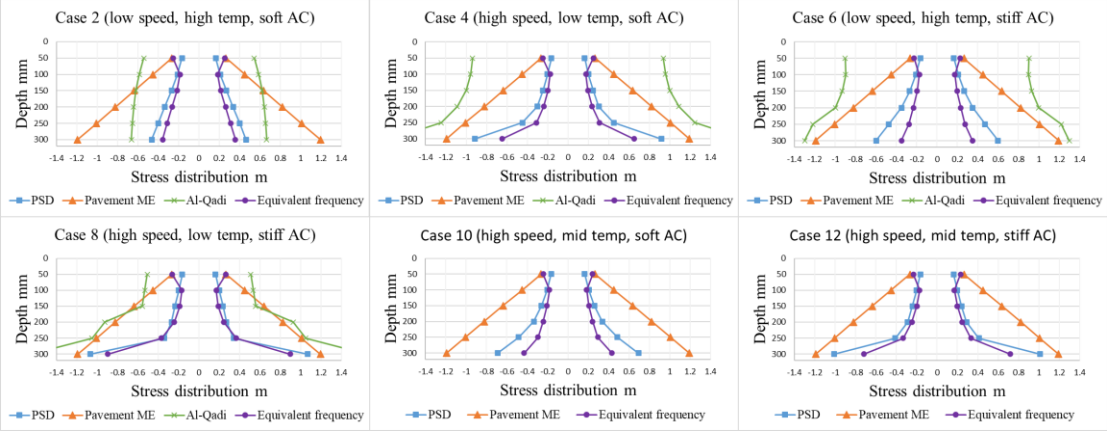

Figure 3.7 Comparison of pulse width from various methods – Thick AC layer.

Frequency and Modulus Comparison

Figure 3.8 and Figure 3.9 show the comparison of frequencies from Pavement ME and PSD methods with the equivalent frequency by iteration for thin and thick pavements, respectively. Even though the conditions in terms of vehicle speed and AC stiffness vary greatly among cases, the comparative trends of the three methods are similar. Both the Pavement ME and the Centroid of PSD methods overestimate loading frequencies near the surface, with the Pavement ME frequency being significantly higher than the equivalent frequency. However, the differences among the three methods are minimized at depths greater than or equal to about 75 mm for both thin and thick pavements.

The Pavement ME frequencies are proportional to the vehicle speed and inversely proportional to the depth. Frequencies calculated as the Centroid of the PSD obtained from the actual vertical stress pulses are

affected by both vehicle speed and pavement layer properties. As shown in Figure 3.8 and Figure 3.9, the "PSD" frequency is only proportional to the vehicle speed near the surface. When the depth is greater, the relationship is nonlinear since the frequency is reduced by the increase in AC stiffness to some extent. For example, the vehicle speed of case 3 is 6.15 times higher than that of case 1 (80 km/h and 13 km/h), but the frequency calculated by the Centroid of PSD method in case 3 at the bottom of the AC layer is only about 3.5 times higher than that of case 1 because the AC layer in case 3 is stiffer than case 1 due to lower temperature (46 °C for case 1 and 10 °C for case 3).

Frequencies can be used to calculate the modulus, which is positively correlated with the frequency. The comparison of modulus is similar to frequency, but the discrepancy among these methods is less significant. Table 3.3 summarizes the percent error of modulus predicted using the frequencies from the Pavement ME and Centroid of PSD methods compared with those obtained by iteration to match the vertical strain profile from the full dynamic viscoelastic analysis (3D-Move). Positive values indicate an overestimation while negative values mean an underestimation. In general, the Centroid of PSD method is better than the Pavement ME method in predicting the equivalent loading frequency and corresponding AC modulus.

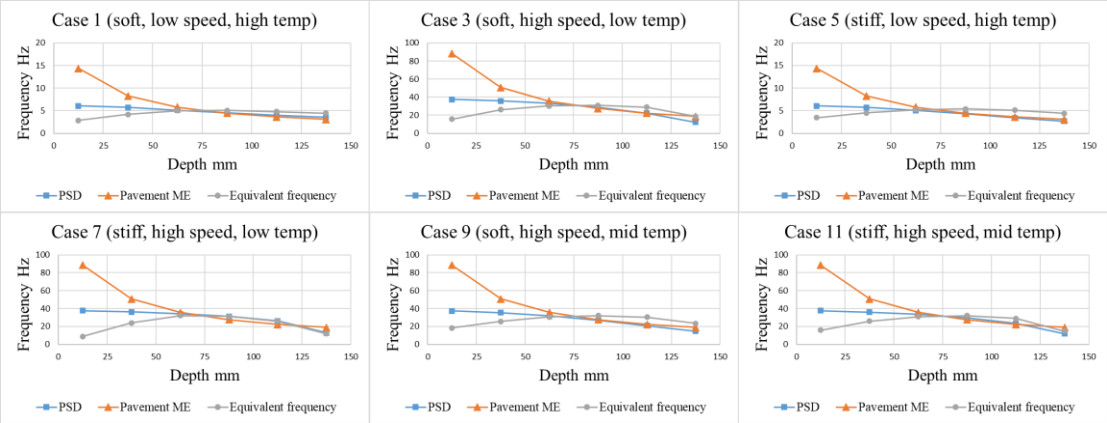

Figure 3.8 Comparison of frequency from various methods – Thin AC layer.

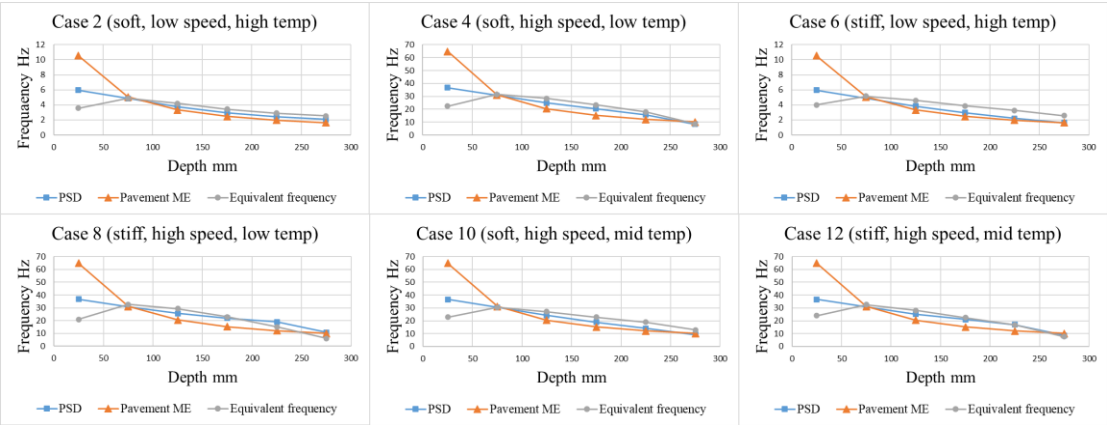

Figure 3.9 Comparison of frequency from various methods – Thick AC layer.

Table 3.3 Percent error in MEPDG and PSD predictions of AC modulus compared to the equivalent modulus by iteration.

Case No.	MEPDG			PSD		
	Top	[a]Within	Bottom	Top	[a]Within	Bottom
1	64.1	4.6	-10.3	25.0	0.8	-6.7
2	39.2	1.1	-11.2	16.4	0.0	-5.2
3	56.0	4.3	0.1	26.4	2.1	-11.2
4	31.7	-0.3	5.1	14.1	-0.7	-0.7
5	87.3	4.4	-15.2	28.5	-1.5	-20.2
6	53.5	-1.0	-18.5	19.3	-2.3	-18.0
7	31.0	1.2	6.2	20.2	0.6	0.9
8	13.2	-0.5	7.5	6.7	-0.6	8.6
9	72.8	5.4	-7.4	28.9	1.2	-15.2
10	43.9	0.8	-8.4	18.1	0.0	-11.3
11	47.6	3.3	6.4	23.2	1.7	-5.8
12	25.1	-1.0	7.9	10.5	-1.3	3.1

[a]Depth of 62.5 mm for thin cases and 75 mm for thick cases.

Strain Comparison

Figure 3.10 to Figure 3.11 show the comparison between vertical strains estimated by the Pavement ME, the Centroid of PSD, and viscoelastic analysis for thin and thick pavements, respectively. The Pavement ME and the Centroid of PSD methods underestimate vertical strains near the surface of the AC layer by up to 55% and 30%, respectively, compared to the viscoelastic solution (considered to be the reference/control). The largest error occurs in cases where the AC is extremely soft (cases 1 and 2). However, cases 1 and 2 are the combination of soft binder and high temperature (46°C), which is not a reasonable

design scheme since soft binder will not be used in such hot climates. Therefore, large errors in such cases may not have a significant impact on design practices. When the AC is extremely stiff (cases 7 and 8), both the strain values and the Pavement ME errors are small. Apart from these extreme cases, other cases (3 to 6, and 9 to 10) are more realistic scenarios with combinations of soft binder and low or mid-temperature ranges, or stiff binder and very low speed ranges. For these cases, the strain values and the Pavement ME errors are significant only near the surface. Thus, it may lead to underestimating rutting in the top AC layer if one uses the Pavement ME loading frequencies for design. However, the discrepancies decrease along the depth, and the differences between each method become insignificant at depths greater than 75 mm in both thin and thick pavements. In general, the Centroid of PSD method gives better predictions than the Pavement ME for vertical strains near the surface.

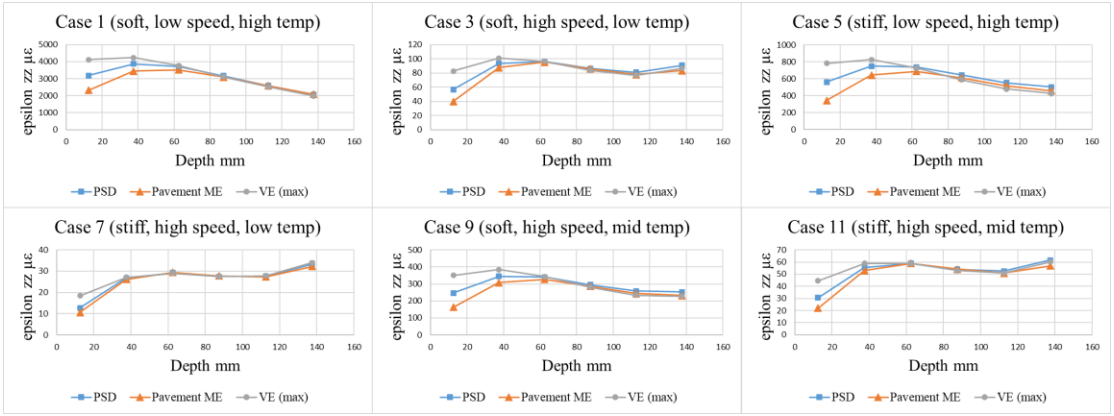

Figure 3.10 Comparison of vertical strain from various methods – Thin AC layer.

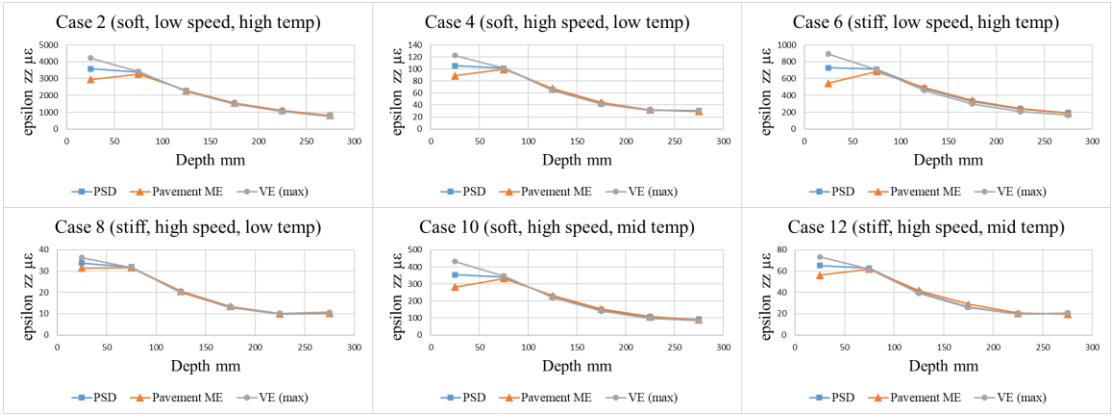

Figure 3.11 Comparison of vertical strain from various methods – Thick AC layer.

Figure 3.12 to Figure 3.13 show the comparison between horizontal (longitudinal and transverse) strains estimated by the Pavement ME, the Centroid of PSD, and equivalent frequency methods with the

viscoelastic analysis for thin and thick pavements, respectively. It should be noted that horizontal strains calculated by linear elastic analysis for a single wheel load are the same in all directions because of symmetry, but this is not true for viscoelastic analysis since the load is moving.

The maximum tensile strain does not always occur at the bottom of the AC layer. When the AC layer is much stiffer than the base layer (cases 7 and 8), it behaves like a beam and the maximum horizontal compressive and tensile strains occur at the top and bottom of the layer, respectively. However, when the AC layer is very soft (cases 1 and 2), its behavior is different from that of a beam. Instead, the combined AC and base/subbase layers behave more like a half-space.

There is no significant difference between the three loading frequency methods when comparing horizontal strains. Even though the equivalent frequency method obtained by iterating with vertical strains can predict vertical strains perfectly, it is not able to estimate horizontal strains with complete accuracy. This means that loading frequencies are different in vertical and horizontal directions. In addition, horizontal strains predicted by the viscoelastic analysis indicate that tensile strains in the transverse direction are more critical, especially in cases with soft binders, and this implies that loading frequencies in the transverse direction are lower than in the longitudinal direction. Both these two phenomena confirm the findings of Losa & Di Natale (2012).

From the design point of view, it is more useful to focus on the maximum tensile strain in each case. The Pavement ME method tends to overestimate the horizontal strain in the longitudinal direction around the middle of the softer AC layers while the errors are much smaller in the transverse direction. This is not a big concern because transverse strains are more critical in most cases and the overestimation of tensile strains is on the safe side for design. For example, the Pavement ME method underestimates the maximum tensile strain up to 86% in the longitudinal direction in case 6, but this number is only 1.5% in the transverse direction. The Pavement ME method does underestimate the maximum tensile strain in some cases, with errors usually below 10%, except in case 8 where the error is around 15% at the bottom of the AC layer (in the longitudinal direction). However, the absolute values of strains in case 8 are very small (less than 15 microstrains), and therefore will not have any significant influence on design results. Table 3.4 summarizes the percent error of strains predicted by the Pavement ME method compared with the viscoelastic analysis.

Positive values indicate an overestimation while negative values mean an underestimation.

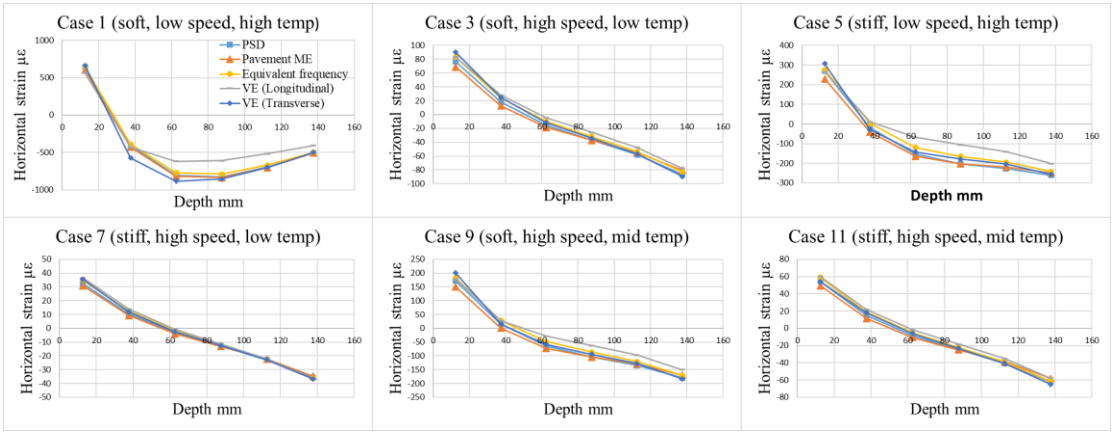

Figure 3.12 Comparison of horizontal (longitudinal and transverse) strain from various methods – Thin AC layer.

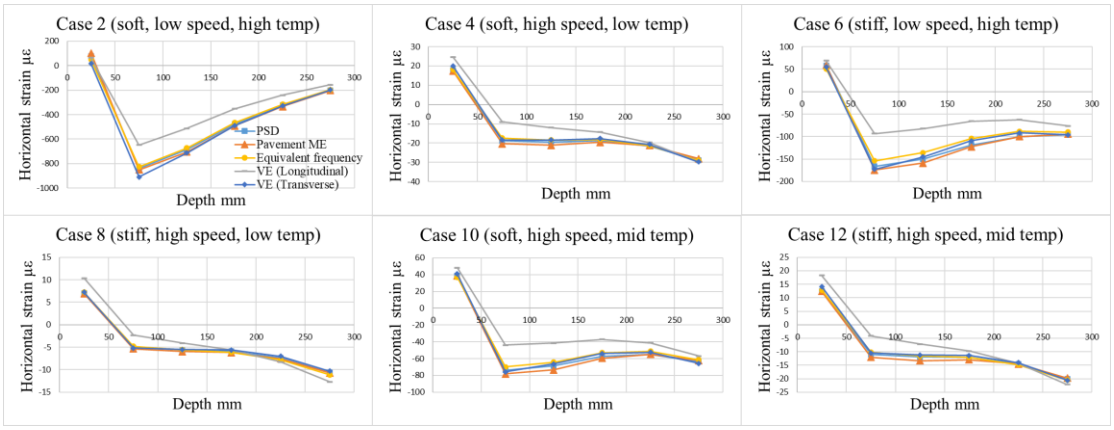

Figure 3.13 Comparison of horizontal (longitudinal and transverse) strain from various methods – Thick AC layer.

Table 3.4 Percent error in MEPDG predictions compared to viscoelastic analysis.

Case No.	Vertical ε_{zz}			Horizontal ε_{xx}		Horizontal ε_{yy}	
	Top	Within *	Bottom	Max **	Bottom	Max ***	Bottom
1	-43.7	-6.6	-5.2	31.8	24.9	-6.8	2.1
2	-30.4	-4.2	-8.1	31.1	30	-5.8	2.1
3	-51.6	-1.3	3.7	3.9	3.9	-10.0	-10.0
4	-27.6	-1.5	3.4	-5.9	-5.9	-5.4	-5.4
5	-55.9	-5.3	-7.4	23.2	23.2	-2.6	-2.6
6	-38.8	-3.5	-13.9	86.5	23.6	1.5	-1.7
7	-42.4	1.3	-5.1	-4.9	-4.9	-5.4	-5.4
8	-13.7	0	-5.9	-15.5	-15.5	3.9	3.9
9	-53.4	-4.7	1.5	13.3	13.3	-6.9	-6.9
10	-34.8	-4.0	5.3	9.2	9.2	3.8	-5.1
11	-50.7	0.4	-5.2	0.4	0.4	-10.5	-10.5
12	-23.72	0.2	-5.4	-10.8	-10.8	-4.2	-4.2

* Depth of 62.5 mm for thin cases and 75 mm for thick cases.

** Depth where the maximum tension occurs; 62.5 mm for case 1, 75 mm for cases 2 and 6; Bottom for all other cases.

*** Depth where the maximum tension occurs; 62.5 mm for case 1, 75 mm for cases 2, 6, and 10; Bottom for all other cases.

3.5 Summary and Conclusions

This chapter first introduces the concepts of predominant and equivalent frequency, provides a brief explanation of the difference between them, and proposes three methods for the calculation of predominant frequency. The properties of the predominant frequency are investigated through pulses of different shapes. In the second part of the paper, the accuracy of the Pavement ME method and the other methods of calculating the predominant frequency is evaluated in terms of frequency and strain by comparing their results with those from dynamic viscoelastic analysis. The following conclusions can be drawn:

- When calculating predominant frequencies by taking the centroid of the area of the transform amplitude in the frequency domain, only the dominant portion of the amplitude should be considered because the high-frequency portion is there to account for the sharpness of the pulse in the Fourier Transform.

- The time-frequency relationship for predominant frequency is closer to $f = 1/(2t)$ than $f = 1/t$, assuming that the pulse duration t is accurate. Overestimating the pulse duration t and using $f = 1/t$, which is higher than the equivalent frequency tend to compensate for the error to some extent.
- The centroid of PSD method agrees well with the equivalent frequency method in estimating the pulse width with depth, except at the surface of the AC layer.
- The Pavement ME method underestimates vertical strains near the surface by up to 55%, while it gives reasonable predictions with increasing depth. A concern over rutting prediction near the top of the AC layer might be raised if one uses Pavement ME loading frequencies for design.
- The Pavement ME method gives reasonable predictions of transverse strains, which are more critical for single-wheel loading. While the error is higher for strains in the longitudinal direction, it is of no consequence since transverse strains are more critical.
- Even though the procedure for Pavement ME frequency calculation is highly simplified and uses an incorrect equation that overestimates the frequency, its overall performance appears to be acceptable for horizontal strains at the bottom of the AC layer and for vertical strains except for near the surface. This is believed to be caused by the simultaneous errors in frequency and pulse duration calculations, which compensate each other to a certain degree.
- Overall, the Centroid of PSD method gives better predictions than the Pavement ME method and may be used to develop a simple correction method for the PAVEMENT ME in the future.

INVESTIGATION OF THE CHARACTERISTICS OF MULTIPLE AXLE LOADING FREQUENCIES AND THE ACCURACY OF PAVEMENT ME METHODOLOGY IN PREDICTING STRAIN RESPONSES UNDER MULTIPLE AXLE LOADINGS IN FLEXIBLE PAVEMENT

4.1 Objectives

Most of the existing literature examining predominant or equivalent loading frequencies for asphalt pavement is confined to single-axle scenarios. There is a notable lack of research addressing the accuracy and validity of the Pavement ME frequency method in the context of multiple-axle scenarios.

The objective of this chapter is to explore the accuracy of using a predominant loading frequency to predict critical strains under multiple axle loading for flexible pavements and evaluate the validity of the current Pavement ME method for different types of axle configurations.

To undertake this investigation, eight cases from Al-Qadi et al. (2008a) and four cases added by the authors (to include mid temperatures) with combinations of different AC temperatures, AC thickness, vehicle speed, and binder stiffness are selected for analysis. The "3-D Move" software (version 2.1) (2013) was used to simulate pavement responses (stress and strain) under tandem and tridem axle loadings with both linear elastic and fully dynamic viscoelastic analysis. The Pavement ME frequencies for tandem and tridem axle loadings were compared with those predominant frequencies calculated by a method named "centroid of PSD" based on the Power Spectra Density (PSD) of the vertical stress pulse (Chen et al., 2024) and equivalent frequencies obtained by iteration with vertical strains at different depths within the AC layer. Vertical strains and horizontal (longitudinal and transverse) strains predicted by the elastic analysis using the Pavement ME frequency were also compared with those predicted using the predominant frequencies by Chen et al. (2024) and Ulloa et al. (2013) (only tandem axle) as well as the dynamic viscoelastic analysis, which is considered to be the truth.

4.2 Pavement Structures and Traffic

This chapter used the "3-D Move" software (version 2.1) (2013) to calculate pavement responses induced by multiple-axle loadings. Twelve cases with combinations of different pavement structures, AC materials, vehicle speed, and AC temperatures are selected for analysis. Eight of the twelve cases were from

Al-Qadi et al (2008a), which include the |E*| data as a function of loading frequency at 10 °C and 46 °C for two AC materials (soft and stiff). The authors added four more realistic cases by constructing two new |E*| master curves at 25 °C based on the time-temperature superposition principle for the soft and stiff AC materials, respectively. Details of the twelve cases are summarized in Table 4.1. The |E*| master curves for the soft and stiff AC materials at different temperatures are shown in Figure 4.1. The base layer and subgrade were treated as linear elastic with moduli of 207 MPa and 41 MPa, respectively. The axle loading information is summarized in Table 4.2.

Table 4.1 Summary of simulation conditions.

Case No.	Pavement T (°C)	HMA Thickness (mm)	Pavement Thickness (mm)	Target Speed (km/h)	Binder
1	46	152	660	13	Soft
2	46	304	813	13	Soft
3	10	152	660	80	Soft
4	10	304	813	80	Soft
5	46	152	660	13	Stiff
6	46	304	813	13	Stiff
7	10	152	660	80	Stiff
8	10	304	813	80	Stiff
9	25	152	660	80	Soft
10	25	304	813	80	Soft
11	25	152	660	80	Stiff
12	25	304	813	80	Stiff

Table 4.2 Summary of axle loading information.

Axle Type	Tire Radius mm	Tire Pressure KPa	Axle Spacing mm	Dual Spacing mm
Tandem	80	862	1067	330
Tridem	80	862	1067	330

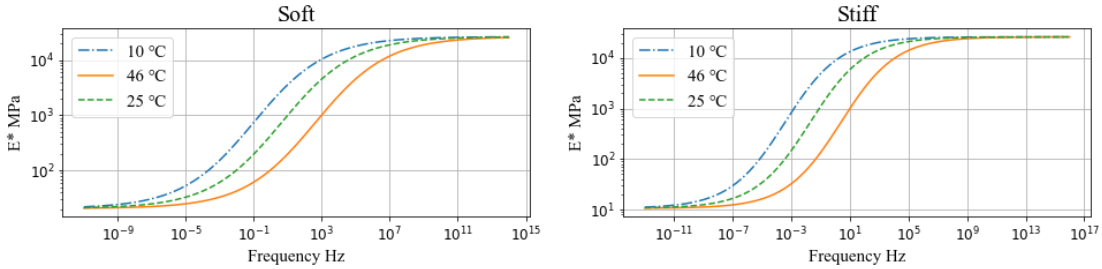

Figure 4.1 Dynamic modulus master curves at different temperatures.

4.3 Methodology

The Pavement ME frequency method for multiple-axle configurations was compared with the equivalent frequency and the other predominant frequency methods developed by Chen et al. (2024) and Ulloa et al. (2013), respectively. The critical strain responses under multiple-axle loadings were calculated by elastic analysis using those predominant or equivalent frequencies and compared with those obtained by dynamic viscoelastic analysis.

Both elastic and dynamic viscoelastic analyses were performed by the "3D Move" software (version 2.1) (2013). The dynamic modulus |E*| master curves displayed in Figure 4.1 as well as the corresponding phase angle values at different temperatures, which can be estimated by taking the derivative of the |E*| function versus frequency (Rowe 2009, Oshone et al. 2017), were used as material inputs for the AC layer for dynamic viscoelastic analysis.

Pavement ME Frequency

The Pavement ME method calculates predominant loading frequencies as the reciprocal of the loading time corresponding to the vertical stress pulse duration. The AC layer is first transformed into an equivalent single layer with an effective thickness based on Odemark's method (Ullidtz 1998) and then the vertical stress is assumed to be distributed at 45 degrees along the depth.

Once the effective depth is obtained, the "effective length of loading" can be calculated for three distinct conditions. Figure 4.2. shows an example of the load distribution of a tandem axle.

Condition #1

If $Z_{eff} <= S_T / 2 - a_c$, where Z_{eff} is effective depth, S_T is the axle spacing, and a_c is the radius of the tire-pavement contact area, there is no interaction between axles (no overlap of stresses) as shown in Figure 4.2.

The effective length can be computed by Equation 4.1:

$$L_{eff} = 2(a_c + Z_{eff}) \tag{4.1}$$

where L_{eff} is the effective length of loading

Condition #2

If $S_T / 2 - a_c < Z_{eff} < 2 (n-1) S_T$, where, n is the number of axles, there is partial interaction between axle loadings, and the logarithmic value of the effective length increases linearly from the depth of $S_T / 2 - a_c$ to $Z_{eff} < 2 (n-1) S_T$. The effective length can be computed by Equations. 4.2 to 4.4:

$$\log L_{eff} = a \log Z_{eff} + b \tag{4.2}$$

$$a = \frac{\log \frac{5S_T(n-1) + 2a_c}{S_T}}{\log \frac{2S_T(n-1)}{\frac{S_T}{2} - a_c}} \tag{4.3}$$

$$b = \log S_T - a \log(\frac{S_T}{2} - a_c) \tag{4.4}$$

Condition #3

If $Z_{eff} > 2 (n-1) S_T$, the axle loadings are considered to be fully overlapped. The effective length can be computed by Equation. 4.5:

$$L_{eff} = S_T(n-1) + 2a_c + 2Z_{eff} \tag{4.5}$$

Finally, the equivalent loading frequency is calculated by Equation. 4.6:

$$\mathrm{f} = \frac{17.6v_s}{L_{eff}} \tag{4.6}$$

Where f is the equivalent frequency in Hz, v_s is the vehicle speed in MPH, and L_{eff} is the effective length inch.

Even though the Pavement ME procedure has specific formulations for different axle types, the equivalent frequency values are computed by Equations. 4.1 to 4.6 are relatively independent of axle type (ARA 2001). In addition, the Pavement ME software uses a set of fixed moduli for the pavement layers when calculating the equivalent loading frequencies. Thus, the Pavement ME equivalent loading frequency is only a function of the depth of interest and the vehicle speed.

Even though the Pavement ME procedure has specific formulations for different axle types, the equivalent frequency values computed by Equations. 4.1 to 4.6 are relatively independent of axle type (ARA 2001) as demonstrated by an example in Figure 4.3 of Pavement ME frequencies for both single and multiple axles for different AC layer thicknesses and vehicle speeds. All Pavement ME loading frequencies analyzed in this paper are derived from the tandem-axle scenario to maintain consistency with Pavement ME software, which uses tandem axle loading frequencies for all axle types for the sake of computational efficiency (ARA 2001). In addition, the Pavement ME software uses a set of fixed moduli for the pavement layers when calculating the equivalent loading frequencies. Thus, the Pavement ME equivalent loading frequency is only a function of the depth of interest and the vehicle speed.

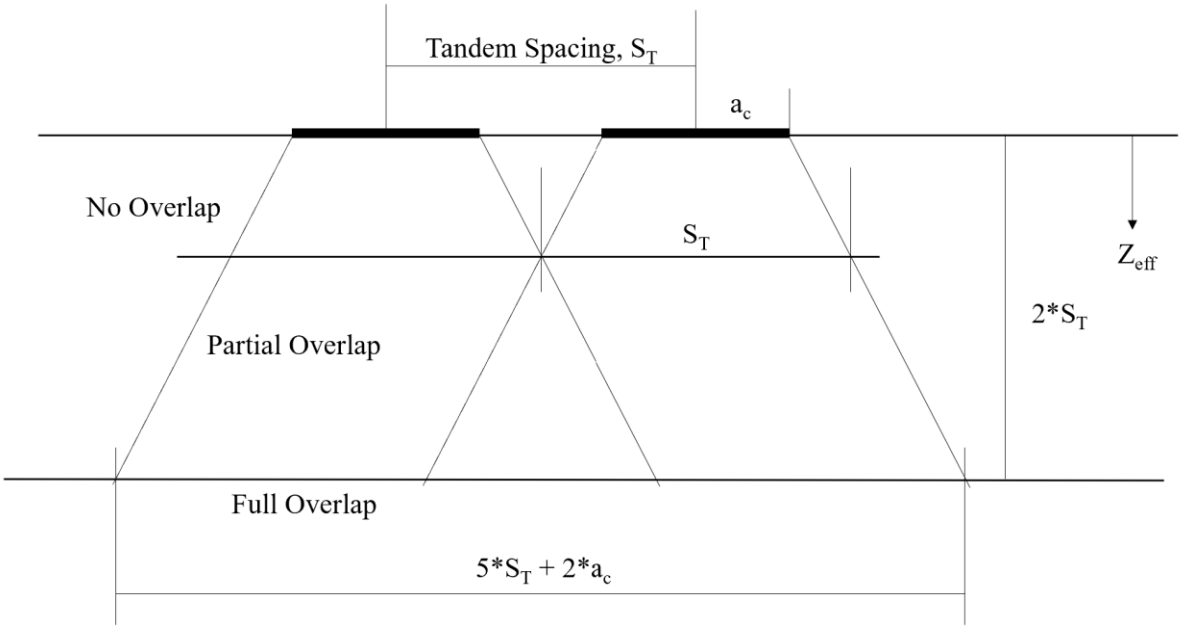

Figure 4.2 Tandem axle load distribution (adapted from ARA 2001).

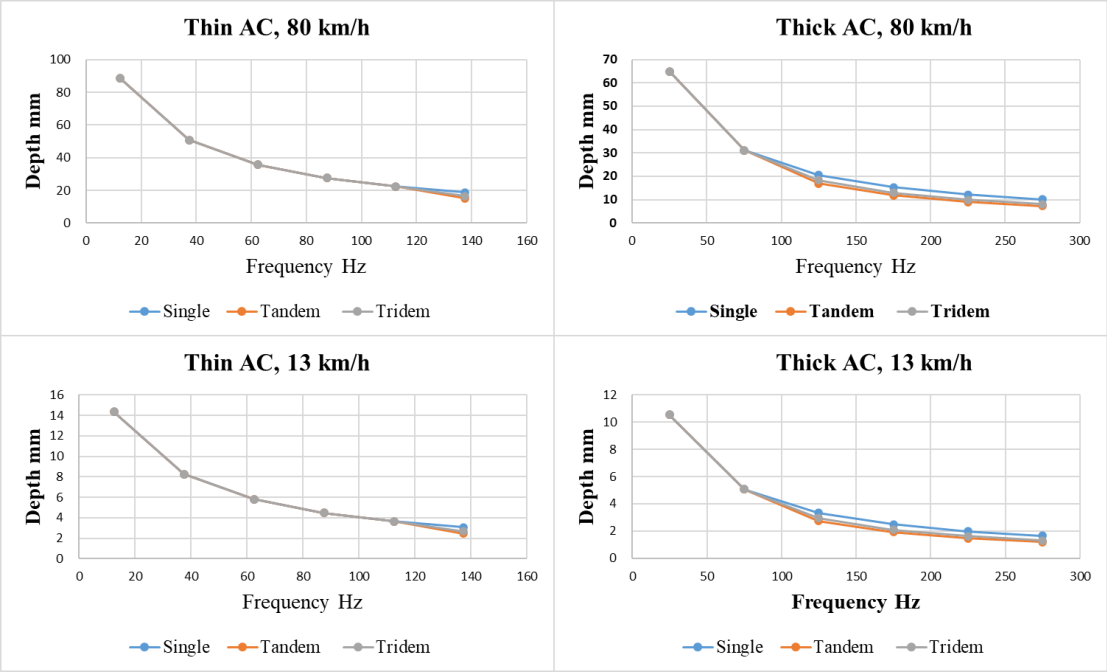

Figure 4.3 Pavement ME frequencies for single and multiple axles for thin and thick AC layer thicknesses and different vehicle speeds.

Predominant Frequency Obtained by the Centroid of PSD Method

One of the dominant axle loading frequency methods explored in this chapter is the Centroid of PSD (Chen et al. 2023). The procedure of this method is described as follows:

Step 1: Simulate the vertical stress histories using full dynamic viscoelastic analysis. Figure 4.4 (a) shows an example of the vertical stress pulse of case 9 at a depth of 125 mm.

Step 2: Perform the Fourier transform to convert the vertical stress histories into Fourier spectra in the frequency domain and draw the envelope of the Fourier spectra as shown in Figure 4.4 (b).

Step 3: Delete the non-dominant portion (right side of the vertical line in Figure 4.4 (b)) of the Fourier spectra, which is believed to accommodate the sharpness of the vertical stress signal in the time domain and does not represent the dominant energy of the stress pulse.

Step 4: Calculate the PSD spectra of the vertical stress pulse by taking the squire of the Fourier amplitude. As shown in Figure 4.4 (c), the frequency value corresponds to the centroid of the area formed by the PSD spectra is the dominant frequency of the pulse.

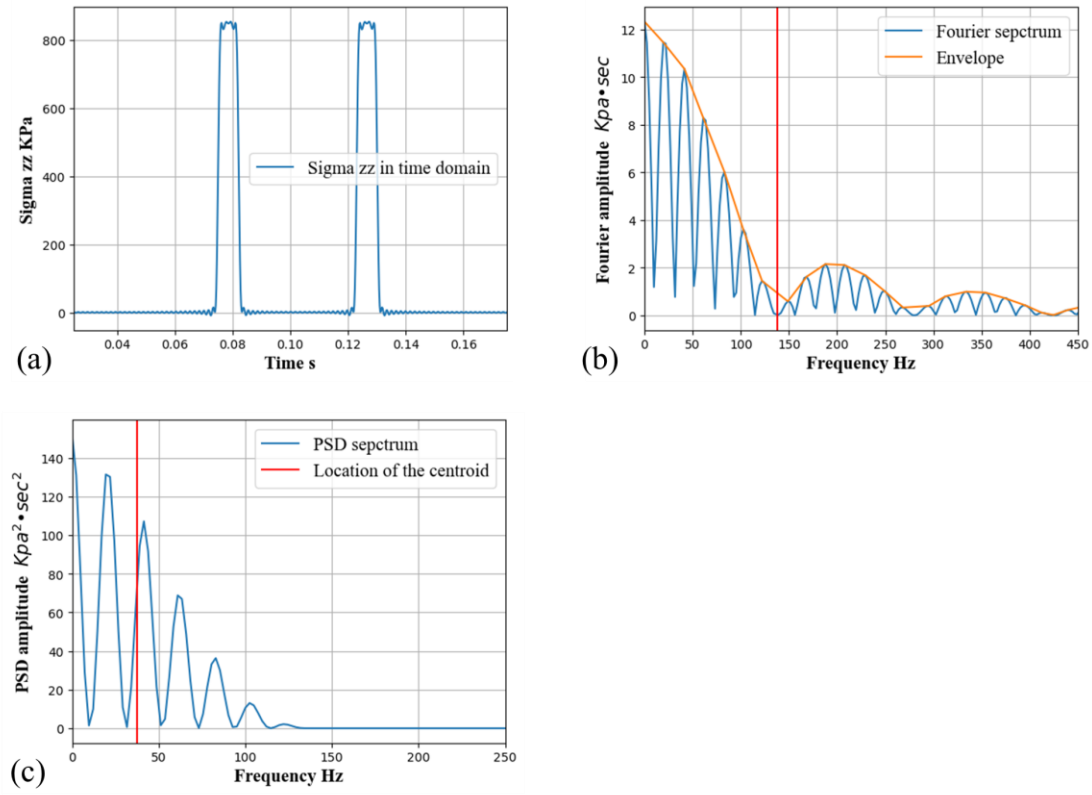

Figure 4.4 Tandem axle vertical stress pulse. (a) time domain; (b) Fourier spectra in the frequency domain; (c) PSD spectra in the frequency domain.

Predominant Frequency Proposed by Ulloa et al.

The method proposed by Ulloa et al (2013) is only applicable to a tandem-axle and it relies on the Fourier spectra of the pavement response (strain and stress) histories. The first two steps of this method are similar to that of the Centroid of PSD method except that:

(a) they use the Fourier spectra as opposed to the Power spectra.

(b) the frequency corresponding to the peak of the Fourier spectra is taken as the predominant frequency of the signal if this peak is not around the zero frequency. Otherwise, the frequency where the next peak occurs is considered to be the predominant frequency as shown in Figure 4.5.

(c) instead of using vertical stress histories to calculate the frequency for all types of responses, this method calculates the frequencies for both vertical stress and strains in the three directions (vertical, longitudinal, and transverse) with the Fourier spectra of those responses.

They also developed regression equations for predominant frequencies of different response types for

4-inch and 8-inch AC layers as shown in Equations. 4.7 and 4.8,

$$f_{p1} = 0.2187(S) \tag{4.7}$$

$$f_{p2} = 0.4681(S) \tag{4.8}$$

where f_{p1} is the predominant frequency in Hz for longitudinal strains at the top 2 inches of the AC layer, vertical strains at any depth greater than 2 inches, or transverse strains and vertical stress throughout the AC layer. f_{p2} is the predominant frequency in Hz for longitudinal strains at any depth greater than 2 inches or vertical strains at the top 2 inches of the AC layer. S is the vehicle speed in km/h.

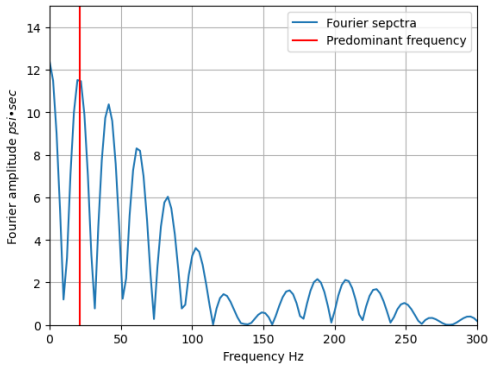

Figure 4.5 Fourier spectra of the vertical stress pulse in the time domain.

Equivalent Frequency

The equivalent frequency is determined through an iterative process involving vertical strains with depth. Initially, frequency values are assumed at various depths within the AC layer, which are then employed to compute the vertical strains within the AC layer. These calculated stresses are subsequently compared to the results obtained from the dynamic viscoelastic analysis. The iterative process continues until the frequencies yield stress values that match with those obtained from dynamic viscoelastic analysis.

4.4 Results and Discussion

Predominant and equivalent frequencies

In this section, the predominant frequency (centroid of PSD) and the equivalent frequency (by iteration) are calculated for both single and multiple axle configurations, and they are compared with the Pavement ME frequency and the frequency obtained by regression equations proposed by Ulloa et al. (2013) (Tandem axle only). These frequencies are shown in Figure 4.6 to Figure 4.7. Frequencies by Ulloa et al. (2013) are

only calculated for the thin pavement because their equations are based on data that were collected from pavements with 100 mm and 200 mm AC layers.

Figure 4.6 shows the comparison of the predominant frequency of single and multiple axles to the frequency by Pavement ME and by Ulloa et al. (2013). It can be seen from the figure that there is no significant difference in the predominant frequencies of single and multiple axles, obtained by the centroid of PSD method, except for near the bottom of the AC layer, where the frequencies for multiple axles are slightly lower than that of single axles due to interaction between axles. This result agrees with one of the conclusions of the Pavement ME methodology that axle loading frequency (also calculated from vertical stress pulse) is independent of axle type.

The Pavement ME frequencies are much higher than that of the centroid of PSD method near the surface of the AC layer but the difference gradually decreases and becomes insignificant when the depth is greater than 75 mm for both thin and thick AC layers. In cases where the AC layers are stiff (e.g. cases 7 and 11), the Pavement ME frequencies are higher than the centroid of PSD at the bottom of the AC layer. This is because the Pavement ME is using the wrong time-frequency relationship of “f = 1/t” rather than " the correct “f = 1/(2t)” (Chen et al. 2024), assuming the vertical stress pulses propagate linearly along the depth, and using fixed AC moduli. The use of “f = 1/t” leads to the overestimation of the Pavement ME frequency at the top of the AC layer by a factor of about 2 compared with the centroid of PSD, because the pulse widths of the two methods are similar near the surface, which approximately equals the diameter of the tire footprint. As depth increases, the Pavement ME method overestimates the vertical pulse width because it assumes the stress distribution along the depth is linear while the stress distribution pattern of the centroid of PSD method is concave (Chen et al. 2024). However, this type of error can be compensated by the wrong time-frequency relationship except at the bottom of very stiff AC layers (e.g. cases 7 and 11) where the pulse width of the centroid of PSD method is also large. Detailed explanations of vertical stress pulse width and propagation pattern are provided by Chen et al. (2024).

Figure 4.7 shows the comparison of the equivalent frequency of single and multiple axles to the frequency by Pavement ME and by Ulloa et al. (2013). Since the equivalent frequency is obtained by iteration to match the vertical strain with dynamic viscoelastic predictions, it can be considered the standard

in terms of vertical strain prediction. The results show that, unlike for the predominant frequency, there are larger differences between the frequencies for different axle types, especially for extremely soft and stiff AC layers.

In most cases, especially when the AC layers are soft, the equivalent frequencies of multiple axles are smaller than that of the single axle by up to 40%. For soft to moderately soft AC layers, the interaction between axles is insignificant; thus, the maximum value of vertical strain responses under multiple axles equals that of the single axle as shown in Figure 4.8 (a). However, due to the delayed response, the maximum value of the vertical strain responses under multiple axles obtained by dynamic viscoelastic analysis is slightly higher than the maximum value of a single axle as shown in Figure 4.8 (b). Consequently, the equivalent loading frequencies of multiple axles need to be higher to reduce the modulus of the AC layer that is used in the elastic analysis and result in a higher vertical strain that matches the one computed by the dynamic viscoelastic analysis.

In Figure 4.7, the equivalent frequencies of tandem axles in cases 7 and 8 are higher than that of single axles. The AC layers of these cases are very stiff, hence, the interaction between axles is relatively high. In the elastic analysis, the maximum vertical strain response under tandem axles is marginally higher than the single axle as shown in Figure 4.9 (a). On the other hand, in the dynamic viscoelastic analysis, the peak vertical strain response of the tandem axle is slightly smaller than that of the single axle. This may possibly be due to the delayed recovery of the negative response under one of the axles overlaying with the peak response of the other axle, as shown in Figure 4.9 (b). As a result, the equivalent frequency for the tandem axle used in the elastic analysis needs to be higher to increase the modulus of the AC layer and reduce the strain responses, in order to match those by the dynamic viscoelastic analysis. It should be noted that in case 7, the peak vertical strain response of the tandem axle at the depth of 37.5 mm of the AC layer is only 3.2% smaller than that of the single axle (20.76 με compared to 21.43 με); and the corresponding modulus at the same location for tandem axle condition is only 4.4% higher than the single axle. However, this results in an increase of equivalent frequency by 49% (from 33.2 Hz to 49.6 Hz). This means that the equivalent frequency is very sensitive to the modulus and vertical strain response when the AC layer is stiff. However, the predicted vertical strain values are much less sensitive to loading frequencies if the AC is stiff.

As shown in Figure 4.6 and Figure 4.7, the loading frequencies calculated by Ulloa's equations agree with the centroid of PSD method at the top 2 inches but are higher than the equivalent frequency. When the depth is greater than 2 inches, frequencies by Ulloa agree with the Pavement ME frequencies at the bottom of the AC layer but they are usually lower than the equivalent frequency except for cases 7 and 11 at the bottom of the AC layer. Another observation from Figure 4.6 and Figure 4.7 is that the distribution shape with the depth for equivalent frequency is concave while this distribution for other predominant frequencies is asymptotic. This implies that to match the vertical strains calculated by elastic analysis with those from dynamic viscoelastic analysis, the equivalent loading frequency (and equivalent elastic modulus) may not consistently decrease with depth; instead, it may initially rise before declining.

Elastic AC modulus

The modulus of the AC layer is positively related to the loading frequency. The comparison trend of the elastic modulus corresponding to the predominant and equivalent frequency is similar to that of frequency but with lesser differences. Examples of cases with soft and stiff AC layers are shown in Figure 4.10 and Figure 4.11. In Figure 4.10, the moduli that correspond to the predominant frequencies by the centroid of PSD method for single and multiple axles are nearly on top of each other. In Figure 4.11, even though there are still gaps between the moduli calculated by equivalent frequencies for various axle configurations, the discrepancies are much smaller than those in Figure 4.7.

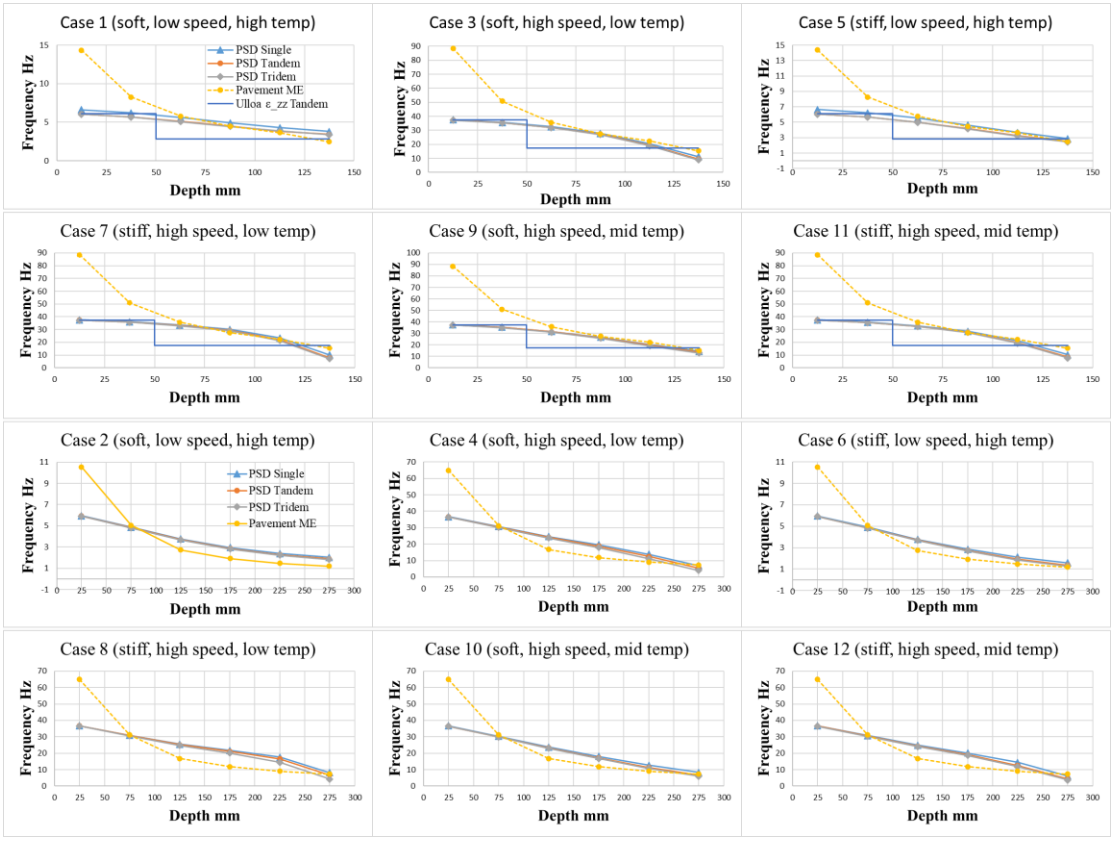

Figure 4.6 Comparison of predominant frequency and other methods for single and multiple axles (a) Thin AC layer; (b) Thick AC layer.

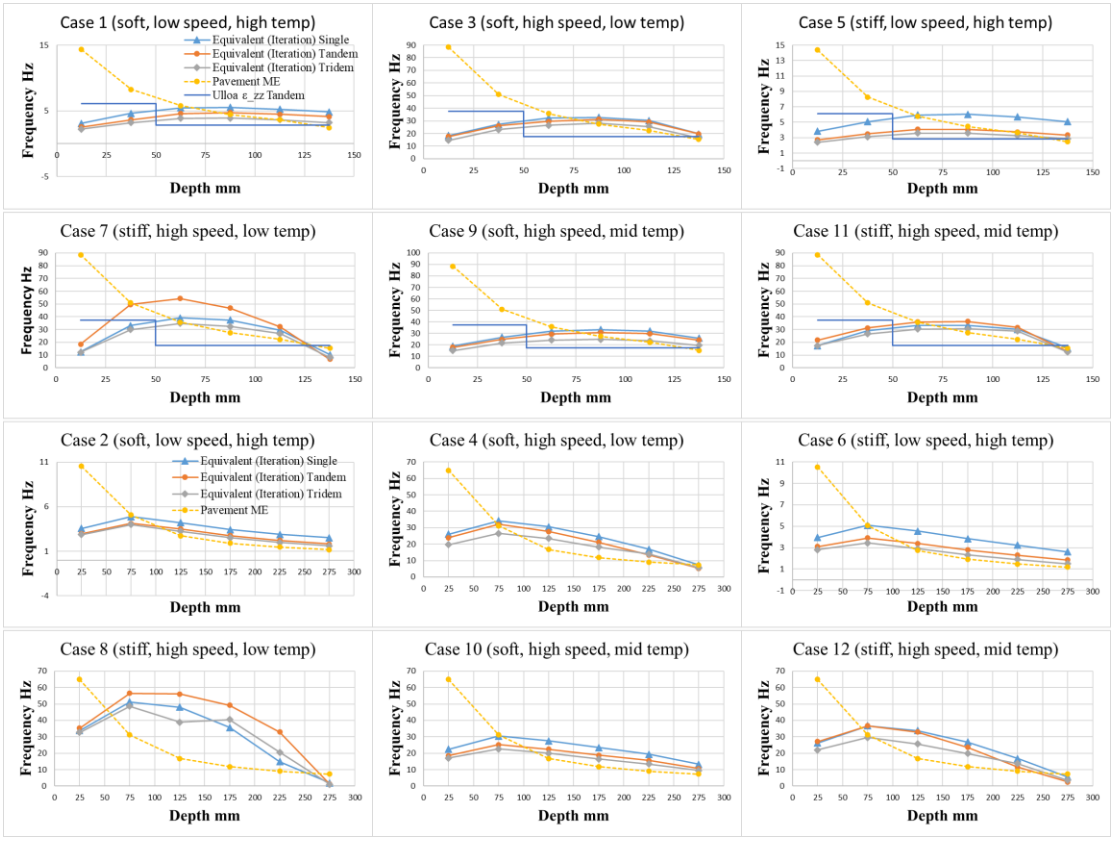

Figure 4.7 Comparison of equivalent frequency and other methods for single and multiple axles (a) Thin AC layer; (b) Thick AC layer.

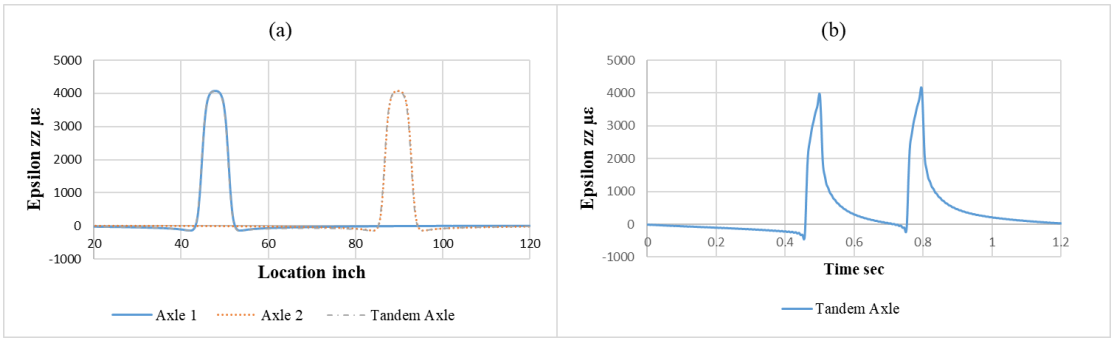

Figure 4.8 Vertical strain responses under axles at a depth of 37.5 mm in case 1. (a) elastic analysis; (b) dynamic viscoelastic analysis.

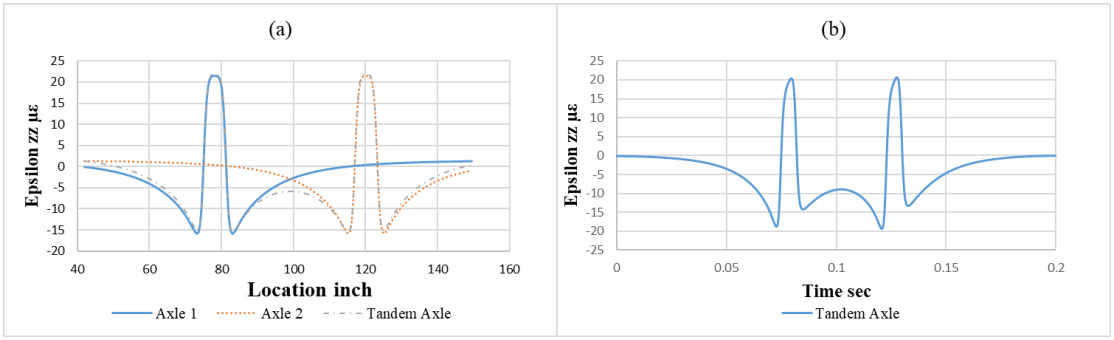

Figure 4.9 Vertical strain responses under axles at the depth of 37.5 mm in case 7. (a) elastic analysis; (b) dynamic viscoelastic analysis.

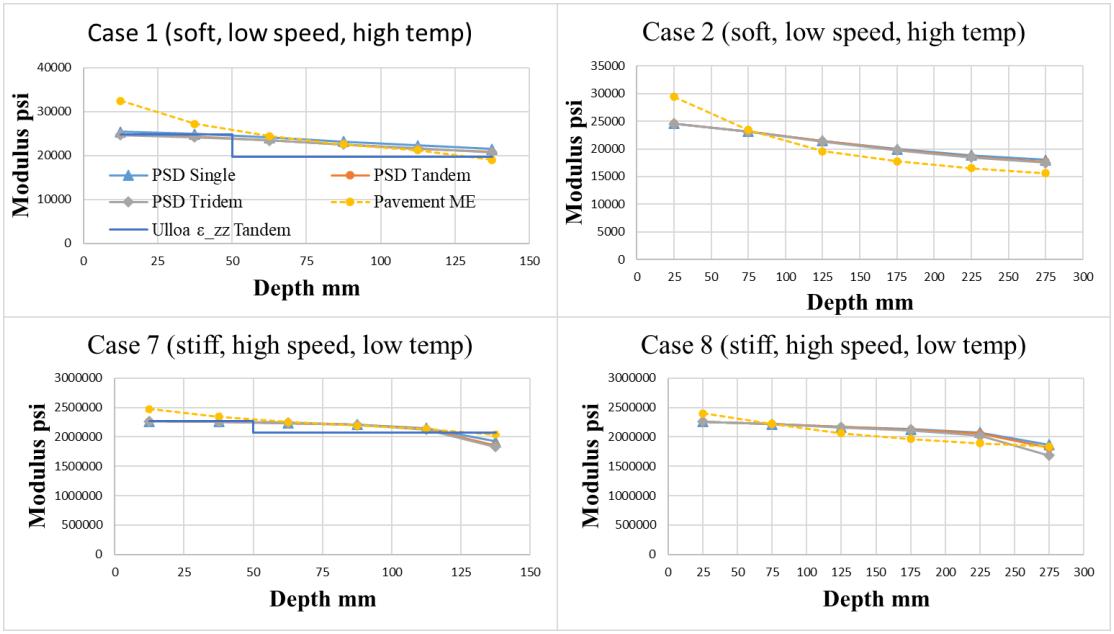

Figure 4.10 Comparison of modulus predicted by predominant frequency and other methods for single and multiple axles.

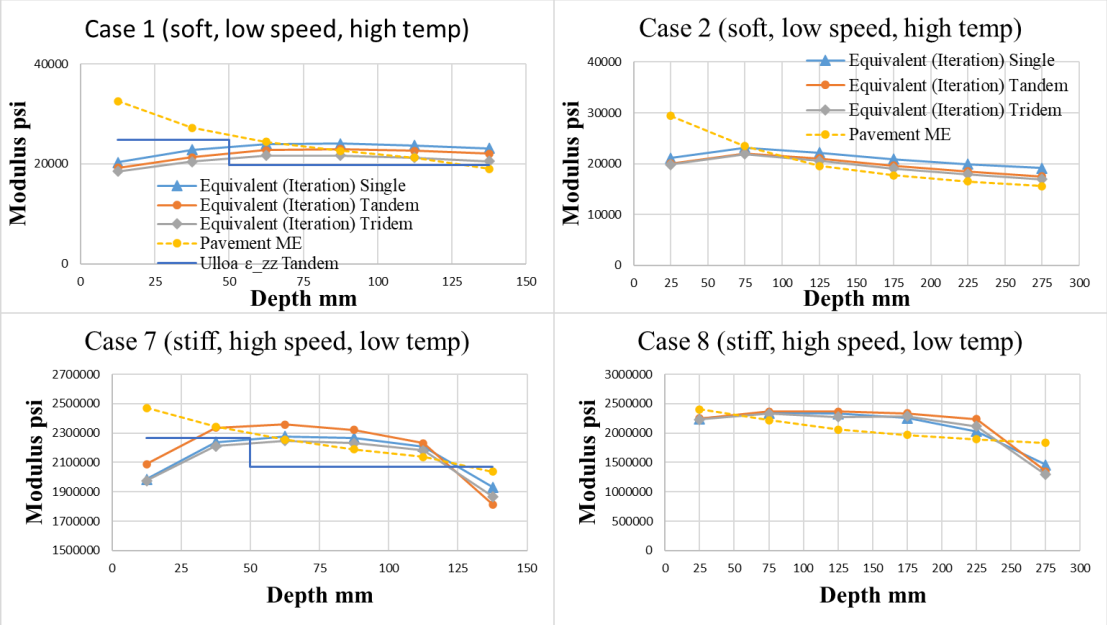

Figure 4.11 Comparison of modulus predicted by equivalent frequency and other methods for single and multiple axles.

Vertical strains within the AC layer

This section explores the influence of axle configurations on loading frequencies in terms of vertical strain (ε_{zz}) predictions within the AC layer. To evaluate the accuracy of only one frequency value for both single and multiple axle configurations, the predominant frequencies by the centroid of PSD method and the equivalent frequencies by iteration for single axle scenarios are used to predict the vertical strains induced by multiple axle loadings. Figure 4.12 shows the vertical strains induced by a tridem axle with dual tires as predicted by various frequency methods and those obtained from the dynamic viscoelastic analysis, which is considered to be the standard. The vertical strains for all single, tandem, and tridem axles are then normalized to the dynamic viscoelastic results and listed in Table 4.3 to Table 4.6 for a more quantitative comparison.

As can be seen in Figure 4.12, the major differences occur at shallow depth near the surface of the AC layer. The strains predicted by different frequencies tend to converge at the bottom of the AC layer with errors usually within 10% compared to the standard in most cases except for case 8. However, the underestimation of vertical strains in case 8 is not a concern from the design point of view considering the strain values are very small.

The Pavement ME frequency underestimates the vertical strains under both single and multiple axle loadings by up to more than 60% near the top of the AC layer, and the errors decrease along the depth. In general, the errors near the AC layer surface marginally increase by less than 5% as the number of axles grows, except for cases 7 and 11, where the errors for the tandem axle are lower than that for the single axle. This is because the dynamic viscoelastic strain responses under the tandem axle are slightly lower than those under the single axle as demonstrated in Figure 4.9. Using the predominant frequency or Pavement ME frequency derived from single axle scenarios to predict the vertical strain under multiple axle loadings can result in an additional error of 5% to 10% near the surface of the AC layer, as can be seen in Figure 4.12 and Table 4.3 to Table 4.6. Overall, the centroid of PSD method performs better than the Pavement ME in terms of vertical strain prediction.

The equivalent frequency is obtained by iteration with vertical strains at each depth of the AC layer. Thus, the equivalent frequencies for single, tandem, and tridem axles are not used for the prediction of vertical strains under these three axle loadings, respectively, because the results should be the same as those from dynamic viscoelastic analysis. Unlike the predominant frequency and the Pavement ME frequency, using the single axle equivalent frequency to calculate strain responses induced by multiple axle loadings will result in lower vertical strains with a difference of 5% to 10% in the cases with soft to moderately soft AC layers except for case 5 where the difference is up to 20%. This implies that using only one frequency will not enable predicting vertical strains induced by different axle loadings with reasonable accuracy, especially for relatively soft AC layers, even though the predominant frequency and Pavement ME frequency show insignificant differences when using different axle configurations.

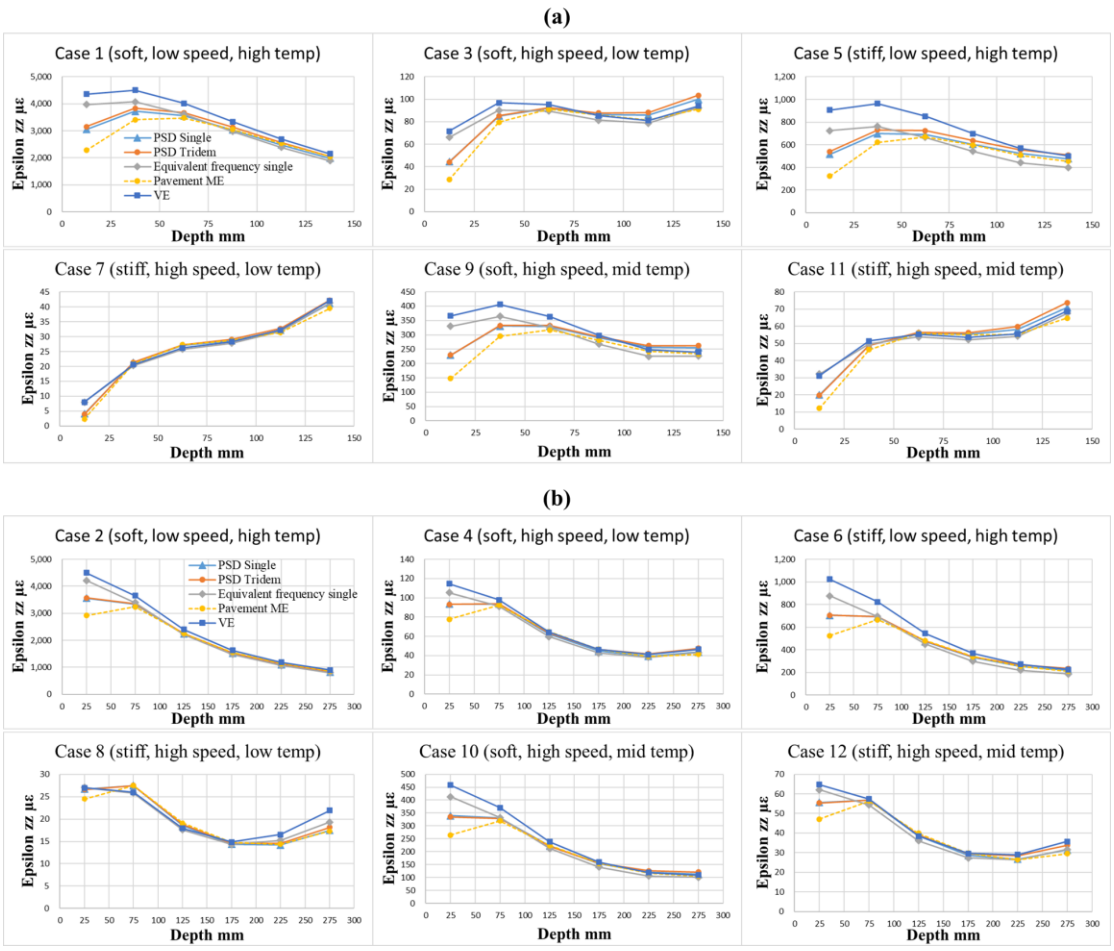

Figure 4.12 Vertical strains under tridem axles calculated using various loading frequencies (a) Thin AC layer; (b) Thick AC layer.

Table 4.3 Vertical strains predicted by various frequencies for single axles (Thin pavement).

Case number	Depth mm	Normalized Vertical Strains	
		PSD Single	[a]P_ME
Case 1	12.5	0.77	0.58
	37.5	0.91	0.84
	62.5	0.98	0.96
	87.5	1.02	1.02
	112.5	1.04	1.07
	137.5	1.05	1.15
Case 3	12.5	0.67	0.41
	37.5	0.95	0.87
	62.5	1.03	1.01
	87.5	1.07	1.05
	112.5	1.09	1.04
	137.5	1.08	1.01
Case 5	12.5	0.72	0.45
	37.5	0.92	0.81
	62.5	1.03	1.00
	87.5	1.12	1.11
	112.5	1.20	1.17
	137.5	1.21	1.23
Case 7	12.5	0.58	0.27
	37.5	1.05	0.99
	62.5	1.05	1.03
	87.5	1.03	1.02
	112.5	1.01	0.99
	137.5	1.00	0.96
Case 9	12.5	0.70	0.45
	37.5	0.91	0.81
	62.5	1.01	0.97
	87.5	1.08	1.05
	112.5	1.14	1.09
	137.5	1.15	1.10
Case 11	12.5	0.65	0.41
	37.5	0.98	0.93
	62.5	1.04	1.04
	87.5	1.06	1.06
	112.5	1.07	1.03
	137.5	1.06	0.99

[a]Pavement ME

Table 4.4 Vertical strains predicted by various frequencies for single and multiple axles (Thin pavement).

Case number	Depth mm	Normalized Vertical Strains								
		Tandem Axle					Tridem Axle			
		PSD Single	PSD Tandem	[a]Equ Single	P_ME	Ulloa	PSD Single	PSD Tridem	Equ Single	P_ME
Case 1	12.5	0.73	0.75	0.95	0.55	0.74	0.70	0.72	0.91	0.52
	37.5	0.87	0.89	0.95	0.79	0.88	0.83	0.85	0.90	0.76
	62.5	0.93	0.96	0.94	0.91	1.13	0.88	0.91	0.90	0.86
	87.5	0.96	0.99	0.94	0.96	1.12	0.91	0.94	0.89	0.91
	112.5	0.98	1.01	0.94	1.00	1.10	0.92	0.95	0.89	0.94
	137.5	0.98	1.02	0.94	1.07	1.07	0.92	0.96	0.88	1.01
Case 3	12.5	0.67	0.67	0.93	0.40	0.65	0.62	0.62	0.92	0.40
	37.5	0.92	0.92	0.94	0.83	0.92	0.88	0.88	0.93	0.82
	62.5	1.00	1.01	0.95	0.97	1.19	0.96	0.97	0.94	0.96
	87.5	1.05	1.06	0.96	1.02	1.14	1.02	1.03	0.95	1.01
	112.5	1.08	1.10	0.98	1.03	1.07	1.06	1.09	0.97	1.02
	137.5	1.08	1.11	0.99	1.00	1.01	1.06	1.10	0.98	1.00
Case 5	12.5	0.60	0.63	0.84	0.37	0.61	0.57	0.60	0.80	0.36
	37.5	0.76	0.80	0.83	0.68	0.79	0.72	0.76	0.79	0.64
	62.5	0.86	0.90	0.82	0.83	1.16	0.81	0.85	0.78	0.78
	87.5	0.92	0.97	0.82	0.90	1.13	0.86	0.91	0.78	0.86
	112.5	0.98	1.03	0.82	0.95	1.09	0.92	0.98	0.78	0.90
	137.5	1.01	1.07	0.84	1.03	1.04	0.95	1.02	0.80	0.97
Case 7	12.5	0.71	0.70	1.18	0.50	1.18	0.51	0.49	1.00	0.28
	37.5	1.11	1.11	1.06	1.09	1.06	1.03	1.03	0.98	1.01
	62.5	1.07	1.08	1.03	1.08	1.03	1.03	1.04	0.98	1.04
	87.5	1.03	1.04	1.00	1.04	1.00	1.01	1.03	0.98	1.02
	112.5	1.00	1.01	0.99	0.99	0.99	1.00	1.02	0.98	0.98
	137.5	0.97	0.99	0.98	0.94	0.98	0.98	1.00	0.98	0.95
Case 9	12.5	0.68	0.68	0.96	0.44	0.66	0.63	0.63	0.90	0.40
	37.5	0.88	0.88	0.96	0.79	0.88	0.81	0.82	0.90	0.73
	62.5	0.98	0.98	0.96	0.94	1.22	0.91	0.91	0.90	0.87
	87.5	1.05	1.05	0.95	1.02	1.19	0.97	0.98	0.90	0.94
	112.5	1.11	1.12	0.96	1.05	1.14	1.04	1.06	0.91	0.99
	137.5	1.12	1.13	0.98	1.07	1.08	1.06	1.09	0.94	1.02
Case 11	12.5	0.72	0.72	1.03	0.46	0.68	0.64	0.63	1.03	0.38
	37.5	1.00	1.00	0.97	0.95	0.99	0.95	0.95	0.96	0.90
	62.5	1.05	1.06	0.98	1.05	1.23	1.01	1.02	0.97	1.01
	87.5	1.06	1.07	0.98	1.06	1.14	1.03	1.05	0.97	1.03
	112.5	1.07	1.09	0.98	1.03	1.04	1.05	1.08	0.98	1.01
	137.5	1.04	1.07	0.99	0.98	0.97	1.03	1.07	0.98	0.96

[a]Equivalent frequency

Table 4.5 Vertical strains predicted by various frequencies for single axles (Thick pavement).

Case number	Depth mm	Normalized Vertical Strains	
		PSD Single	[a]P_ME
Case 2	25	0.84	0.69
	75	0.98	0.95
	125	1.01	1.06
	175	1.02	1.11
	225	1.03	1.14
	275	1.04	1.16
Case 4	25	0.88	0.71
	75	1.03	1.00
	125	1.06	1.14
	175	1.06	1.17
	225	1.05	1.12
	275	1.01	1.03
Case 6	25	0.80	0.59
	75	0.99	0.94
	125	1.05	1.14
	175	1.10	1.24
	225	1.16	1.29
	275	1.17	1.27
Case 8	25	0.99	0.86
	75	1.06	1.02
	125	1.06	1.08
	175	1.01	1.07
	225	0.94	1.01
	275	0.89	0.95
Case 10	25	0.81	0.63
	75	0.99	0.95
	125	1.04	1.12
	175	1.08	1.19
	225	1.13	1.21
	275	1.12	1.15
Case 12	25	0.90	0.74
	75	1.04	1.01
	125	1.06	1.13
	175	1.05	1.15
	225	1.02	1.08
	275	0.98	0.99

[a]Pavement ME

Table 4.6 Vertical strains predicted by various frequencies for multiple axles (Thick pavement).

Case number	Depth mm	Normalized Vertical Strains							
		Tandem Axle				Tridem Axle			
		PSD Single	PSD Tandem	[a]Equ Single	P_ME	PSD Single	PSD Tridem	Equ Single	P_ME
Case 2	25	0.81	0.81	0.95	0.66	0.79	0.79	0.94	0.64
	75	0.93	0.94	0.95	0.90	0.92	0.92	0.93	0.88
	125	0.95	0.96	0.94	1.00	0.93	0.94	0.92	0.98
	175	0.96	0.96	0.93	1.04	0.93	0.94	0.91	1.01
	225	0.96	0.97	0.92	1.06	0.93	0.95	0.90	1.03
	275	0.96	0.97	0.91	1.07	0.92	0.95	0.88	1.03
Case 4	25	0.87	0.87	0.94	0.69	0.82	0.81	0.92	0.67
	75	1.01	1.02	0.96	0.97	0.96	0.96	0.93	0.94
	125	1.03	1.04	0.95	1.09	0.97	0.99	0.93	1.06
	175	1.02	1.04	0.95	1.11	0.97	1.00	0.92	1.08
	225	0.99	1.02	0.97	1.06	0.96	1.02	0.93	1.02
	275	0.95	0.99	0.97	0.98	0.94	1.02	0.93	0.94
Case 6	25	0.73	0.73	0.89	0.53	0.69	0.69	0.86	0.51
	75	0.89	0.89	0.88	0.84	0.84	0.84	0.84	0.80
	125	0.93	0.93	0.87	1.00	0.87	0.88	0.83	0.95
	175	0.96	0.98	0.86	1.07	0.89	0.92	0.81	1.01
	225	1.01	1.04	0.85	1.12	0.93	0.98	0.80	1.05
	275	1.03	1.09	0.87	1.11	0.96	1.04	0.82	1.05
Case 8	25	1.00	1.00	0.90	0.81	0.99	0.99	1.00	0.90
	75	1.07	1.07	0.93	0.99	1.06	1.06	0.99	1.06
	125	1.08	1.08	0.95	1.06	1.04	1.05	0.98	1.10
	175	1.03	1.04	1.00	1.07	0.97	0.98	0.96	1.03
	225	0.95	0.98	1.07	1.04	0.86	0.88	0.92	0.90
	275	0.90	0.93	1.09	1.01	0.80	0.83	0.88	0.81
Case 10	25	0.76	0.76	0.93	0.59	0.74	0.73	0.90	0.57
	75	0.92	0.92	0.92	0.88	0.89	0.89	0.90	0.86
	125	0.96	0.97	0.92	1.03	0.93	0.92	0.89	1.00
	175	1.00	1.01	0.91	1.09	0.96	0.97	0.88	1.06
	225	1.04	1.08	0.92	1.11	1.01	1.05	0.89	1.07
	275	1.05	1.11	0.94	1.08	1.03	1.10	0.92	1.05
Case 12	25	0.92	0.92	0.96	0.72	0.86	0.85	0.96	0.72
	75	1.05	1.05	0.96	0.99	0.99	0.99	0.95	0.98
	125	1.05	1.06	0.95	1.10	1.00	1.01	0.94	1.09
	175	1.00	1.02	0.94	1.09	0.97	1.00	0.92	1.07
	225	0.93	0.97	0.94	1.00	0.92	0.98	0.91	0.97
	275	0.87	0.91	0.92	0.91	0.88	0.95	0.89	0.87

[a]Equivalent frequency

Horizontal strains within the AC layer

The horizontal strains in both longitudinal (ε_{xx}) and transverse (ε_{yy}) directions under single and multiple axle loadings (with dual tires) are calculated using various frequencies. The maximum tensile strains are normalized to results from the dynamic viscoelastic and listed in Table 4.7 to Table 4.9. Except for cases 1 and 2 for ε_{xx} and for case 6 for ε_{yy}, where the maximum tensile value occurs within the AC layer, all other maximum tensile values occur at the bottom of the layer for all three axle configurations. However, these results are not shown here for brevity. Note that the horizontal viscoelastic tensile strains under a single axle with a single tire are greater in the transverse direction than in the longitudinal direction (Chen et al. 2024). On the other hand, Table 4.7 shows that for a single axle with dual tires, the horizontal tensile strains in the longitudinal direction are larger (highlighted) than in the transverse direction for most conditions except when the AC is very soft (cases 1, 2, and 6). This is due to the interaction effect of two tires except when the AC layer is very soft where the interaction is small enough so that the dual tires behave independently as two single tires. However, Table 4.8 and Table 4.9show that for tandem and tridem axles scenarios, even though in some cases the AC layer is not soft, the transverse strain (ε_{yy}) becomes the critical horizontal strain. This may be due to the compound interaction between tires and axles, which is out of the scope of this research.

As shown in Table 4.7 to Table 4.9, the differences between maximum tensile strains predicted by various loading frequencies are much smaller than those between vertical strains, and the errors compared with the dynamic viscoelastic results are acceptable in general. For both the predominant frequency and equivalent frequency, the errors of normalized horizontal strain values predicted by each method are similar regardless of whether the frequency is derived for single or multiple axle scenarios. The errors in the critical horizontal strain calculated using the Pavement ME frequency are within 15% in most cases except for cases 5, 8, and 12. The maximum error in the longitudinal strain ε_{xx} in case 5 is an overestimation of up to 35% on the conservative side. The Pavement ME frequency underestimates the critical horizontal strains for tandem and tridem axle loadings by up to 33% and 23% in cases 8 and 12, respectively. However, due to the high stiffness of the AC layer, the absolute values of strains in these cases are very small (less than 50 micro strains) which will not cause any concern from a practical point of view. Finally, it is noted that

obtaining the equivalent frequency by iteration, so that it allows for predicting the vertical strains with almost zero error, does not lead to similarly accurate predictions of horizontal stains.

In summary, the maximum horizontal strains are less sensitive to loading frequency than vertical stains for both single and multiple axles. This may be because the maximum tensile strains usually occur at the bottom of the AC layer where loading frequencies also tend to converge. The accuracy of loading frequencies in terms of maximum horizontal strain prediction is generally independent of the number of axles but is mainly affected by the AC layer stiffness and vehicle speed.

Table 4.7 Maximum horizontal strains predicted by various frequencies (Single axle).

Case number	Longitudinal strain (ε_{xx})				Transverse strain (ε_{yy})			
	Normalized to VE			[d]VE	Normalized to VE			VE
	[a]PSD	[b]P_ME	[c]Iteration	(με)	PSD	P_ME	Iteration	(με)
1	1.44	1.52	1.36	537	0.92	0.96	0.88	812
3	1.12	1.06	1.05	101	1.01	0.96	0.95	77
5	1.37	1.37	1.26	206	1.07	1.07	0.98	191
7	0.97	0.95	0.98	52	1.02	0.99	1.02	36
9	1.23	1.21	1.15	170	1.03	1.01	0.96	142
11	1.07	1.02	1.03	79	1.01	0.96	0.97	59
2	1.32	1.37	1.33	616	0.93	0.95	0.94	847
4	0.95	0.97	0.94	48	1.02	1.05	1.02	32
6	1.31	1.34	1.22	100	1.03	1.08	0.96	147
8	0.88	0.94	0.96	20	0.88	0.96	0.97	15
10	1.18	1.20	1.11	79	1.05	1.06	1.00	58
12	1.00	1.02	1.01	33	0.90	0.92	0.91	27

[a]Predominant frequency from single axles using PSD method

[b]Pavement ME

[c]Equivalent frequency by iteration over vertical strains

[d]Full dynamic viscoelastic

Table 4.8 Maximum horizontal strains predicted by various frequencies (Tandem axle).

Case number	Longitudinal strain (ε_{xx})						Transverse strain (ε_{yy})					
	Normalized to VE					[d]VE (με)	Normalized to VE					VE (με)
	[a]PSD		[b]P_ME	[c]Iteration			PSD		P_ME	Iteration		
	[e]S	[f]Tan		S	Tan		S	Tan		S	Tan	
1	1.44	1.49	1.51	1.35	1.53	551	0.84	0.87	0.87	0.79	0.91	857
3	1.15	1.17	1.08	1.07	1.09	93	1.03	1.04	0.97	0.95	0.97	80
5	1.30	1.33	1.28	1.17	1.29	217	1.18	1.22	1.17	1.05	1.18	168
7	0.90	0.91	0.87	0.90	0.91	51	1.05	1.07	1.03	1.06	1.06	40
9	1.22	1.23	1.19	1.12	1.15	169	1.03	1.03	1.01	0.93	0.96	142
11	1.10	1.13	1.04	1.05	1.07	71	0.96	0.98	0.92	0.91	0.94	67
2	1.34	1.34	1.38	1.29	1.42	621	0.88	0.88	0.90	0.85	0.94	874
4	0.83	0.86	0.87	0.86	0.86	49	1.06	1.09	1.09	1.08	1.09	38
6	1.32	1.35	1.34	1.20	1.31	93	0.96	0.96	1.00	0.84	1.03	147
8	0.68	0.71	0.78	0.84	0.74	23	1.22	1.26	1.35	1.46	1.32	15
10	1.18	1.12	1.20	1.11	1.16	71	1.08	1.10	1.08	1.01	1.05	63
12	0.93	0.97	0.99	1.00	1.04	31	0.82	0.85	0.86	0.86	0.90	38

[a]Predominant frequency from single and tandem axles using PSD method

[b]Pavement ME

[c]Equivalent frequency by iteration over vertical strains

[d]Full dynamic viscoelastic

[e]Single axle

[f]Tandem axle

Table 4.9 Maximum horizontal strains predicted by various frequencies (Tridem axle).

Case number	Longitudinal strain (ε_{xx})						Transverse strain (ε_{yy})					
	Normalized to VE					VE[d] (με)	Normalized to VE					VE (με)
	[a]PSD		[b]P_ME	[c]Iteration			PSD		P_ME	Iteration		
	[e]S	[f]Tri		S	Tri		S	Tri		S	Tri	
1	1.28	1.33	1.34	1.21	1.40	598	0.80	0.83	0.84	0.77	0.89	874
3	1.13	1.16	1.07	1.06	1.10	92	0.99	1.01	0.95	0.93	0.95	83
5	1.27	1.31	1.28	1.17	1.30	220	1.16	1.20	1.18	1.06	1.18	165
7	1.01	1.03	0.98	1.01	1.03	44	0.89	0.91	0.87	0.89	0.90	49
9	1.22	1.24	1.19	1.13	1.19	168	1.10	1.11	1.08	1.01	1.06	129
11	1.08	1.12	1.02	1.04	1.07	71	0.91	0.94	0.88	0.87	0.90	71
2	1.32	1.33	1.37	1.29	1.40	628	0.84	0.85	0.86	0.83	0.90	888
4	1.01	1.08	1.02	1.00	1.05	39	0.83	0.88	0.84	0.83	0.85	52
6	1.29	1.33	1.33	1.20	1.33	93	0.86	0.87	0.95	0.79	1.00	150
8	0.74	0.76	0.75	0.81	0.84	22	0.84	0.87	0.85	0.92	0.95	26
10	1.19	1.21	1.17	1.09	1.16	71	1.03	1.08	1.06	0.98	1.02	65
12	0.95	1.01	0.95	0.96	1.02	30	0.80	0.85	0.80	0.81	0.85	43

[a]Predominant frequency from single and tridem axles using PSD method
[b]Pavement ME
[c]Equivalent frequency by iteration over vertical strains
[d]Full dynamic viscoelastic
[e]Single axle
[f]Tridem axle

4.5 Conclusion

This chapter investigates the frequency characteristics of multiple axle loadings and the accuracy of using one frequency to predict the strain responses induced by different axle configurations. The pavement ME frequency is compared with those from other methods including the centroid of PSD method and the equivalent frequency derived by iteration. Multiple cases in terms of pavement structure, AC layer stiffness, and vehicle speed were simulated using single and multiple axles scenarios. Several conclusions can be drawn as follows:

- The Pavement ME method significantly overestimates the loading frequency near the surface of the AC layer, but the error gradually decreases with depth. This is because Pavement ME uses the wrong frequency-time relationship of "*f = 1/t*" rather than "*f = 1/(2t)*". This error is partially compensated by the overestimation of pulse duration within the AC layer.

- The differences between the predominant frequencies obtained by the centroid of PSD method for single and multiple axles are negligible. The equivalent frequencies developed for multiple axle loadings are smaller than that for single axle loadings by up to 40%, except for very stiff AC layers.
- Even though both the Pavement ME and the centroid of PSD methods yield almost identical frequencies for single and multiple axle configurations, using these frequencies derived from single axle scenarios to predict vertical strain under multiple axle loadings can result in an additional error of up to 5% to 10% near the surface of the AC layer. Errors of vertical strains predicted by the equivalent frequency developed for single axle loading conditions are generally acceptable, except for structures with soft to moderately soft AC materials, where these errors can reach up to 20%.
- The maximum horizontal strains are less sensitive to loading frequency than vertical stains for both single and multiple axles. The accuracy of all loading frequencies in terms of maximum horizontal strain prediction is generally independent of the number of axles but is mainly affected by the AC layer stiffness and vehicle speed.
- The overall behavior of the Pavement ME frequency in the prediction of strain responses under single and multiple axles loadings is similar.
- The equivalent frequency of multiple-axle loading configurations is smaller than that of single-axle loading configurations for AC layers with low to moderate stiffness.

A CORRECTION METHOD FOR THE CURRENT PAVEMENT ME METHODOLOGY IN EQUIVALENT LOADING FREQUENCY CALCULATION

This chapter will present a simple correction method for the current Pavement ME method in loading frequency calculations based on the "centroid of PSD" and the equivalent frequency developed in Chapter 3. The correction procedure is straightforward, computationally efficient, and can be easily implemented in the Pavement ME design software.

5.1 Limitations of the Original Pavement ME Method

The original Pavement ME method transfers the AC layer into an equivalent layer with a different thickness (effective thickness) as a function of the ratio between the AC and subgrade based on the revised Odemark's method as shown in Figure 5.1. Then it assumes the vertical stress pulse propagates linearly at 45 degrees within the transformed AC layer and the pulse width can be calculated by geometry relationships as shown in Figure 5.1 (b). Finally, the frequency is calculated as the reciprocal of the loading time, which is simply equal to the pulse width divided by the vehicle speed. A detailed description of the Pavement ME method is presented in Chapter 3.

In Figure 5.1, if the slope of vertical stress distribution in the original AC layer is defined as $S = h/[(L - 2a_c)/2]$, then it can be mathematically proven that the inverse of this slope, S^{-1} is a linear function of $(Eac / Esg)^{1/3}$ (or S is proportional to $(Esg / E_{AC})^{1/3}$) based on the assumption that the distribution slope is a constant in the transformed AC layer. This relationship will be assumed to be still valid in the correction procedure.

Three major sources of errors are identified in the Pavement ME method based on the analysis in Chapter 3 and Hu et al. (2010). These errors will be addressed in the correction procedure. Firstly, the frequency-time relationship of "$f = 1/(2t)$" should be used, instead of "$f = 1/t$". Secondly, the vertical stress pulse width, which is inversely proportional to the stress distribution slope, is influenced by the ratio between the moduli of the AC layer and the layer immediately beneath it, typically the base layer. Thus, the actual AC and base moduli values, instead of dummy moduli values should be used; and the subgrade modulus E_{sg} in the equation "$(E_{AC} / E_{sg})^{1/3}$" should be replaced by the base modulus E_{Base}. Thirdly, by comparing the vertical stress pulses obtained by the original Pavement ME and the equivalent frequency as

demonstrated in Figure 5.2 and Figure 5.3, it can be found that the Pavement ME method always underestimates the pulse width near the surface of the AC layer.

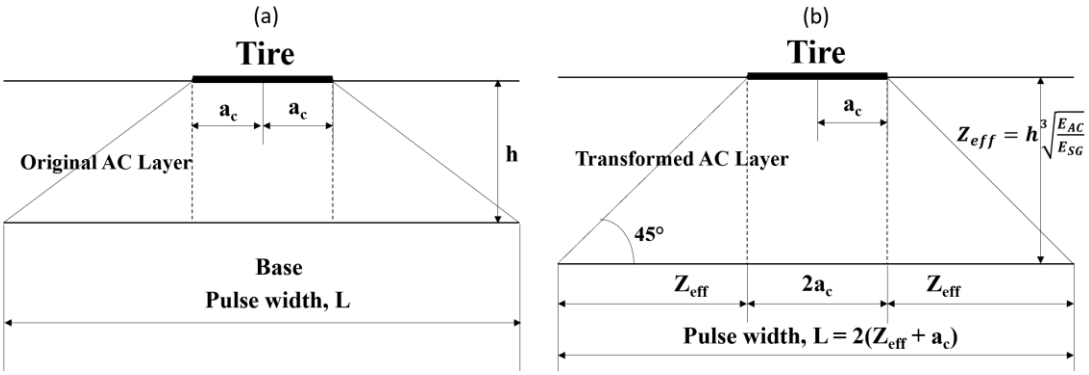

Figure 5.1 Transformation of AC layer based on Odemark's method (a) original AC thickness; (b) transformed AC thickness (adapted from ARA 2001).

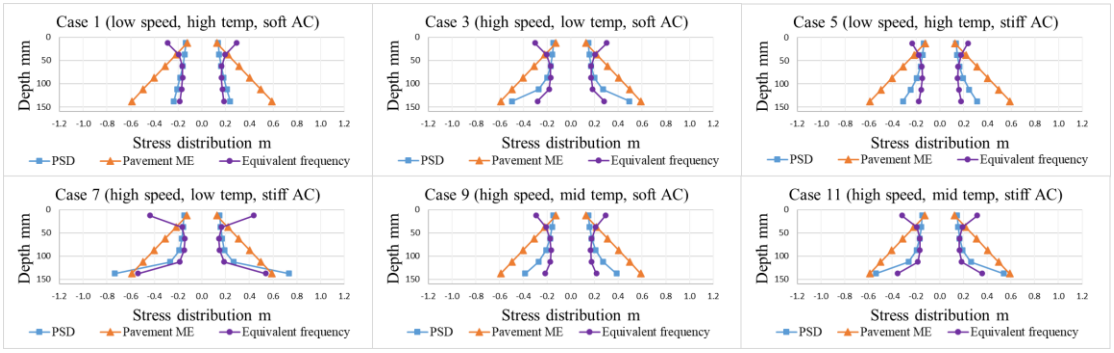

Figure 5.2 Pulse width from Pavement ME and PSD methods – Thin AC layer.

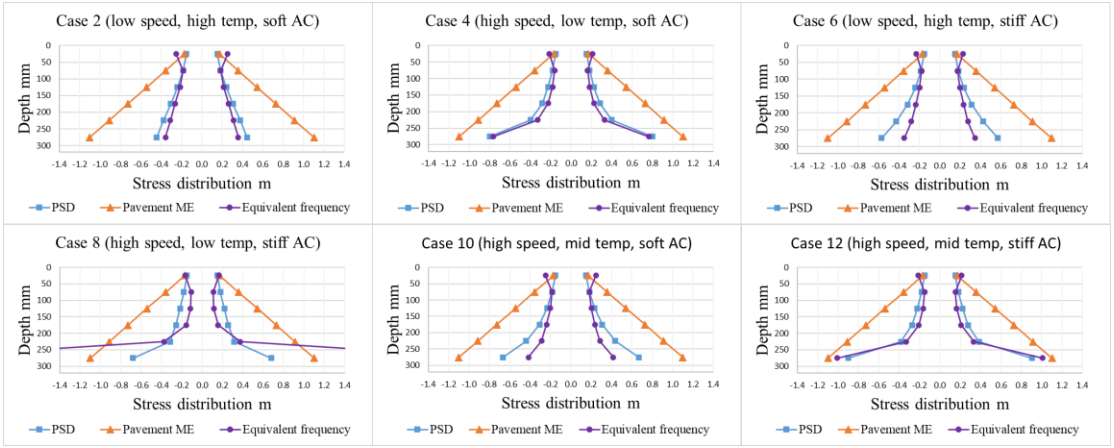

Figure 5.3 Pulse width from Pavement ME and PSD methods – Thick AC layer.

5.2 Correction Procedure

The correction method is based on the pulse duration (or width) of the vertical stress induced by axle

loadings and is accomplished through two phases. In phase one, the predominant frequency method, "centroid of PSD" is used to derive the vertical stress pulse distribution slope along the depth as a function of the ratio between the moduli of the AC layer and the base layer. Then, in phase two, the equivalent frequency presented in Chapters 3 and 4 is employed to correct the pulse width only near the surface of the AC layer. Once the stress pulse width has been accurately calculated at various depths of the AC layer, the pulse duration can be determined by dividing the pulse width by the vehicle speed. Subsequently, the frequency-time relationship given by "*f = 1/(2t)*" is utilized to obtain the loading frequency. According to the analysis provided in Chapter 4, the differences between predominant frequencies for single and multiple axle configurations, as well as the equivalent frequencies near the surface for different axle configurations, are insignificant. Thus, all correction procedures presented in this chapter are based upon single-axle dual-tire scenarios.

Phase I: Correction for Vertical Stress Distribution Slope

In the initial stage of Phase I, the overall distribution slope of the pulse obtained by the "centroid of PSD" method is calculated as if the pulse is propagating linearly from the surface to the bottom of the AC layer. Then, the concave shape of the slope distribution pattern is addressed by reducing the pulse width within the AC layer.

Calculate the slope of the vertical stress pulse distribution:

The "centroid of PSD" method relies on the Fourier Transform to convert the stress pulses from the time domain to the frequency domain and does not calculate pulse duration explicitly, its pulse duration can be estimated by the time-frequency relation of "*f = 1/(2t)*". The loading time and pulse width are calculated by Equations 5.1 and 5.2 respectively:

$$t = \frac{1}{2f} \tag{5.1}$$

$$L = t * V \tag{5.2}$$

where *f* is the loading frequency, *t* is the loading time, *L* is the pulse width, and *V* is the vehicle speed.

As shown in Figure 5.1, the slope of the vertical stress pulse distribution in the untransformed AC layer can be calculated by Equation 5.3:

$$S = \frac{h}{(L_b - L_s)/2} \tag{5.3}$$

where S is the slope of the stress distribution, h the thickness of the AC layer, L_b and L_s are pulse widths at the bottom and surface of the AC layer respectively.

Calculate the elastic modulus of the AC layer:

Because the distribution slope of the vertical stress pulse is influenced by the ratio between the moduli of the AC and base layers, the average elastic modulus of the AC layer needs to be estimated. In Pavement ME, the material properties of the AC layer are characterized by the dynamic modulus sweep data, and the magnitude of the dynamic modulus, which is a function of loading frequency itself and temperature, is used as the elastic modulus of the AC layer. In this correction procedure, the modulus at each sub-layer of the AC layer is computed using the original Pavement ME frequency, and then the average of those moduli is used as the equivalent elastic modulus of the entire AC layer. When calculating the average modulus of the AC layer, the whole layer is modeled as a one-dimensional elastic spring. The average elastic modulus should result in the same total strain when the spring is subjected to identical vertical stress along its length. Based on this logic, the average modulus of the AC layer is calculated by Equation 5.4:

$$E_{AC} = (\frac{1}{h_{AC}} \sum_{1}^{n} h_i \times \frac{1}{E_i})^{-1} \tag{5.4}$$

where: E_{AC} is the average of the entire AC layer, h_{AC} is the thickness of the entire AC layer, h_i is the thickness of each sublayer, n is the number of sublayers, and E_i is the modulus of each sublayer, which is obtained from the dynamic modulus E* master curve as a function temperature and the Pavement ME loading frequency.

Determine the relationship between the "slope" and "$(E_{Base} / E_{AC})^{1/3}$":

As mentioned previously, the vertical stress distribution slope within the untransformed AC layer, S is a linear function of $(Esg / E_{AC})^{1/3}$, where E_{AC} is the AC modulus, and E_{sg} is the subgrade modulus. This relation is also valid when E_{sg} is replaced by the base modulus, E_{Base}.

The necessary information obtained from the "centroid of PSD" frequencies for the development of the slope of the vertical stress pulse distribution as a function of the modulus ratio between the AC and the base layer is summarized in Table 5.1. The relationship between the vertical stress distribution slope and

$(E_{Base} / E_{AC})^{1/3}$ is shown in Figure 5.4 and Equation 5.5. As anticipated, a linear relationship is observed between the two quantities. In Figure 5.4, some data points deviate from the trendline when the $(E_{Base} / E_{AC})^{1/3}$ are minimum and maximum. These data points are extreme cases where AC layers are either unrealistically soft and would not be used for design or very stiff, in which the strains are too small to cause damage. In Figure 5.4, the intersection of the linear trendline is forced to zero. Because when $(E_{Base} / E_{AC})^{1/3}$ tends to zero, which means the AC layer is extremely stiff. In such a scenario, the slope should be close to zero because the vertical stress distribution along the depth is very flat as demonstrated in Figure 5.5.

Table 5.1 Summary of information for stress pulses obtained by the "centroid of PSD" method.

Case #	AC thickness, in	AC modulus, psi	Base modulus, psi	$\sqrt[3]{\frac{E_{Base}}{E_{AC}}}$	Slope
1	6	23,778	30,000	1.081	1.233
3	6	728,091	30,000	0.345	0.361
5	6	109,978	30,000	0.649	0.709
7	6	2,240,852	30,000	0.237	0.310
9	6	224,256	30,000	0.511	0.529
11	6	1,156,023	30,000	0.296	0.320
2	12	20,526	30,000	1.135	0.853
4	12	627,803	30,000	0.363	0.386
6	12	85,857	30,000	0.704	0.596
8	12	2,100,188	30,000	0.243	0.474
10	12	184,481	30,000	0.546	0.485
12	12	1,011,485	30,000	0.310	0.333

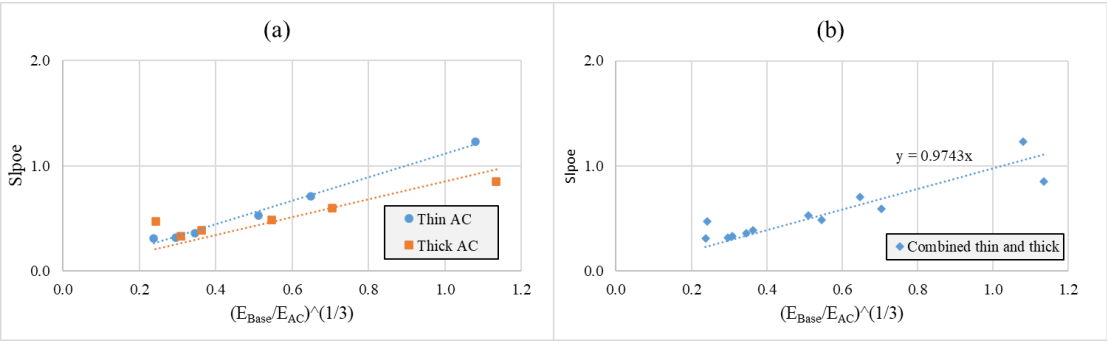

Figure 5.4 Vertical stress pulse distribution slope verse the ratio between AC and base moduli (a) separate thin and thick AC layers; (b) combined thin and thick AC layers.

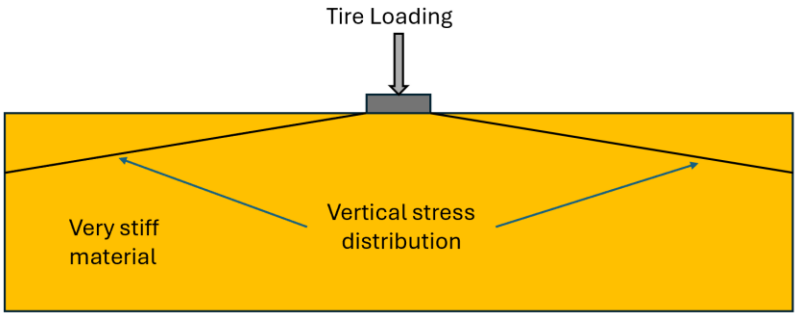

Figure 5.5 Vertical stress distribution in extremely stiff materials.

Generalize the relationship between the "slope" and "$(E_{Base} / E_{AC})^{1/3}$":

It should be noted that the relationship demonstrated in Figure 5.4 and Equation 5.5 is based on the base layer modulus of 30,000 psi only. To generalize this relationship, an additional 24 hypothetical cases with varying AC and base moduli have been generated. The new analysis uses the same structure subjecting to single axle loadings (thin and thick) as the previous 12 cases. The range of elastic moduli for the AC and base layers is sufficiently broad to cover the most realistic design scenarios. The detailed combination of the 24 cases is listed in Table 5.2. The vertical stress pulses obtained by the "centroid of PSD" method for the new 24 cases (cases 13 to 36) are shown in Figure 5.6. A similar analysis to that presented in Table 5.1 and Figure 5.4 has been conducted for cases 13 to 36, with the corresponding results displayed in Table 5.3 and Figures 7 to 8. From Figure 5.4 and Figure 5.7, it is evident that the relationship between "slope" and "(E_{Base}/E_{AC}) ^ (1/3)" is consistent across scenarios with varying base layer moduli, in that all coefficients of linear trendlines for these scenarios are close to "1". Additionally, the trendline for the combined newly created 24 cases is plotted in Figure 5.8. Given that the relationship between "slope" and "(E_{Base}/E_{AC}) ^ (1/3)" is independent of the base layer modulus, Equation 5.5 remains valid for a base layer modulus other than 30,000 psi. In this context, the constant coefficient in Equation 5.5 is replaced by "1," resulting in the final relationship between "(E_{Base}/E_{AC}) ^ (1/3)" as presented in Equation 5.6.

Table 5.2 Table 2. Summary of simulation conditions of the new 24 cases.

Target Speed	50 mph (80 km/h)
AC thickness	6 inch (152 mm), 12 inch (305 mm)
AC moduli	50,000 psi, 100,000 psi, 500,000 psi, 1,000,000 psi
Base moduli	10,000 psi, 50,000 psi, 100,000 psi

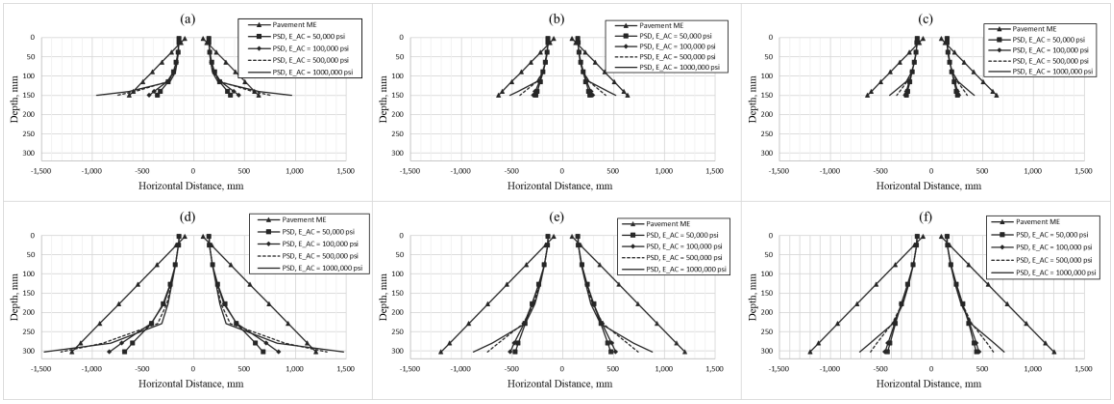

Figure 5.6 Vertical stress distribution alone depth (a) Thin AC, base modulus = 10,000 psi; (b) Thin AC, base modulus = 50,000 psi; (c) Thin AC, base modulus = 100,000 psi; (d) Thick AC, base modulus = 10,000 psi; (e) Thick AC, base modulus = 50,000 psi.

Table 5.3 Summary of information for stress pulses obtained by the "centroid of PSD" method for the new 24 cases.

Case #	AC thickness, in	AC modulus, psi	Base modulus, psi	$\sqrt[3]{\frac{E_{Base}}{E_{AC}}}$	Slope
13	6	50,000	10,000	0.585	0.688
15	6	100,000	10,000	0.464	0.501
17	6	500,000	10,000	0.271	0.241
19	6	1,000,000	10,000	0.215	0.181
21	6	50,000	50,000	0.585	1.241
23	6	100,000	50,000	0.464	1.022
25	6	500,000	50,000	0.271	0.535
27	6	1,000,000	50,000	0.215	0.393
29	6	50,000	100,000	1.000	1.423
31	6	100,000	100,000	0.794	1.251
33	6	500,000	100,000	0.464	0.738
35	6	1,000,000	100,000	0.368	0.548
14	12	50,000	10,000	1.000	0.562
16	12	100,000	10,000	0.794	0.437
18	12	500,000	10,000	0.464	0.258
20	12	1,000,000	10,000	0.368	0.226
22	12	50,000	50,000	1.260	0.925
24	12	100,000	50,000	1.000	0.806
26	12	500,000	50,000	0.585	0.504
28	12	1,000,000	50,000	0.464	0.408
30	12	50,000	100,000	1.260	1.030
32	12	100,000	100,000	1.000	0.949
34	12	500,000	100,000	0.585	0.655
36	12	1,000,000	100,000	0.464	0.533

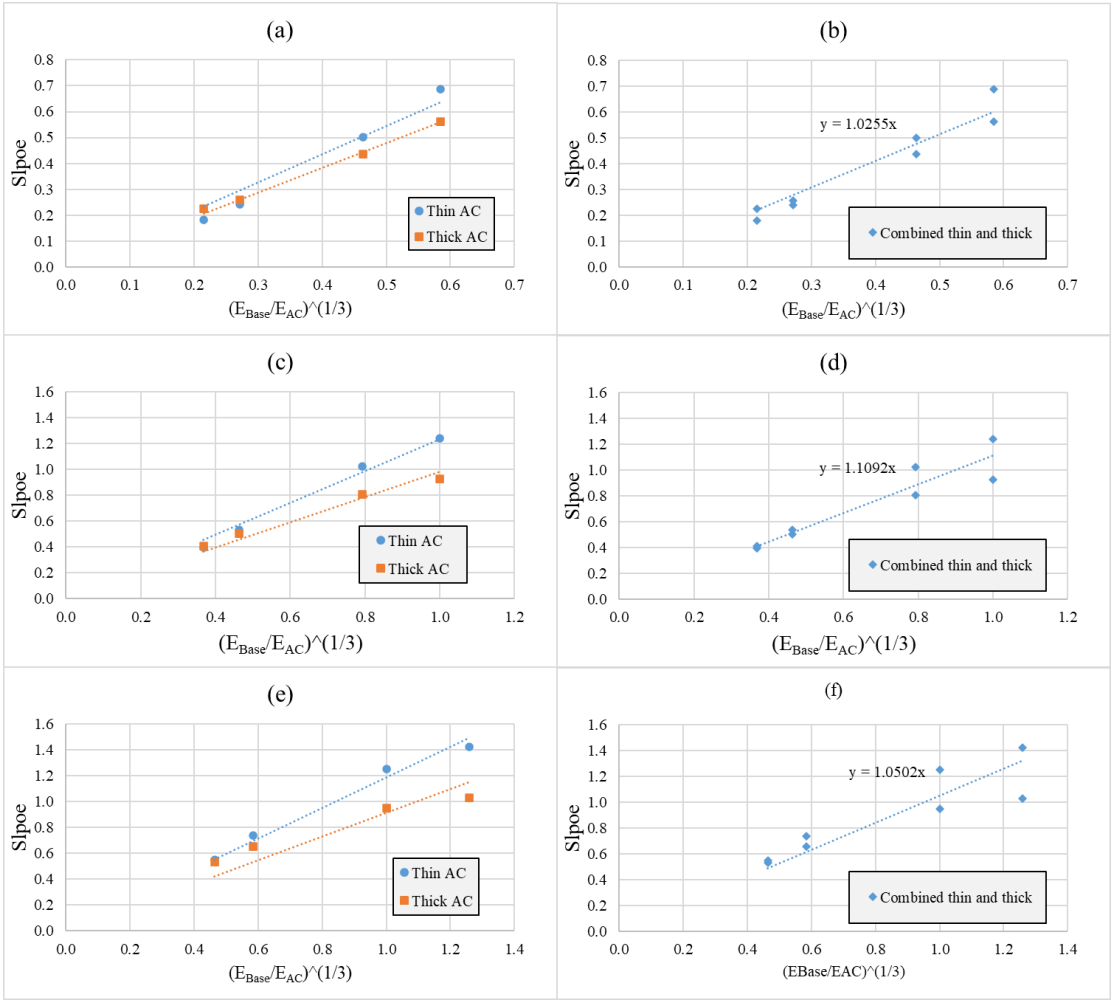

Figure 5.7 Vertical stress pulse distribution slope versus the ratio between AC and base moduli (a) base modulus = 50,000 psi, separate thin and thick AC layer; (b) base modulus = 50,000 psi, combined thin and thick AC layer; (c) base modulus = 100,000 psi, separate thin and thick AC layer; (d) base modulus = 100,000 psi, combined thin and thick AC layer; (e) base modulus = 500,000 psi, separate thin and thick AC layer; (f) base modulus = 500,000 psi, combined thin and thick AC layer.

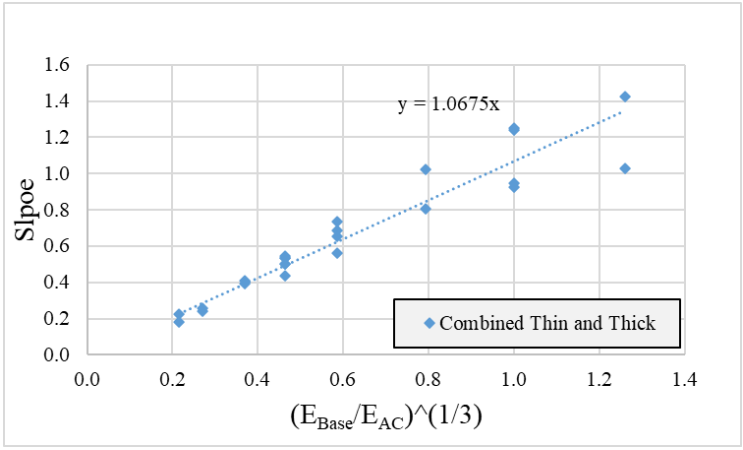

Figure 5.8 Vertical stress pulse distribution slope versus the ratio between AC and base moduli (combined cases 13 to 36).

$$Slope = \frac{1}{\left(\sqrt[3]{\frac{E_{AC}}{E_{base}}}\right)} \tag{5.6}$$

Correct the pulse width for the Pavement ME method:

Based on the geometric relations illustrated in Figure 5.1 (a), and the linear relationships between the stress pulse distribution slope and modulus ratio as depicted in Figure 5.4 and Equation 5.6, the vertical stress pulse width at any depth within the AC layer can be calculated using Equation 5.7:

$$L = 2\left(\frac{h}{Slope} + a_c\right) \tag{5.7}$$

where h is the depth of interest, L is the pulse width at the depth of h, and a_c is the radius of the tire footprint.

The pulse width calculated by Equations 5.6 and 5.7 will agree with that of the “centroid of PSD” method only at the surface and the bottom of the AC layer. This is because these equations assume linear pulse propagation along the depth, whereas the pulse distribution shape of the "centroid of PSD" method exhibits a concave profile, as depicted in Figure 5.2, Figure 5.3, and Figure 5.6 , and will be addressed in the second stage of Phase I.

By observing Figure 5.2, Figure 5.3, and Figure 5.6, it can be found that the stress pulse distribution, as determined by the “centroid of PSD” method, can be approximately segmented into two sections along

the depth within the AC layer. In the first section, the pulse exhibits an approximately linear distribution from the surface of the AC layer at a large slope (steep). Subsequently, in the second section, the slope abruptly flattens as it approaches the bottom of the AC layer. The boundary between the two sections, identified as the inflection point of the slope, is observed at a depth of approximately 4.5 inches in thin AC layers (6 inches) and at a depth of 6 inches in thick AC layers (12 inches). This means that the boundary between the two sections always occurs at a depth of 75% of the AC layer thickness regardless of pavement structures. Considering this fact, the pulse width calculated using a uniform slope (Equation 5.7) will be further refined by applying distinct slopes for the top 75% and the remaining 25% of the AC layer, respectively.

According to Figure 5.2, Figure 5.3, and Figure 5.6, the reduction in pulse width by the "centroid of PSD" method at a depth corresponding to 75% of the AC layer thickness is also influenced by the moduli of both the AC and base layers. Figure 5.9 shows that the ratio between pulse widths of the "centroid of PSD" method and pulse widths calculated by uniform slopes at a depth of 75% of the AC layer thickness is also a linear function of "(E_{Base}/E_{AC}) ^ (1/3)". According to the analysis presented in Figure 5.9, this ratio can be determined using Equation 5.8:

$$R_{75} = 1.35 \times \sqrt[3]{\frac{E_{Base}}{E_{AC}}} \tag{5.8}$$

where R_{75} is the ratio between the pulse width of the "centroid of PSD" method and the pulse width calculated by uniform slopes at a depth of 75% of the AC layer thickness. Once R_{75} is obtained, the stress pulse distribution slopes and the corresponding pulse widths for the two sections of the AC layers can be determined using Equations 5.9 to 5.12:

$$Slope_1 = \frac{Slope}{R_{75}} = 0.741 \tag{5.9}$$

$$Slope_2 = \frac{0.25}{1/Slope - 0.75/Slope_1} \tag{5.10}$$

$$L_1 = 2 \times (\frac{h}{Slope_1} + a_c) \tag{5.11}$$

$$L_2 = 2 \times \left(\frac{h - 0.75h_{AC}}{Slope_2} + \frac{0.75h_{AC}}{Slope_1} + a_c\right) \quad (5.12)$$

where *Slope* is the uniform stress pulse distribution slope obtained from Equation 5.6; $Slope_1$ and $Slope_2$ are stress pulse distribution slopes within the top 75% and the remaining 25% of the AC layer, respectively; h is the depth of interest; h_{ac} is the thickness of the AC layer; ac is the radius of the tire footprint; and L_1 and L_2 are the pulse width slope of within the top 75% and the remaining 25% of the AC layer, respectively.

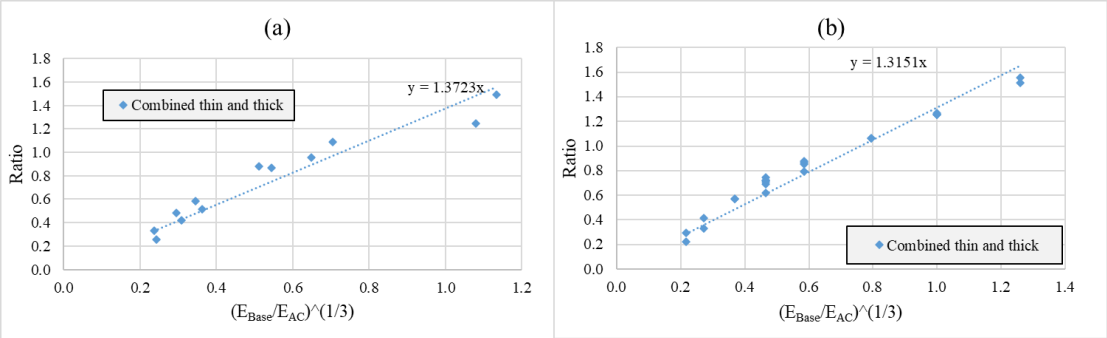

Figure 5.9 Ratios between pulse widths of the "centroid of PSD" method and pulse widths calculated by uniform slopes at a depth of 75% of the AC layer thickness (a) cases 1 to 12; (b) cases 13 to 36.

Phase II: Correction for the stress pulse near the surface of the AC layer

Phase II of the correction procedure will be focused on the vertical pulse width near the surface using the "equivalent frequency" developed in Chapters 3 and 4 as a reference. Because the "equivalent frequency" is obtained by recursive procedure and is backcalculated from vertical strains obtained via dynamic viscoelastic analysis for cases 1 to 12, it is regarded as the "truth".

Although the "centroid of PSD" method generally aligns with the "equivalent frequency" at most locations within the AC layer, it markedly underestimates the pulse width near the AC surface. By examining Figure 5.2 and Figure 5.3, it is evident that the pulse width derived from the "equivalent frequency" method is substantially broader than that obtained via the "centroid of PSD" method at the AC surface. However, this discrepancy diminishes progressively with increasing depth, and the pulse widths determined by these two methods tend to converge at a depth of approximately 2.5 inches regardless of pavement structures. Based on this observation, the pulse width corrected from Phase I can be further refined by applying correction factors specifically to the top 2.5 inches of the AC layer.

The pulse width calculated by Equation 5.11 in Phase I equals the diameter of the tire-pavement contact footprint. The correction factor is defined as the difference between pulse widths obtained by the "equivalent frequency" method and Equation 5.1 divided by the diameter of the tire-pavement contact footprint as demonstrated in Equivalent 5.13:

$$CF = (L_e - L_1)/(2 \times a_c) \tag{5.13}$$

where CF is the correction factor, L_e is the pulse width determined by the "equivalent frequency", L_1 is the pulse width determined by Equation 11, and a_c is the radius of the tire-pavement contact footprint. The correction factor is at its maximum at the AC surface (depth = 0) and decreases linearly until it reaches zero at a depth of 2.5 inches. The maximum correction factor is also affected by the modulus of the AC layer, though it exhibits significantly less sensitivity compared to the pulse distribution slope. Figure 5.10 illustrates an approximate linear correlation between the maximum correction factor and the logarithm of the modulus of the AC layer. The correction factor, within the top 2.5 inches of the AC layer can be calculated by Equations 5.14 and 5.15:

$$CF_{max} = 0.62 \times \log(E_{AC}) \tag{5.14}$$

$$CF = \frac{-CF_{max}}{2.5} h + CF_{max} \tag{5.15}$$

where CF_{max} is the correction factor at the surface of the AC layer (depth = 0), E_{AC} is the average modulus of the AC layer obtained by Equation 5.4, h is the depth of interest, and CF is the correction factor (CF = 0 when h > 2.5 inches).

By applying the correction factor, the pulse width of the corrected Pavement ME frequency method is determined by Equation 5.16:

$$L_{corrected} = L_i + CF \times 2a_c \tag{5.16}$$

where $L_{corrected}$ is the pulse width of the corrected Pavement ME frequency method, L_i (i = 1, 2) is the pulse width calculated by Equations 5.11 or 5.12. Finally, the loading frequency of the corrected Pavement ME method is calculated by Equation 5.17 based on the time-frequency relationship of "f = 1/(2t)":

$$f_{corrected} = \frac{1}{2 \times L_{correct}/V} \tag{5.17}$$

where V is the vehicle speed.

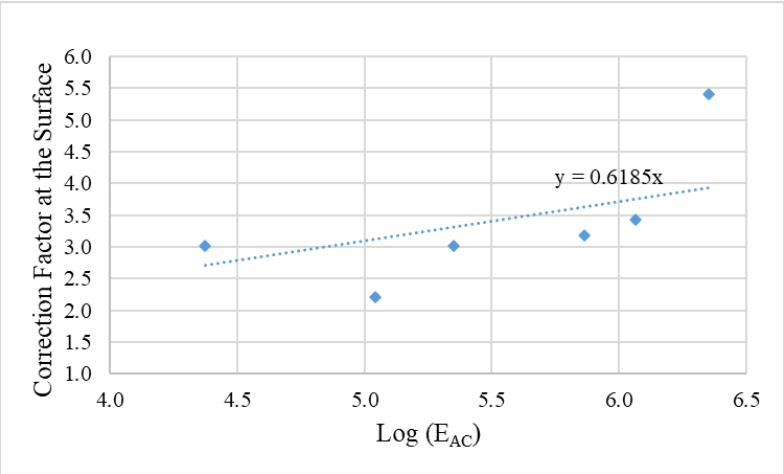

Figure 5.10 Correction factor at the AC surface for different AC moduli.

5.3 Summary of the calculation procedure for the corrected Pavement ME method

Step 1: Calculate the average modulus of the AC layer using Equation 5.4.

Step 2: Calculate the uniform slope of the vertical stress pulse distribution using Equation 5.6.

Step 3: Calculate the pulse distribution slopes for the top 75% of and remaining 25% of the AC layer respectively using Equations 5.9 and 5.10.

Step 4: Calculate the pulse width for the top 75% of and remaining 25% of the AC layer respectively using Equations 5.11 and 5.12.

Step 5: Calculate the correction factor for the top 2.5 inches of the AC layer using Equations 5.14 and 5.15.

Step 6: Calculate the pulse width of the corrected Pavement ME method using Equation 5.16.

Step 7: Calculate the corrected loading frequency using Equation 5.17.

5.4 Verification of the corrected Pavement ME loading frequency

In this section, the correction method for Pavement ME loading frequency developed in previous sections of this chapter is verified with several realistic cases. This verification is accomplished through a comparative analysis of pulse widths and loading frequencies calculated by the corrected method and the "equivalent frequency." Additionally, it involves comparing the critical strains predicted by the corrected method with those obtained through dynamic viscoelastic analysis.

Figure 5.11 and Figure 5.12 present the pulse widths and loading frequencies calculated using various methods for cases 9 to 12. These cases encompass combinations of thin and thick asphalt concrete layers

with both soft and stiff binders, all at the temperature of 25 degrees Celsius. It is evident that both the pulse width and loading frequency computed by the corrected Pavement ME method exhibit significantly better agreement with the "equivalent frequency" compared to those determined by the original Pavement ME method.

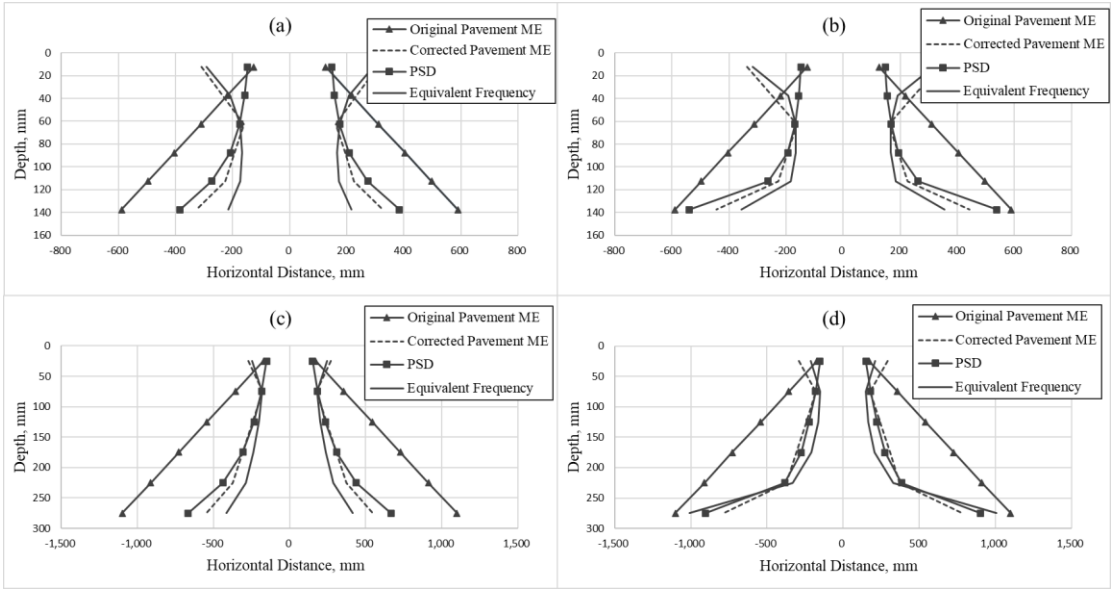

Figure 5.11 Comparison of pulse width before and after correction (a) case 9, soft binder; (b) case 11, stiff binder; (c) case 10, soft binder; (d) case 12, stiff binder.

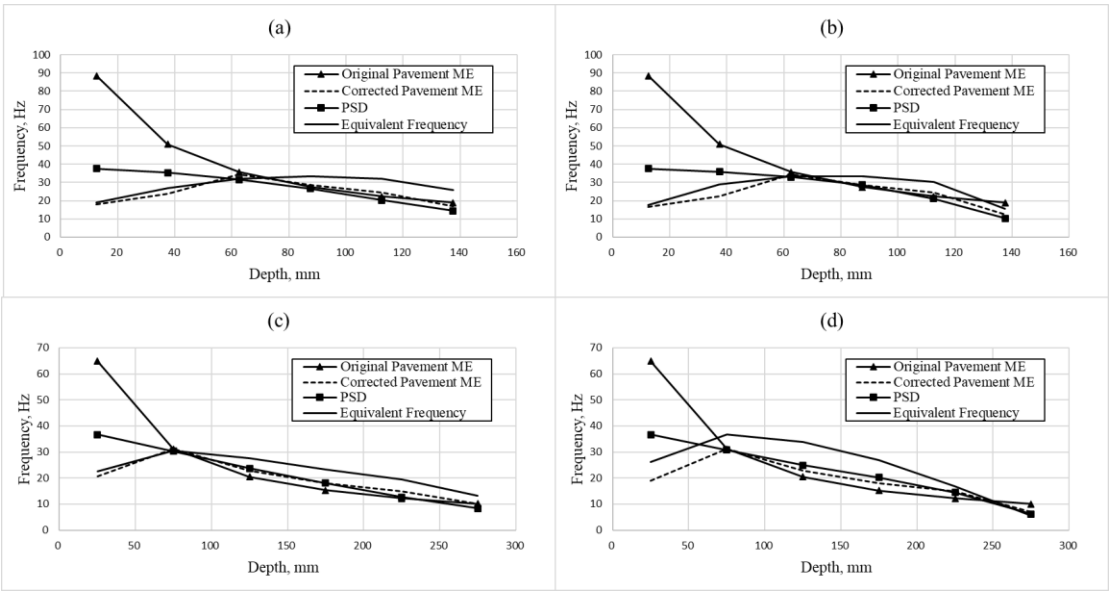

Figure 5.12 Comparison of frequency before and after correction (a) case 9, soft binder; (b) case 11, stiff binder; (c) case 10, soft binder; (d) case 12, stiff binder.

The corrected Pavement ME method is also employed to predict critical strains using linear elastic analysis, and these predicted strains are then compared with those derived from dynamic viscoelastic analysis. The simulation scenario involves three hypothetical pavement structures situated in the climate conditions of East Lansing, Traverse City, and Detroit, Michigan. These structures comprise AC layers with different thicknesses (8-inch, 6-inch, and 12-inch) subjected to a 36-kip tandem-axle load traveling at a speed of 60 miles per hour. The PG grade and aggregate gradation of the AC material for these pavement structures are 64-28 and 4E10, 58-28 and 3E3, and 64-28 and 3E30, respectively. Detailed dynamic modulus and phase angle data for these AC materials can be found in Appendix A. For this analysis, two temperature quintiles (shown in Table 5.4 to Table 5.6) from the month of July have been selected for each pavement structure, as July is the hottest month of the year and represents the most critical conditions for pavement response.

Table 5.4 Pavement temperature gradient of two quintiles in July for East Lansing, Michigan.

Depth in	Quintile 1 of July		Quintile 5 of July	
	Fahrenheit	Celsius	Fahrenheit	Celsius
0.50	63.9	17.7	103.3	39.6
1.50	67.3	19.6	99.5	37.5
2.50	69.8	21.0	96.5	35.9
3.50	71.7	22.1	94.3	34.6
4.50	72.9	22.7	92.7	33.7
5.50	73.8	23.2	91.5	33.1
7.00	74.5	23.6	90.3	32.4

Table 5.5 Pavement temperature gradient of two quintiles in July for Traverse City, Michigan.

Depth in	Quintile 1 of July		Quintile 5 of July	
	Fahrenheit	Celsius	Fahrenheit	Celsius
0.50	60.5	15.8	100.2	37.9
1.50	63.9	17.7	96.4	35.8
2.50	66.6	19.2	93.3	34.1
3.50	68.6	20.3	90.9	32.7
4.50	70.1	21.2	89.0	31.6
5.50	71.3	21.8	87.4	30.8

Table 5.6 Pavement temperature gradient of two quintiles in July for Detroit, Michigan.

Depth in	Quintile 1 of July		Quintile 5 of July	
	Fahrenheit	Celsius	Fahrenheit	Celsius
0.50	67.7	19.8	106.5	41.4
1.50	71.0	21.6	102.8	39.3
3.00	74.5	23.6	98.6	37.0
5.00	77.5	25.3	94.7	34.8
7.00	79.1	26.2	92.1	33.4
9.00	80.0	26.7	90.4	32.4
11.00	80.4	26.9	89.1	31.7

The vertical strains within the asphalt concrete (AC) layer and the maximum horizontal strains at the bottom of the AC layer, as predicted by both the original and corrected Pavement ME, as well as the dynamic viscoelastic analysis, are presented in Table 5.7 to Table 5.9 and Figure 5.13, respectively. The corrected Pavement ME method significantly enhanced the prediction of vertical strain at the shallow depth of the AC layer, demonstrating strong agreement with the results of viscoelastic analysis within Quintile 5

(highest temperature) for all three pavement structures. In Temperature Quintile 1, where strain values are small and discrepancies among different methods are insignificant, the corrected Pavement ME demonstrates slightly better performance than the original version at the surface and bottom of the AC layer. The disparity between the maximum horizontal tensile strains obtained by these methods is significantly smaller compared to that of vertical strains. The maximum horizontal strains at the bottom of the AC layers predicted by the corrected Pavement ME frequency agree well with and are slightly higher than (by 17%, on the conservative side) those predicted by the dynamic viscoelastic analysis for the thin AC layer (6-inch) and the medium AC layer (8-inch), respectively (Table 5.7 and Table 5.8). For the structure with a thick AC layer (12-inch), the corrected frequency method still underestimates the maximum horizontal strains at the bottom of the AC layer by up to 15% (Table 5.9). However, these strain values are so small that they do not pose any concern from a design perspective. The improvement achieved by the corrected Pavement ME method in predicting maximum horizontal strains is more evident in Temperature Quintile 5 of July, where the strain values reach the highest within a year.

Table 5.7 Horizontal strains at the bottom of the AC layer for the structure in East Lansing climate.

Methods	Temperature Quintile 1 of July		Temperature Quintile 5 of July	
	Epsilon xx (με)	Epsilon yy (με)	Epsilon xx (με)	Epsilon yy (με)
Original Pavement ME	-59.1	-57.2	-93.7	-80.5
Corrected Pavement ME	-62.1	-59.3	-99.0	-92.2
Dynamic viscoelastic	-69.5	-59.8	-98.3	-84.3

Table 5.8 Horizontal strains at the bottom of the AC layer for the structure in Traverse City climate.

Methods	Temperature Quintile 1 of July		Temperature Quintile 5 of July	
	Epsilon xx (με)	Epsilon yy (με)	Epsilon xx (με)	Epsilon yy (με)
Original Pavement ME	-100.3	-82.1	-168.8	-122.1
Corrected Pavement ME	-107.5	-86.0	-177.4	-125.3
Dynamic viscoelastic	-106.0	-90.5	-151.2	-126.0

Table 5.9 Horizontal strains at the bottom of the AC layer for the structure in Detroit climate.

Methods	Temperature Quintile 1 of July		Temperature Quintile 5 of July	
	Epsilon xx (με)	Epsilon yy (με)	Epsilon xx (με)	Epsilon yy (με)
Original Pavement ME	-41.1	-43.8	-60.3	-58.3
Corrected Pavement ME	-42.7	-45.1	-62.3	-59.4
Dynamic viscoelastic	-58.9	-45.5	-72.9	-61.3

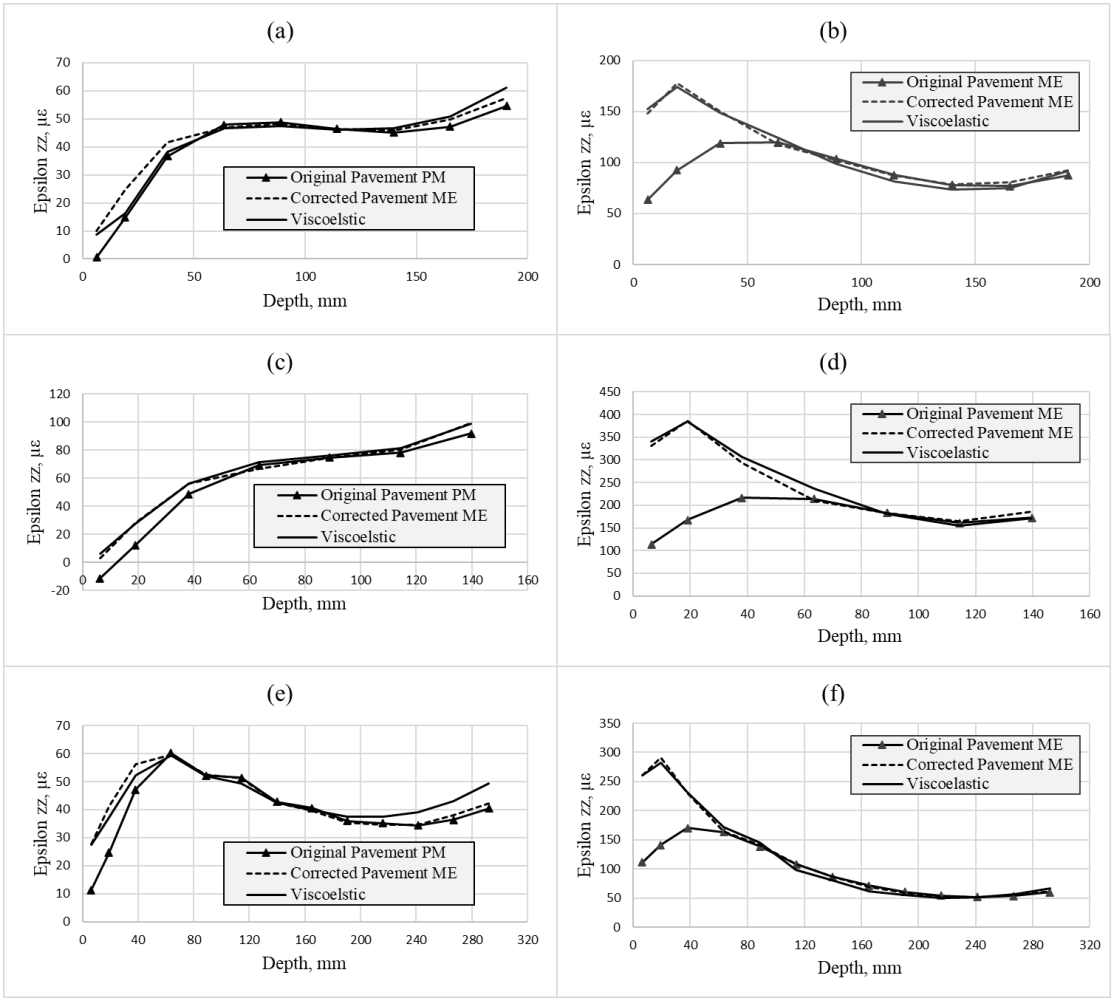

Figure 5.13 Vertical strains predicted by different methods (a) quintile 1 of July for East Lansing climate; (b) quintile 5 of July for East Lansing climate; (c) quintile 1 of July for Traverse City climate; (d) quintile 5 of July for Traverse City climate; (e) quintile 1 of July for Detroit climate; (f) quintile 5 of July for Detroit climate.

IMPACT OF AXLE LOADING FREQUENCIES ON LONG-TERM PAVEMENT DISTRESS PREDICTION

6.1 Introduction

The research presented in Chapters 3 and 4 indicates that the current Pavement ME method significantly overestimates loading frequencies near the surface of the asphalt concrete (AC) layer, but the errors gradually decrease with greater depth. As a result, vertical strains were underestimated near the surface with errors of 50% to 70% depending on pavement conditions and axle configuration, while the calculated maximum tensile strains were reasonable (errors within 15%). The correction method for Pavement ME loading frequency calculation developed in Chapter 5 exhibits robust performance in predicting critical strain. Notably, it addresses the limitation of the original Pavement ME frequency, which tends to significantly underestimate the vertical strain near the AC surface.

In this chapter, the effect of loading frequencies on the prediction of long-term pavement distress is analyzed. Four pavement structures, based on actual freeway designs in Michigan are selected to examine the effects of loading frequencies on long-term (20-year) pavement distress prediction using the mechanistic-empirical pavement analysis (MEAPA) software.

6.2 MEAPA

MEAPA is a web-based pavement design application developed at Michigan State University. The engine of the software implements the original formulations of the Pavement ME methodology with a few improvements and simplifications on the climatic model and improvements on the top-down cracking model (Kutay and Lanotte, 2020; Ghazavi et al, 2020; Ghazavi et al. 2022).

The AC rutting prediction model used by MEAPA is based on the vertical compressive strain and temperature of the AC layer. Equation 6.1 is used to calculate the rutting (Ayres Jr and Witczak, 1998; Kaloush and Witczak, 2000; Leahy, 1989), and the default values provided by MEAPA for coefficients of the transfer function are utilized for this analysis:

$$\Delta_{p(HMA)} = \varepsilon_{p(HMA)} h_{HMA} = \beta_{1r} k_z \varepsilon_{r(HMA)} 10^{k_{1r}} n^{k_{2r}\beta_{2r}} T^{k_{3r}\beta_{3r}} \quad (6.1)$$

where:

$\Delta_{p(HMA)}$ = Accumulated permanent or plastic vertical deformation in the HMA layer/sub-layer,

in.

$\varepsilon_{p(HMA)}$ = Accumulated permanent or plastic vertical axial strain in the HMA layer/sub-layer, in.

$\varepsilon_{r(HMA)}$ = Resilient or elastic strain calculated by the structural responses model at the mid-depth of each HMA sub-layer, in.

h_{HMA} = Thickness of the HMA layer/sub-layer, in.

n = Number of axle load repetitions.

T = Mix or pavement temperature, °F.

k_z = Depth confinement factor. ($k_z = k_1$ below – Page 3.3.49 in MEPDG formulation)

$$k_1 = (C_1 + C_2 * depth) * 0.328196^{depth}$$

$$C_1 = -0.1039 * h_{ac}^2 + 2.4868 * h_{ac} - 17.342$$

$$C_2 = -0.0172 * h_{ac}^2 - 1.7331 * h_{ac} + 27.428$$

k_1 = function of total asphalt layers thickness (h_{ac}, in) and depth (depth, in) to computational point, to correct for the confining pressure at different depths.

$k_{1r,2r,3r}$ = Global field calibration parameters (k_{1r} = -2.45, $k2_r$ = 3.01, $k3_r$ = 0.22)

$\beta_{1r}, \beta_{2r}, \beta_{3r}$ = Local or mixture field calibration constants (β_{1r} = 0.4, β_{2r} = 0.52, and β_{3r} = 1.36)

The bottom-up fatigue cracking used by MEAPA is based on the traditional fatigue life formulation, Miner's law of linear damage growth, and transfer functions converting damage to observed fatigue cracking in the field. The material-level traditional fatigue life formulation used by MEAPA is described through Equations 6.2 to 6.5 (NCHRP 2004), and the coefficients of the bottom-up fatigue cracking transfer function, recalibrated for Michigan as developed by Haider et al. (2023), are utilized in this analysis:

$$N_f = C_h C \beta_{f1} k_{f1} (\frac{1}{\varepsilon_t})^{\beta_{f2} k_{f2}} (\frac{1}{E})^{\beta_{f3} k_{f3}} \quad (6.2)$$

$$C = 10^{4.84(\frac{v_{be}}{v_a + v_{be}} - 0.69)} \quad (6.3)$$

$$C_{H-bu} = (b_{bu1} + \frac{b_{bu2}}{1 + e^{(b_{bu3} - b_{bu4} h_{ac})}})^{-1} \quad (6.4)$$

where:

ε_t = Tensile strain at the bottom of AC.

N_f = Number of cycles to failure, for bottom-up cracks.

k_{f1}, k_{f2}, k_{f3} = Global field calibration parameters (k_{f1} = 3.75, k_{f2} = 2.87, and k_{f3} = 1.46).

$\beta_{f1}, \beta_{f2}, \beta_{f3}$ = Local or mixture-specific field calibration constants (β_{f1} = 0.0202, β_{f2} = 1.38, β_{f3} = 0.88).

h_{ac} = Height of the AC layer.

b_{bui} = Coefficients: b_{bu1} = 0.000398, b_{bu2} = 0.003602, b_{bu3} = 11.02, b_{bu4} = 3.49

E = Equivalent modulus of bottom layer (at the given temperature/frequency)

v_{be} = Effective asphalt content by volume, %.

v_a = Percent air voids in the HMA mixture, %

$$FC_{bottom-up}(t) = (\frac{1}{60})(\frac{C_{4-bu}}{1 + e^{(C_{1-bu} * C_1^* + C_{2-bu}^* \log(D_{cum}(t)))}}) \quad (6.5)$$

where:

$FC_{bottom-up}(t)$ = Area of alligator cracking that initiates at the bottom of the HMA layers, percent of total lane area.

$D_{cum}(t)$ = Cumulative damage at the bottom of the HMA layers.

C_{i-bu} = Transfer function regression constants (local calibration for Michigan, Haider et. al., 2023); $C_{4\text{-}bu}$ = 6,000; $C_{1\text{-}bu}$ = 0.25; and $C_{2\text{-}bu}$ = 0.27

C_1^* = $-2 * C_2^*$

C_2^* = $-2.40874 - 39.748(1 + h_{ac})^{-2.856}$

The top-down fatigue model utilized by MEAPA is the same as the bottom-up fatigue cracking model described in Equations 6.2 to 6.5, with the exception that the tensile strain at the bottom of the AC layer in Equation 6.2 is substituted with the maximum principal tensile strain within the top 0.5 inches of the AC surface layer, and several coefficients are adjusted accordingly. The analysis in this chapter employs the default coefficient values for the transfer function as provided by MEAPA.

6.3 Simulation Conditions

Four pavement structures, created based on real freeway designs in Michigan, featuring varying asphalt concrete (AC) layer thicknesses, temperatures, and traffic volumes, were selected for analysis.

Detailed information on these four pavement structures is summarized in Table 6.1. The dynamic modulus and phase angle for the HMA materials listed in Table 6.1 are reported in Appendix A.

A standard tandem axle (36 kips) is used as the traffic loading for all simulation cases because the tandem axle is the dominant axle type among heavy vehicles. Detailed information on axle loadings is presented in Table 6.2. According to the Comprehensive Truck Size and Weight (TS&W) Study (FHWA, 1995), a 34-kip tandem axle has an equivalent single axle load (ESAL) value of 1.1 on flexible pavement. Applying the fourth power law, the ESAL value for a 36-kip tandem axle is approximately 1.38. Then, the equivalent number of repetitions of tandem axle per day can be calculated as ESALs per day divided by 1.38 as presented in Table 6.2.

The MEAPA climate model addresses the temporal variation of pavement temperatures by delineating five temperature quintiles for each month, with Quintile 1 representing the lowest temperatures and Quintile 5 representing the highest temperatures within the given month. The temperatures estimated by MEAPA exhibited fluctuations over the years; however, the overall variation remained relatively minor. The average temperature for each quintile over a 20-year period is utilized to represent that quintile. These 60 distinct temperature quintiles for each pavement structure are then employed to calculate loading frequencies.

Because the original Pavement ME frequency is only a function of vehicle speed and the AC layer thickness, this frequency is identical in all temperature quintiles for a certain pavement structure. However, the calculation of the corrected Pavement ME method incorporates the modulus of the AC layer, which is dependent on temperature. Both the original and corrected Pavement ME loading frequencies for all structures can be found in Appendix B. Consequently, the frequency values of the corrected method vary for each temperature quintile. Table 6.3 presents an example of the pavement temperature gradient and loading frequencies for I-94, specifically for Temperature Quintile 1 in January and Temperature Quintile 5 in July. Detailed pavement temperatures for all structures are presented in Appendix B.

Table 6.1 Summary of design information of pavement structures.

Roadway	BL-I-94	US-127	US-131	I-94
Region	Metro	Bay	North	Metro
Climate	Detroit	Lansing	Traverse City	Detroit
HMA (top) thickness, inch	2	2	1	2
HMA (top) binder type	PG64-22	PG64-28	PG58-28	PG70-22P
HMA (top) aggregate gradation	4E3	5E10	5E3	4E30
HMA leveling thickness, inch	3	2	2	3
HMA leveling binder type	PG58-22	PG64-28	PG58-28	PG64-28
HMA leveling aggregate gradation	3E3	4E10	3E3	3E30
HMA base thickness, inch	3	4	3	7
HMA base binder type	PG58-22	PG58-28	PG58-28	PG64-28
HMA base aggregate gradation	3E3	3E10	3E3	3E30
HMA layer total thickness, inch	8	8	6	12
Base layer thickness, inch	4	6	6	6
Base layer modulus, psi	33,000	33,000	33,000	33,000
Subbase layer thickness, inch	18	18	18	18
Subbase layer modulus, psi	20,000	20,000	20,000	20,000
Subgrade resilient modulus, psi	4,400	4,400	7,000	4,400
20-year traffic, ESALs	1.53 Millions	7.98 Millions	30.33 Millions	26.97 Millions
20-year traffic, equivalent 36-kip tandem axle per day	152	793	3022	2679

Table 6.2 Summary of axle loading information.

Axle Type	Tire Radius (inch)	Tire Pressure (psi)	Axle Loading (kip)	Axle Spacing (inch)	Dual Spacing (inch)	Speed (mph)
Tandem	3.455	120	36	42	13	60

Table 6.3 Pavement temperature gradient and loading frequencies for I-94.

Depth (inch)	Pavement ME frequency (Hz)	January Quintile 1		July Quintile 5	
		Temperature (Fahrenheit)	Corrected Pavement ME frequency (Hz)	Temperature (Fahrenheit)	Corrected Pavement ME frequency (Hz)
0.25	120.47	16.59	16.13	107.51	17.92
0.75	84.64	17.45	18.53	105.53	20.34
1.5	58.53	18.63	23.85	102.77	25.52
2.5	41.47	19.93	38.64	99.77	38.64
3.5	32.11	21.01	32.27	97.36	32.27
4.5	26.20	21.90	27.70	95.48	27.70
5.5	21.82	22.67	24.26	93.91	24.26
6.5	18.28	23.32	21.58	92.66	21.58
7.5	15.71	23.91	19.44	91.60	19.44
8.5	13.76	24.42	17.68	90.75	17.68
9.5	12.24	24.88	12.97	90.01	16.60
10.5	11.01	25.28	7.35	89.39	11.70
11.5	10.00	25.66	5.13	88.85	9.03

6.4 Results and Discussion

The cumulative damage overtime at the bottom and top of the AC layer predicted using the original and corrected pavement ME method for the four pavement structures are presented in Table 6.4 and Figure 6.1. It should be noted that this damage is calculated as a function of the number of cycles to failure, which is calibrated by several global and local as shown in Equations 6.2 to 6.4. Due to the absence of a calibration parameter specifically developed for the corrected Pavement ME method, the same calibration parameters developed for the original Pavement ME method are utilized in the corrected method.

Table 6.4 and Figure 6.1 shows the cumulative damage at the bottom and top of the AC layer, which is calculated based on the maximum tensile strains at the bottom of the AC layer and the maximum principal tensile strains at the top of the AC layer, respectively. The damage at the bottom of the AC layer predicted by the corrected Pavement ME method is higher than that by the original one. The differences are not substantial in structures with thin and medium AC layers (BL-I94, US-127, and US-131), ranging from less than 10% to nearly 20%. This discrepancy is negligible (1.12 %) in the structure with a thick AC layer (I-

94, 12-inch AC). The discrepancies between the original and corrected Pavement ME methods in the prediction of cumulative damage at the top of the AC layer are substantial. The corrected method forecasts 50% to 75% higher damage for all the four structures. This can be attributed to Pavement ME's substantial overestimation of the loading frequency near the asphalt concrete surface, which consequently results in an overestimation of the elastic modulus.

By applying the transfer function as shown in Equation 6.5 to the cumulative damage at the bottom and top of the AC layer, the corresponding distress, bottom-up fatigue cracking and top-down fatigue cracking can be obtained. Table 6.5 demonstrates that the bottom-up fatigue cracking predicted by both the original and corrected Pavement ME frequency methods for well-designed pavement structures (BL-I94, US-127, and I-94) remains below the 25% threshold, irrespective of pavement thickness and traffic volumes. The pavement structure of US-131 is inadequately designed, as the AC layer is only 6 inches thick, and the aggregate gradation is intended for 10 million equivalent ESALs. However, the actual traffic volumes on this road section exceed 30 million ESALs. In such a scenario, the bottom-up fatigue cracking yielded by these two loading frequencies marginally surpasses the threshold.

The differences between bottom-up fatigue predicted using the original and corrected Pavement ME loading frequencies are below 4% for all pavement structures. This is because the bottom-up fatigue is predominantly influenced by the tensile strains at the bottom of the AC layer and the original Pavement ME method effectively predicts the maximum tensile strains at the bottom of the AC layer with an acceptable error.

The top-down fatigue cracking predicted by both the original and corrected loading frequencies falls significantly below the established threshold of 2,000 feet per mile for properly designed pavement structures. On US-131, where the pavement structure is inadequately designed to accommodate real traffic volumes, distress predictions approach the threshold. The corrected loading frequency method consistently forecasts substantially higher levels of top-down cracking compared to the original Pavement ME, with discrepancies reaching up to 130%. It should be noted that the corrected loading frequency developed in Chapter 5 is not specifically designed for principal tensile strains near the surface, which are critical factors in the top-down fatigue cracking model employed by MEAPA. Consequently, the analysis presented in

Table 6.5 does not support the conclusion that the Pavement ME frequency method significantly underestimates top-down fatigue cracking. However, the Pavement ME model underestimates vertical strains near the AC surface. Given that vertical strain is mechanistically related to principal strain, there remains a concern that Pavement ME will consequently underestimate principal tensile strains within the top of the AC layer.

Table 6.6 presents the predicted AC rutting and total rutting at the end of the pavement design life (20 years) as calculated using the two loading frequency methods. Similar to fatigue damage, the calibration parameters in the rutting model developed for the original Pavement ME method are utilized in the corrected method. As expected, the rutting depth in US-131, which was inadequately designed, is the highest among all pavement structures. Both the asphalt concrete (AC) and total rutting depths simulated using the corrected Pavement ME method are up to 24% and 10% higher, respectively, compared to the original Pavement ME method. These discrepancies are more pronounced in pavement structures with thin to medium AC layers subjected to low to medium traffic (US-127 and US-131). Nevertheless, these discrepancies are significantly smaller than those observed in vertical strain calculations using different loading frequencies, where the Pavement ME method underestimates vertical strains by up to 55% to 70% near the surface of the AC layer. This is because the pavement ME loading frequency only underestimates vertical strains within the upper portion of the AC layer (typically 2.5 to 3 inches). In contrast, the AC rutting and total rutting are calculated as the cumulative permanent deformation throughout the entire AC layer and all pavement layers, respectively.

Table 6.4 Cumulative damage at the bottom and top of the AC layer using different loading frequencies after 20 years.

Roadway	Cumulative damage at the bottom of AC (%)			Cumulative damage at the top of AC (%)		
	Pavement ME	Corrected Pavement ME	% difference	Pavement ME	Corrected Pavement ME	% difference
BL-I-94	2.55E-04	2.75E-04	7.96%	2.37E-03	3.52E-03	48.68%
US-127	1.41E-03	1.56E-03	11.16%	2.07E-02	3.61E-02	74.18%
US-131	2.38E-02	2.81E-02	18.03%	1.49E-01	2.62E-01	75.98%
I-94	2.51E-04	2.54E-04	1.12%	1.11E-02	1.76E-02	58.93%

Table 6.5 Fatigue cracking predicted using different loading frequencies after 20 years.

Roadway	Bottom-up fatigue cracking			Top-down fatigue cracking (feet/mile)		
	Pavement ME	Corrected Pavement ME	% difference	Pavement ME	Corrected Pavement ME	% difference
BL-I-94	9.02%	9.21%	2.05%	1.08	1.97	82.72%
US-127	14.02%	14.40%	2.68%	29.06	67.31	131.60%
US-131	26.50%	27.48%	3.70%	551.85	1216.39	120.42%
I-94	9.37%	9.39%	0.29%	11.27%	22.76%	102.01%

Table 6.6 Rutting predicted using different loading frequencies after 20 years.

Roadway	AC Rutting (inch)			Total Rutting (inch)		
	Pavement ME	Corrected Pavement ME	% difference	Pavement ME	Corrected Pavement ME	% difference
BL-I-94	0.04	0.05	15.25%	0.18	0.19	5.51%
US-127	0.09	0.11	23.91%	0.26	0.29	9.93%
US-131	0.16	0.19	21.99%	0.38	0.41	9.57%
I-94	0.05	0.06	17.39%	0.18	0.19	6.98%

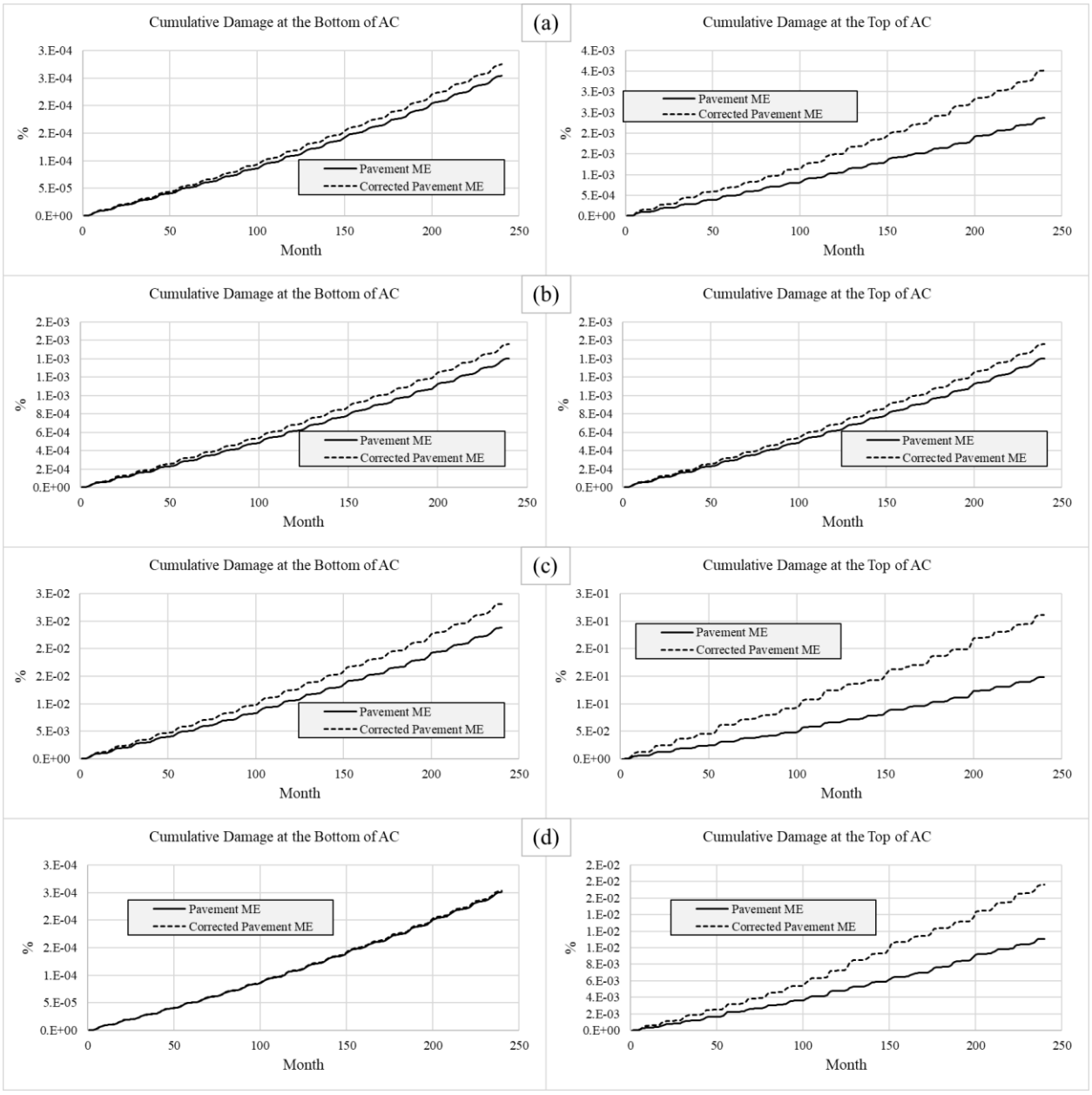

Figure 6.1 Cumulative damage at the bottom and top of the AC layer predicted over time using different loading frequencies (a) BL-I-94; (b) US-127; (c) US-131; (d) I-94.

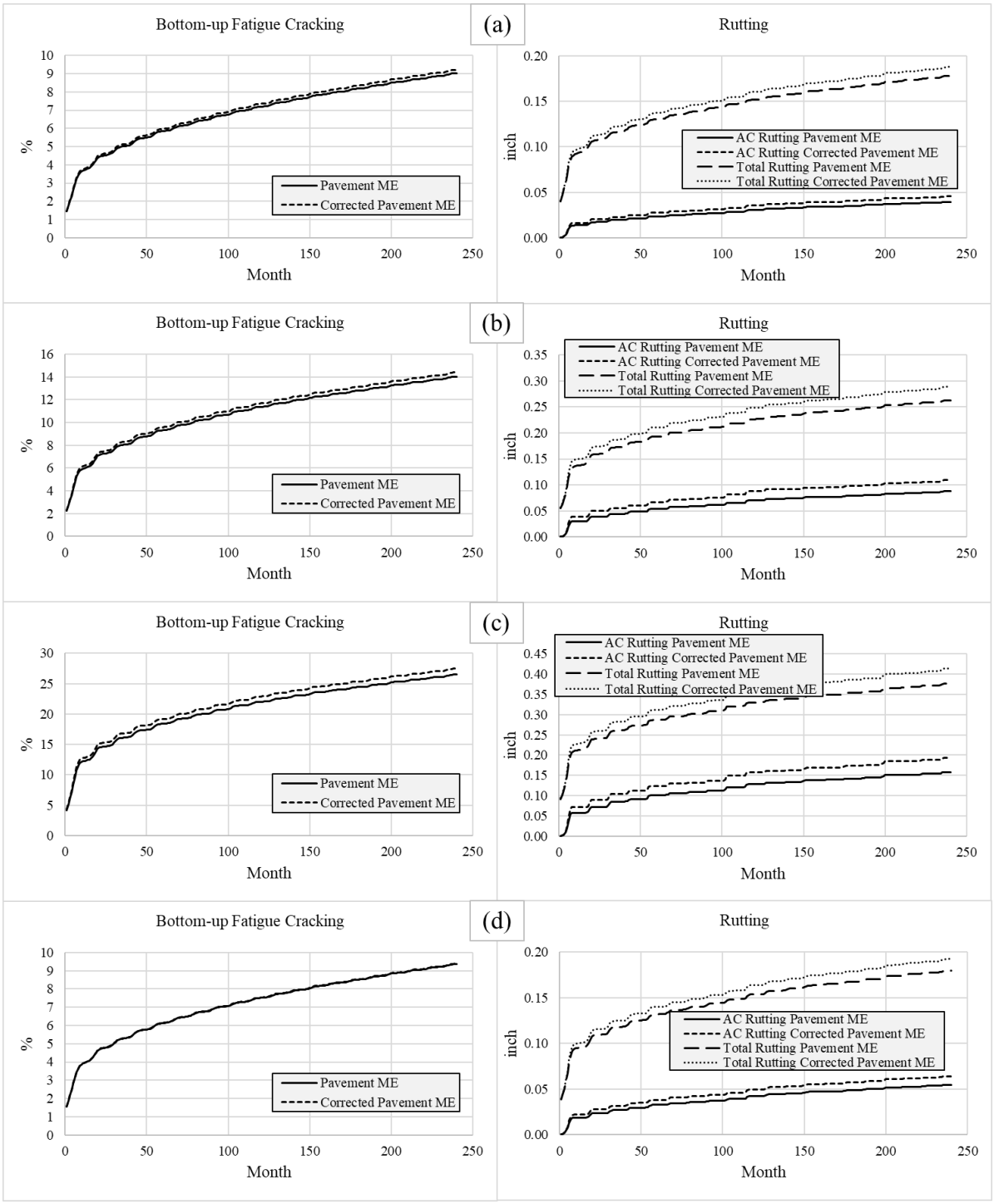

Figure 6.2 Bottom-up fatigue and rutting predicted over time using different loading frequencies (a) BL-I-94; (b) US-127; (c) US-131; (d) I-94.

6.5 Conclusions

This chapter presents a comparative analysis of the long-term distress predicted by both the original

and corrected Pavement ME loading frequency methods for four pavement structures, based on real-world projects in Michigan, simulated using the MEAPA software. Several conclusions can be drawn as follows:

- The difference between bottom-up fatigue cracking predicted by the original and corrected Pavement ME frequencies is negligible.
- The corrected frequency yields higher rutting predictions compared to the original Pavement ME method, ranging from approximately 15% to over 20% for AC rutting and 5% to 10% for total rutting, depending on pavement structures and traffic volumes.
- There is a potential concern that the original Pavement ME method may substantially underestimate the extent of top-down fatigue cracking.

GENERAL CONCLUSIONS AND FUTURE WORK

7.1 General Conclusions

This study provides a comprehensive investigation into the characteristics and physical significance of equivalent axle loading frequency for flexible pavement. Two novel frequency calculation methods were introduced, and the accuracy and validity of the loading frequency method used by the prevalent Pavement ME methodology were evaluated. This evaluation was conducted from the perspective of frequency, elastic modulus, critical strains, and predicted long-term distress. Furthermore, a practical correction method for Pavement ME loading frequency calculation was developed, which can be readily implemented into its design software. The following conclusions have been drawn from this thesis:

- The predominant frequency refers to the frequency that carries the most significant energy of the axle loading pulse. This is a fundamental physical property of the signal, and it can be calculated using either the loading time or actual loading pulses. On the other hand, the equivalent frequency is not a physical property of the signal and has no direct relationship with the loading time or loading pulses.
- When calculating predominant frequencies by taking the centroid of the area of the transform amplitude in the frequency domain, only the dominant portion of the amplitude should be considered because the high-frequency portion is there to account for the sharpness of the pulse in the Fourier Transform.
- The time-frequency relationship for predominant frequency is closer to $f = 1/(2t)$ than $f = 1/t$, assuming that the pulse duration t is accurate. Overestimating the pulse duration t and using $f = 1/t$, which is higher than the equivalent frequency tends to compensate for the error to some extent.
- The predominant frequency method proposed by this study, the centroid of PSD method, agrees well with the equivalent frequency method in estimating the pulse width with depth, except at the surface of the AC layer.
- The Pavement ME method substantially overestimates the loading frequency near the surface of the AC layer for both single-axle and multiple-axle loading configurations; however, these discrepancies diminish with increasing depth.
- The differences between the predominant frequencies obtained by the centroid of PSD method for

single and multiple axles are negligible. However, the equivalent frequencies from multiple axle loadings are smaller than that from single axle loadings by up to 40% for AC layers with soft to moderate stiffness.

- The Pavement ME method underestimates vertical strains near the surface by up to 55% and 70% for single-axle and multiple-axle loading configurations, respectively, while it gives reasonable predictions with increasing depth.
- The maximum horizontal strains are less sensitive to loading frequency than vertical stains for both single and multiple axles. The accuracy of all loading frequencies in terms of maximum horizontal strain prediction is generally independent of the number of axles but is mainly affected by the AC layer stiffness and vehicle speed.
- The Pavement ME method gives reasonable predictions of transverse strains for both single-axle and multiple-axle loading configurations. The critical orientation of tensile strains at the bottom of the AC layer is transverse under single-wheel loading, whereas it is typically longitudinal under dual-wheel loading.
- Even though both the Pavement ME and the centroid of PSD methods yield almost identical frequencies for single and multiple axle configurations, using these frequencies derived from single axle scenarios to predict vertical strain under multiple axle loadings can result in an additional error of up to 5% to 10% near the surface of the AC layer. Errors of vertical strains predicted by the equivalent frequency developed for single axle loading conditions are generally acceptable, except for structures with soft to moderately soft AC materials, where these errors can reach up to 20%.
- Even though the procedure for Pavement ME frequency calculation is highly simplified and uses an incorrect equation that overestimates the frequency, its overall performance appears to be acceptable for horizontal strains at the bottom of the AC layer and for vertical strains except for near the surface. This is because Pavement ME overestimates the pulse duration t and uses the wrong time-frequency relationship of "f = 1/t", which tends to compensate for the error to some extent. In other words, two simultaneous errors in frequency and pulse duration calculations compensate each other to a certain degree.

- The overall behavior of the Pavement ME frequency in the prediction of strain responses under single and multiple axles loadings is similar.
- The correction method for Pavement ME loading frequency developed in this thesis demonstrates strong agreement with the equivalent frequency and significantly outperforms the original Pavement ME in predicting vertical strains.
- The difference between bottom-up fatigue cracking predicted by the original and corrected Pavement ME frequencies is negligible.
- The corrected frequency yields higher rutting predictions compared to the original Pavement ME method, ranging from approximately 15% to over 20% for AC rutting and 5% to 10% for total rutting, depending on pavement structures and traffic volumes.
- There is a potential concern that the original Pavement ME method may substantially underestimate the extent of top-down fatigue cracking.
- The overall performance of the current Pavement ME loading frequency method in terms of long-term pavement distress prediction is acceptable.

7.2 Future Study

This thesis does not examine the axle loading frequency in relation to shear strain or principal tensile strains near the AC layer surface, which are considered to be the primary causes of top-down fatigue cracking in flexible pavements. However, it has been proved that the Pavement ME loading frequency significantly underestimates vertical strains near the AC surface. Given that vertical strain is mechanistically related to principal strain, there remains a concern that Pavement ME will consequently underestimate principal tensile strains within the top of the AC layer.

In the future, it is imperative to evaluate the accuracy of the Pavement ME frequency concerning the prediction of shear and principal tensile strains near the surface of the AC layer. Additionally, the development of an alternative correction method for the current Pavement ME frequency may be necessary to improve the prediction of top-down cracking.

BIBLIOGRAPHY

3D-Move Analysis, Version 2.1. [Computer software]. Reno, NV.

AASHTO Guide for Design of Pavement Structures. AASHTO, Washington, D.C., 1993.

Al-Qadi, I. L., Elseifi, M. A., Yoo, P. J., Dessouky, S. H., Gibson, N., Harman, T., D'Angelo, J., & Petros, K. (2008a). Accuracy of current complex modulus selection procedure from vehicular load pulse: NCHRP Project 1-37A mechanistic-empirical pavement design guide. Transportation research record, 2087(1), 81-90.

Al-Qadi, I. L., Loulizi, A., Elseifi, M., & Lahouar, S. (2004). The Virginia Smart Road: The impact of pavement instrumentation on understanding pavement performance. Journal of the Association of Asphalt Paving Technologists, 73(3), 427-465.

Al-Qadi, I. L., Xie, W., & Elseifi, M. A. (2008b). Frequency determination from vehicular loading time pulse to predict appropriate complex modulus in MEPDG. Asphalt Paving Technology-Proceedings, 77, 739.

Al-Qadi, I. L., Yoo, P. J., Elseifi, M. A., Janajreh, I., Chehab, G., & Collop, A. (2005). Effects of tire configurations on pavement damage. Journal of the Association of Asphalt Paving Technologists, 74(1), 921-961.

ARA, Inc., ERES Division. (2001). Appendix CC-3 of the Guide for Mechanistic-Empirical Design of New and Rehabilitated Pavement Structures. NCHRP 1-37A. https://onlinepubs.trb.org/onlinepubs/archive/mepdg/2appendices_CC.pdf

Ayres Jr, M., & Witczak, M. W. (1998). AYMA: Mechanistic probabilistic system to evaluate flexible pavement performance. Transportation Research Record, 1629(1), 137-148.

Barksdale, R. D. (1971). Compressive stress pulse times in flexible pavements for use in dynamic testing. Highway research record, 345(4), 32-44.

Bodin, D., Chupin, O., & Denneman, E. (2017). Viscoelastic asphalt pavement simulations and simplified elastic pavement models based on an “equivalent asphalt modulus” concept. Journal of Testing and Evaluation, 45(6), 1887-1895.

Brown, S. F. (1973). Determination of Young's modulus for bituminous materials in pavement design. Highway Research Record, (431).

Chen, P., Chatti, K., Cetin, B. (2023). Evaluation of the Accuracy of Pavement ME Methodology in Calculating Equivalent Loading Frequency and Its Effect on Strain Response Predictions in Flexible Pavements. Journal of Transportation Engineering, Part B: Pavements,

D"Angelo, J. A., Dongre, R. N., & Myers, L. A. (2006). Conversion of testing frequency to loading time: Impact on performance predictions obtained from mechanistic-empirical pavement design guide (No. 06-2394).

Ferry, J. D. (1980). Viscoelastic properties of polymers. John Wiley & Sons.

Ghanizadeh, A. R., & Fakhri, M. (2018). Quasi-static analysis of flexible pavements based on predicted frequencies using Fast Fourier Transform and Artificial Neural Network. International Journal of Pavement Research and Technology, 11(1), 47-57.

Ghazavi, M., Abdollahi, S. F., & Kutay, M. E. (2022). Implementation of NCHRP 9-44A fatigue endurance limit prediction model in mechanistic-empirical asphalt pavement analysis web application. *Transportation Research Record*, *2676*(6), 696-706.

Ghazavi, M., Seitllari, A., & Kutay, M. E. (2020). Performance Evaluation of Long-Life Pavements Using the Mechanistic-Empirical Asphalt Pavement Analysis (MEAPA) Web Application. In *Proceedings of the 9th International Conference on Maintenance and Rehabilitation of Pavements—Mairepav9* (pp. 79-89). Springer International Publishing.

Gu, F., Luo, X., West, R. C., Taylor, A. J., & Moore, N. D. (2018). Energy-based crack initiation model for load-related top-down cracking in asphalt pavement. *Construction and Building Materials*, *159*, 587-597.

Haider, S. W., Kutay, M. E., Cetin, B., Singh, R. R., Muslim, H. B., Santos, C., ... & Zhong, Y. (2023). *Testing Protocol, Data Storage, and Recalibration for Pavement-ME Design* (No. SPR-1723). Michigan. Dept. of Transportation. Research Administration.

Huang, H. Y. Pavement Analysis and Design. Prentice Hall, Upper Saddle River, N.J., 1993.

Huang, Y. H. (2004). *Pavement analysis and design* (Vol. 2, pp. 401-409). Upper Saddle River, NJ: Pearson Prentice Hall.

Kaloush, K. E., & Witczak, M. W. (2000). Development of a permanent to elastic strain ratio model for asphalt mixtures. Development of the 2002 guide for the design of new and rehabilitated pavement structures. NCHRP, 1-37.

Kaloush, K. E., & Witczak, M. W. (2000). Development of the 2002 Guide for the Design of New and Rehabilitated Pavement Structures.

Kramer, S. L. (1996). Geotechnical earthquake engineering. Pearson Education India.

Kutay, M. E., & Lanotte, M. (2020). Formulations of the pavement performance prediction models in the mechanistics-empirical asphalt pavement analysis (MEAPA) Web application. *Michigan State University*.

Leahy, R. B. (1989). Permanent deformation characteristics of asphalt concrete. University of Maryland, College Park.

Lei, L. (2011). Backcalculation of asphalt concrete complex modulus curve by layered viscoelastic solution. Michigan State University. Civil Engineering.

Losa, M. & Di Natale, A. (2012). Evaluation of representative loading frequency for linear elastic analysis of asphalt pavements. Transportation research record, 2305(1), 150-161.

Loulizi, A., Al-Qadi, I. L., Lahouar, S., & Freeman, T. E. (2002). Measurement of vertical compressive stress pulse in flexible pavements: representation for dynamic loading tests. Transportation Research Record, 1816(1), 125-136.

Ma, Z., Liu, L., Sun, L., 2018. Investigation of top-down cracking performance of in-situ asphalt mixtures based on accelerated pavement testing and laboratory tests. Construction and Building Materials 179, 277e284.

NCHRP. Guide for Mechanistic-Empirical Design of New and Rehabilitated Pavement Structures, Appendix L1-1: Calibration of Fatigue Cracking Models for Flexible Pavements. Transportation Research Board, National Research Council, Washington, D.C., 2004.

Oshone, M., Dave, E., Daniel, J. S., & Rowe, G. M. (2017). Prediction of phase angles from dynamic modulus data and implications for cracking performance evaluation. Road Materials and Pavement Design, 18(sup4), 491-513.

Rowe, G. (2009). Phase angle determination and interrelationships within bituminous materials. In Advanced Testing and Characterization of Bituminous Materials, Two Volume Set (pp. 59-68). CRC Press.

Team, B. (1995). Comprehensive Truck Size and Weight (TS&W) Study Phase 1-Synthesis. *Federal Highway Administration, US Department of Transportation: Columbus, OH, USA*.

Ullidtz, P. (2005). Frequency/Loading Time. NCHRP 1-40A (01), Committee Notes. Transportation Research Board of the National Academies, Washington, DC.

Ulloa, A., Hajj, E. Y., Siddharthan, R. V., & Sebaaly, P. E. (2013). Equivalent loading frequencies for dynamic analysis of asphalt pavements. Journal of Materials in Civil Engineering, 25(9), 1162-1170.

Underwood, B. S., & Kim, Y. R. (2009). Determination of the appropriate representative elastic modulus for asphalt concrete. International Journal of Pavement Engineering, 10(2), 77-86.

Wu, S., & Muhunthan, B. (2019). A mechanistic-empirical model for predicting top-down fatigue cracking in an asphalt pavement overlay. Road Materials and Pavement Design, 20(6), 1322-1353

APPENDIX A: DYNAMIC MODULUS E* OF THE ASPHALT CONCRETE (AC) MATERIALS

In this section, the dynamic modulus data of AC materials used in the analyses in Chapters 5 and 6 are reported.

Table 9.1 Dynamic modulus of 4E10, PG64-28.

Temperature	Modulus (psi) at Different Frequencies (Hz)					
(Fahrenheit)	25.1	10.1	5.1	1.01	0.5	0.1
13.82	3795626	3628061	3492729	3140324	2974437	2570754
39.20	2664149	2427574	2246484	1815062	1631226	1232302
69.80	1257004	1049503	905724	612301	506945	315442
98.60	455227	347827	280859	163028	126913	69812
129.20	136466	97898	75801	40770	31069	16777

Table 9.2 Phase angle of 4E10, PG64-28.

Temperature	Phase angle (degree) at Different Frequencies (Hz)					
(Fahrenheit)	25.1	10.1	5.1	1.01	0.5	0.1
13.82	4.37	4.99	6.74	7.61	9.87	4.37
39.20	10.7	11.8	14.6	15.9	19	10.7
69.80	20.5	21.8	24.6	25.8	28	20.5
98.60	27.6	28.5	30	30.4	30.8	27.6
129.20	30.7	30.8	30.5	30.1	28.7	30.7

Table 9.3 Dynamic modulus of 5E3, PG58-28.

Temperature	Modulus (psi) at Different Frequencies (Hz)					
(Fahrenheit)	25.1	10.1	5.1	1.01	0.5	0.1
13.82	2838734	2704116	2592697	2293402	2148981	1792117
39.20	1879751	1669613	1509002	1132469	977006	657173
69.80	749468	585308	477220	275921	211688	109281
98.60	242269	169721	127920	62708	45408	21458
129.20	84742	56189	40993	19279	13949	6842

Table 9.4 Phase angle of 5E3, PG58-28.

Temperature (Fahrenheit)	Phase angle (degree) at Different Frequencies (Hz)					
	25.1	10.1	5.1	1.01	0.5	0.1
13.82	5.49	6.65	7.63	10.3	11.6	15
39.20	14.1	16.1	17.7	21.5	23.1	26.8
69.80	25.7	27.7	29	31.8	32.8	34.2
98.60	32.3	33.4	34	34.6	34.5	33.5
129.20	34.5	34.6	34.4	33.3	32.4	29.9

Table 9.5 Dynamic modulus of 3E3, PG58-28.

Temperature (Fahrenheit)	Modulus (psi) at Different Frequencies (Hz)					
	25.1	10.1	5.1	1.01	0.5	0.1
13.82	3059179	2849322	2681184	2252913	2057853	1606595
39.20	1967204	1711404	1521640	1096222	928642	599387
69.80	761549	587331	474816	270151	206245	105806
98.60	201099	138728	103617	50169	36275	17213
129.20	38732	25391	18507	8900	6563	3416

Table 9.6 Phase angle of 3E3, PG58-28.

Temperature (Fahrenheit)	Phase angle (degree) at Different Frequencies (Hz)					
	25.1	10.1	5.1	1.01	0.5	0.1
13.82	6.13	7.57	8.78	12.1	13.7	17.7
39.20	14.5	16.8	18.5	22.7	24.5	28.1
69.80	26.3	28.3	29.6	31.9	32.5	32.9
98.60	32.5	32.9	32.8	31.7	30.8	28
129.20	31	29.6	28.3	24.6	22.9	18.7

Table 9.7 Dynamic modulus of 4E3, PG64-22.

Temperature (Fahrenheit)	Modulus (psi) at Different Frequencies (Hz)					
	25.1	10.1	5.1	1.01	0.5	0.1
13.82	3531037	3400931	3294458	3011350	2875113	2535369
39.20	2689639	2490525	2334563	1949453	1778957	1393727
69.80	1474795	1263272	1111470	785657	662354	427240
98.60	607842	474497	388509	230788	180526	98978
129.20	184598	132360	102030	53513	40080	20521

Table 9.8 Phase angle of 4E3, PG64-22.

Temperature (Fahrenheit)	Phase angle (degree) at Different Frequencies (Hz)					
	25.1	10.1	5.1	1.01	0.5	0.1
13.82	3.01	3.63	4.17	5.66	6.41	8.4
39.20	7.48	8.68	9.65	12.2	13.4	16.3
69.80	15.7	17.4	18.7	21.9	23.3	26.3
98.60	23.9	25.6	26.9	29.5	30.5	32.3
129.20	30.4	31.5	32.2	33.4	33.7	33.7

Table 9.9 Dynamic modulus of 3E3, PG58-22.

Temperature (Fahrenheit)	Modulus (psi) at Different Frequencies (Hz)					
	25.1	10.1	5.1	1.01	0.5	0.1
13.82	3711094	3540331	3401725	3038760	2867274	2449676
39.20	2672805	2432253	2247276	1804709	1615788	1206640
69.80	1302973	1085580	934764	627342	517414	319004
98.60	461049	350295	281713	162332	126188	69613
129.20	120421	86128	66727	36358	28020	15731

Table 9.10 Phase angle of 3E3, PG58-22.

Temperature (Fahrenheit)	Phase angle (degree) at Different Frequencies (Hz)					
	25.1	10.1	5.1	1.01	0.5	0.1
13.82	3.12	3.86	4.5	6.33	7.26	9.73
39.20	8.38	9.84	11	14.1	15.5	19
69.80	18.1	20.1	21.5	24.9	26.2	28.8
98.60	26.9	28.4	29.4	31.1	31.6	31.9
129.20	31.6	31.9	31.9	31.1	30.5	28.4

Table 9.11 Dynamic modulus of 5E10, PG64-28.

Temperature (Fahrenheit)	Modulus (psi) at Different Frequencies (Hz)					
	25.1	10.1	5.1	1.01	0.5	0.1
13.82	2992073	2848911	2733217	2432225	2290935	1949110
39.20	2028238	1829164	1677896	1322550	1173800	858151
69.80	880113	719984	611302	396624	322392	192491
98.60	289022	215840	171441	96170	73989	40003
129.20	81078	57456	44210	23702	18138	10017

Table 9.12 Phase angle of 5E10, PG64-28.

Temperature (Fahrenheit)	Phase angle (degree) at Different Frequencies (Hz)					
	25.1	10.1	5.1	1.01	0.5	0.1
13.82	4.68	5.54	6.26	8.21	9.17	11.6
39.20	11	12.5	13.7	16.7	18	21.1
69.80	20.9	22.7	24	26.9	28.1	30.5
98.60	28.7	30	30.9	32.6	33.1	33.8
129.20	33	33.5	33.7	33.7	33.4	32.3

Table 9.13 Dynamic modulus of 3E10, PG58-28.

Temperature (Fahrenheit)	Modulus (psi) at Different Frequencies (Hz)					
	25.1	10.1	5.1	1.01	0.5	0.1
13.82	3132557	3005441	2901532	2626103	2494176	2167551
39.20	2225833	2031216	1880802	1518027	1361818	1020461
69.80	1029505	852211	729548	480901	392703	235245
98.60	348380	260420	206484	114198	86903	45300
129.20	95280	66352	50222	25613	19096	9858

Table 9.14 Phase angle of 3E10, PG58-28.

Temperature (Fahrenheit)	Phase angle (degree) at Different Frequencies (Hz)					
	25.1	10.1	5.1	1.01	0.5	0.1
13.82	3.95	4.68	5.29	6.96	7.8	9.94
39.20	9.55	10.9	11.9	14.7	15.9	18.9
69.80	18.8	20.6	21.9	25	26.3	29
98.60	27	28.5	29.6	31.9	32.7	34.1
129.20	32.4	33.4	33.9	34.8	34.9	34.7

Table 9.15 Dynamic modulus of 4E10, PG70-22P.

Temperature (Fahrenheit)	Modulus (psi) at Different Frequencies (Hz)					
	25.1	10.1	5.1	1.01	0.5	0.1
13.82	3259256	3101129	2974274	2647505	2495470	2130338
39.20	2434196	2227959	2069582	1690047	1527150	1170494
69.80	1302769	1108199	970769	681844	574556	372738
98.60	496700	387192	317457	191044	151001	85797
129.20	118801	85939	67023	36780	28308	15667

Table 9.16 Phase angle of 4E10, PG70-22P.

Temperature (Fahrenheit)	Phase angle (degree) at Different Frequencies (Hz)					
	25.1	10.1	5.1	1.01	0.5	0.1
13.82	3.97	4.75	5.4	7.19	8.09	10.4
39.20	8.46	9.76	10.8	13.5	14.8	17.9
69.80	16.7	18.5	19.8	23.1	24.5	27.5
98.60	25.6	27.3	28.5	31	31.9	33.6
129.20	32.7	33.5	34	34.6	34.6	34

Table 9.17 Dynamic modulus of 3E10, PG58-22.

Temperature (Fahrenheit)	Modulus (psi) at Different Frequencies (Hz)					
	25.1	10.1	5.1	1.01	0.5	0.1
13.82	3115350	2970432	2851297	2534011	2381938	2007648
39.20	2214633	1998631	1831824	1432417	1262818	900814
69.80	1024709	831839	700040	439534	350289	197445
98.60	340379	247740	192281	100923	75126	37468
129.20	87573	59434	44198	21822	16130	8288

Table 9.18 Phase angle of 3E10, PG58-22.

Temperature (Fahrenheit)	Phase angle (degree) at Different Frequencies (Hz)					
	25.1	10.1	5.1	1.01	0.5	0.1
13.82	3.89	4.83	5.63	7.91	9.07	12.1
39.20	10.4	12.1	13.5	17.1	18.7	22.4
69.80	21.1	23.2	24.7	27.8	29	31
98.60	29.1	30.4	31.1	32	32.1	31.4
129.20	32.1	32	31.6	30.1	29.1	26.2

Table 9.19 Dynamic modulus of 4E30, PG70-22P.

Temperature (Fahrenheit)	Modulus (psi) at Different Frequencies (Hz)					
	25.1	10.1	5.1	1.01	0.5	0.1
13.82	3351862	3193675	3066165	2735507	2580702	2206821
39.20	2468870	2256035	2092504	1700836	1533054	1167091
69.80	1314515	1114674	973954.2	679791.7	571333.3	368891.4
98.60	542280.6	424567	349377.5	212506.2	168939.7	97615.03
129.20	170212	125263.2	98932.12	55886.75	43541.63	24765.23

Table 9.20 Phase angle of 4E30, PG70-22P.

Temperature (Fahrenheit)	Phase angle (degree) at Different Frequencies (Hz)					
	25.1	10.1	5.1	1.01	0.5	0.1
13.82	3.29	4.03	4.67	6.46	7.37	9.74
39.20	8.05	9.41	10.5	13.4	14.7	17.8
69.80	16.5	18.3	19.7	22.8	24.1	26.6
98.60	24.4	25.9	26.9	28.8	29.4	30.1
129.20	29.4	29.9	30.1	29.9	29.5	28

Table 9.21 Dynamic modulus of 3E30, PG64-28.

Temperature (Fahrenheit)	Modulus (psi) at Different Frequencies (Hz)					
	25.1	10.1	5.1	1.01	0.5	0.1
13.82	3725165	3560667	3424326	3056855	2878705	2435365
39.20	2660367	2402601	2202464	1720228	1514519	1074671
69.80	1214884	981484.7	822428.5	510131	404185.4	224855.5
98.60	394766.3	285281	220301.5	114577.3	85126.15	42561.65
129.20	102486.6	69518.67	51770.14	25837.31	19255.74	10164.69

Table 9.22 Phase angle of 3E30, PG64-28.

Temperature (Fahrenheit)	Phase angle (degree) at Different Frequencies (Hz)					
	25.1	10.1	5.1	1.01	0.5	0.1
13.82	3.47	4.37	5.16	7.42	8.58	11.6
39.20	10.1	11.9	13.3	17	18.7	22.6
69.80	21.3	23.5	25	28.2	29.4	31.4
98.60	29.5	30.7	31.4	32.1	32.1	31
129.20	32.1	31.9	31.4	29.5	28.3	25.1

APPENDIX B: CLIMATE AND LOADING FREQUENCY

In this section, the climate data and loading frequencies used for the analysis in Chapter 6 are reported.

Table 10.1 Pavement temperatures for climate condition of East Lansing, Michigan.

Month	Depth (inch)	Temperature (Fahrenheit) for Each Quintile				
		Quintile 1	Quintile 2	Quintile 3	Quintile 4	Quintile 5
January	0.25	12.9	21.5	27.4	33.4	41.9
	0.75	13.7	21.8	27.5	33.1	41.3
	1.5	14.8	22.3	27.6	32.8	40.4
	2.5	15.9	22.9	27.7	32.5	39.5
	3.5	16.8	23.3	27.8	32.3	38.9
	4.5	17.5	23.7	28.0	32.2	38.4
	5.5	18.1	24.0	28.1	32.2	38.1
	6.5	18.6	24.3	28.2	32.2	37.9
	7.5	19.0	24.5	28.3	32.2	37.7
February	0.25	15.8	25.0	31.4	37.8	47.0
	0.75	16.8	25.4	31.4	37.5	46.1
	1.5	18.0	26.0	31.5	37.0	44.9
	2.5	19.3	26.5	31.5	36.5	43.8
	3.5	20.2	26.9	31.6	36.2	42.9
	4.5	20.9	27.3	31.6	36.0	42.3
	5.5	21.5	27.5	31.7	35.8	41.8
	6.5	21.9	27.7	31.7	35.7	41.5
	7.5	22.3	27.9	31.8	35.7	41.2
March	0.25	23.7	34.7	42.3	49.9	60.8
	0.75	24.8	35.1	42.2	49.4	59.7
	1.5	26.2	35.6	42.2	48.7	58.2
	2.5	27.5	36.1	42.1	48.0	56.6
	3.5	28.5	36.5	42.0	47.5	55.5
	4.5	29.2	36.7	41.9	47.1	54.7
	5.5	29.7	36.9	41.9	46.8	54.0
	6.5	30.1	37.0	41.8	46.6	53.6
	7.5	30.4	37.1	41.8	46.4	53.1
April	0.25	37.5	48.8	56.6	64.4	75.7
	0.75	38.8	49.2	56.5	63.7	74.2
	1.5	40.5	49.9	56.4	62.9	72.2
	2.5	42.2	50.5	56.2	62.0	70.2
	3.5	43.5	50.9	56.1	61.2	68.7
	4.5	44.3	51.2	55.9	60.7	67.6
	5.5	44.8	51.3	55.8	60.3	66.8
	6.5	45.2	51.4	55.7	60.0	66.2
	7.5	45.5	51.4	55.6	59.7	65.6

Table 10.1 (cont'd).

May	0.25	48.7	60.9	69.3	77.8	89.9
	0.75	50.3	61.5	69.2	77.0	88.1
	1.5	52.4	62.3	69.1	75.9	85.7
	2.5	54.6	63.0	68.9	74.7	83.1
	3.5	56.1	63.5	68.7	73.8	81.2
	4.5	57.1	63.8	68.5	73.1	79.8
	5.5	57.8	64.0	68.3	72.6	78.8
	6.5	58.2	64.0	68.1	72.2	78.0
	7.5	58.4	64.0	67.9	71.8	77.4
June	0.25	57.8	70.2	78.8	87.4	99.8
	0.75	59.6	70.9	78.7	86.5	97.8
	1.5	62.0	71.8	78.6	85.3	95.1
	2.5	64.4	72.6	78.4	84.1	92.3
	3.5	66.2	73.2	78.2	83.1	90.1
	4.5	67.3	73.6	78.0	82.3	88.6
	5.5	68.0	73.8	77.8	81.7	87.5
	6.5	68.5	73.8	77.6	81.3	86.6
	7.5	68.8	73.9	77.4	80.9	85.9
July	0.25	62.9	75.2	83.6	92.1	104.3
	0.75	64.8	75.8	83.5	91.2	102.3
	1.5	67.3	76.8	83.4	90.0	99.5
	2.5	69.8	77.7	83.2	88.7	96.5
	3.5	71.7	78.4	83.0	87.6	94.3
	4.5	72.9	78.8	82.8	86.9	92.7
	5.5	73.8	79.0	82.6	86.3	91.5
	6.5	74.3	79.1	82.5	85.8	90.6
	7.5	74.6	79.1	82.3	85.4	89.9
August	0.25	60.2	72.3	80.7	89.0	101.1
	0.75	62.0	73.0	80.6	88.2	99.2
	1.5	64.5	74.0	80.5	87.1	96.6
	2.5	67.0	74.9	80.4	85.9	93.8
	3.5	68.9	75.6	80.3	85.0	91.8
	4.5	70.1	76.1	80.2	84.4	90.3
	5.5	70.9	76.4	80.1	83.9	89.3
	6.5	71.5	76.5	80.0	83.5	88.5
	7.5	71.8	76.6	79.9	83.2	87.9

Table 10.1 (cont'd).

September	0.25	49.7	61.6	69.9	78.1	90.1
	0.75	51.3	62.3	69.9	77.5	88.5
	1.5	53.5	63.2	69.9	76.6	86.3
	2.5	55.8	64.1	69.9	75.7	84.1
	3.5	57.4	64.8	69.9	75.1	82.5
	4.5	58.5	65.2	70.0	74.7	81.4
	5.5	59.2	65.6	70.0	74.3	80.7
	6.5	59.8	65.8	70.0	74.1	80.1
	7.5	60.2	66.0	69.9	73.9	79.7
October	0.25	40.2	49.9	56.6	63.3	73.0
	0.75	41.4	50.4	56.7	62.9	71.9
	1.5	43.1	51.1	56.7	62.3	70.4
	2.5	44.8	51.9	56.8	61.7	68.8
	3.5	46.1	52.5	56.9	61.3	67.8
	4.5	46.9	52.9	57.0	61.1	67.0
	5.5	47.6	53.2	57.1	60.9	66.5
	6.5	48.1	53.4	57.1	60.8	66.2
	7.5	48.5	53.6	57.2	60.8	65.9
November	0.25	29.4	38.0	44.0	50.0	58.6
	0.75	30.3	38.4	44.1	49.7	57.9
	1.5	31.5	39.0	44.2	49.4	56.9
	2.5	32.7	39.6	44.3	49.1	55.9
	3.5	33.7	40.1	44.5	48.9	55.3
	4.5	34.4	40.4	44.6	48.8	54.9
	5.5	35.0	40.8	44.8	48.8	54.6
	6.5	35.4	41.0	44.9	48.8	54.3
	7.5	35.9	41.3	45.0	48.8	54.2
December	0.25	18.4	26.7	32.5	38.2	46.6
	0.75	19.2	27.1	32.6	38.1	46.0
	1.5	20.2	27.6	32.7	37.8	45.2
	2.5	21.3	28.2	32.9	37.7	44.5
	3.5	22.2	28.6	33.1	37.6	44.0
	4.5	22.9	29.0	33.3	37.5	43.7
	5.5	23.5	29.4	33.5	37.6	43.5
	6.5	24.0	29.7	33.6	37.6	43.3
	7.5	24.4	30.0	33.8	37.7	43.2

Table 10.2 Pavement temperatures for climate condition of Traverse City, Michigan.

Month	Depth (inch)	Temperature (Fahrenheit) for Each Quintile				
		Quintile 1	Quintile 2	Quintile 3	Quintile 4	Quintile 5
January	0.25	12.5	20.4	25.8	31.2	39.0
	0.75	13.4	20.7	25.9	31.0	38.3
	1.5	14.5	21.3	26.0	30.7	37.5
	2.5	15.8	21.9	26.1	30.4	36.5
	3.5	16.8	22.4	26.3	30.2	35.8
	4.5	17.7	22.9	26.5	30.0	35.2
	5.5	18.5	23.3	26.6	30.0	34.8
	6.5	19.1	23.7	26.8	29.9	34.4
	7.5	19.7	24.0	26.9	29.9	34.1
	8.5	20.3	24.3	27.1	29.9	33.9
	9.5	20.7	24.6	27.2	29.9	33.8
	10.5	21.2	24.9	27.4	30.0	33.6
	11.5	21.6	25.1	27.6	30.0	33.6
February	0.25	14.7	23.1	28.9	34.7	43.1
	0.75	15.6	23.5	28.9	34.4	42.3
	1.5	16.8	24.0	28.9	33.9	41.1
	2.5	18.1	24.6	29.0	33.4	39.8
	3.5	19.2	25.0	29.1	33.1	38.9
	4.5	20.1	25.4	29.1	32.8	38.1
	5.5	20.8	25.7	29.2	32.6	37.5
	6.5	21.4	26.0	29.2	32.4	37.1
	7.5	21.9	26.3	29.3	32.3	36.7
	8.5	22.4	26.5	29.4	32.2	36.4
	9.5	22.8	26.7	29.4	32.2	36.1
	10.5	23.1	26.9	29.5	32.1	35.9
	11.5	23.4	27.1	29.6	32.1	35.7
March	0.25	22.3	32.5	39.6	46.6	56.8
	0.75	23.3	32.9	39.5	46.1	55.7
	1.5	24.7	33.4	39.4	45.4	54.1
	2.5	26.1	33.9	39.3	44.7	52.5
	3.5	27.2	34.3	39.2	44.1	51.2
	4.5	28.0	34.6	39.1	43.7	50.2
	5.5	28.7	34.8	39.0	43.3	49.4
	6.5	29.2	35.0	39.0	43.0	48.7
	7.5	29.6	35.1	38.9	42.7	48.2
	8.5	29.9	35.2	38.8	42.5	47.7
	9.5	30.2	35.3	38.8	42.3	47.3
	10.5	30.5	35.3	38.7	42.1	47.0
	11.5	30.7	35.4	38.7	41.9	46.7

Table 10.2 (cont'd).

April	0.25	35.2	46.2	53.7	61.3	72.2
	0.75	36.5	46.6	53.6	60.7	70.8
	1.5	38.1	47.2	53.5	59.8	68.8
	2.5	39.9	47.8	53.3	58.8	66.7
	3.5	41.2	48.2	53.1	58.0	65.0
	4.5	42.1	48.5	52.9	57.3	63.7
	5.5	42.9	48.7	52.7	56.8	62.6
	6.5	43.4	48.8	52.6	56.3	61.8
	7.5	43.8	48.9	52.4	55.9	61.0
	8.5	44.1	48.9	52.3	55.6	60.4
	9.5	44.4	49.0	52.1	55.3	59.9
	10.5	44.5	48.9	52.0	55.0	59.4
	11.5	44.7	48.9	51.8	54.8	59.0
May	0.25	46.6	58.5	66.8	75.0	87.0
	0.75	48.1	59.1	66.6	74.2	85.2
	1.5	50.2	59.8	66.5	73.1	82.7
	2.5	52.4	60.6	66.2	71.9	80.0
	3.5	54.1	61.1	66.0	70.8	77.9
	4.5	55.3	61.5	65.7	70.0	76.2
	5.5	56.2	61.7	65.5	69.3	74.8
	6.5	56.8	61.8	65.3	68.8	73.7
	7.5	57.3	61.9	65.1	68.3	72.8
	8.5	57.6	61.9	64.9	67.8	72.1
	9.5	57.9	61.9	64.7	67.4	71.5
	10.5	58.0	61.8	64.5	67.1	70.9
	11.5	58.1	61.7	64.3	66.8	70.5
June	0.25	55.2	67.1	75.4	83.7	95.7
	0.75	56.9	67.8	75.3	82.9	93.7
	1.5	59.2	68.6	75.2	81.7	91.1
	2.5	61.7	69.5	74.9	80.3	88.2
	3.5	63.6	70.2	74.7	79.3	85.8
	4.5	65.0	70.6	74.5	78.4	84.0
	5.5	66.0	70.9	74.3	77.7	82.6
	6.5	66.8	71.1	74.1	77.1	81.4
	7.5	67.4	71.2	73.9	76.6	80.4
	8.5	67.7	71.2	73.7	76.1	79.7
	9.5	68.0	71.2	73.5	75.7	79.0
	10.5	68.1	71.2	73.3	75.4	78.5
	11.5	68.2	71.1	73.1	75.1	78.0

Table 10.2 (cont'd).

July	0.25	59.6	71.9	80.4	88.9	101.2
	0.75	61.4	72.6	80.3	88.0	99.2
	1.5	63.9	73.5	80.2	86.8	96.4
	2.5	66.6	74.5	80.0	85.4	93.3
	3.5	68.6	75.2	79.7	84.3	90.9
	4.5	70.1	75.7	79.5	83.4	89.0
	5.5	71.3	76.1	79.3	82.6	87.4
	6.5	72.2	76.3	79.1	82.0	86.1
	7.5	72.8	76.4	78.9	81.5	85.1
	8.5	73.3	76.5	78.7	81.0	84.2
	9.5	73.6	76.5	78.6	80.6	83.5
	10.5	73.8	76.5	78.4	80.2	82.9
	11.5	73.9	76.4	78.2	79.9	82.4
August	0.25	0.25	57.5	69.3	77.6	85.8
	0.75	0.75	59.3	70.0	77.5	85.0
	1.5	1.5	61.8	71.0	77.5	83.9
	2.5	2.5	64.4	72.1	77.4	82.7
	3.5	3.5	66.4	72.9	77.3	81.7
	4.5	4.5	68.0	73.4	77.2	81.0
	5.5	5.5	69.1	73.9	77.1	80.4
	6.5	6.5	70.0	74.2	77.0	79.9
	7.5	7.5	70.7	74.4	76.9	79.5
	8.5	8.5	71.2	74.5	76.8	79.1
	9.5	9.5	71.6	74.6	76.7	78.8
	10.5	10.5	71.8	74.7	76.6	78.5
	11.5	11.5	72.0	74.7	76.5	78.3
September	0.25	0.25	48.7	59.6	67.1	74.7
	0.75	0.75	50.2	60.2	67.1	74.1
	1.5	1.5	52.3	61.1	67.2	73.3
	2.5	2.5	54.6	62.1	67.3	72.4
	3.5	3.5	56.3	62.8	67.3	71.8
	4.5	4.5	57.6	63.4	67.4	71.4
	5.5	5.5	58.6	63.8	67.4	71.0
	6.5	6.5	59.4	64.2	67.5	70.7
	7.5	7.5	60.0	64.4	67.5	70.5
	8.5	8.5	60.5	64.6	67.5	70.4
	9.5	9.5	60.9	64.8	67.5	70.3
	10.5	10.5	61.1	64.9	67.6	70.2
	11.5	11.5	61.4	65.0	67.6	70.1

Table 10.2 (cont'd).

October	0.25	40.3	48.8	54.8	60.7	69.3
	0.75	41.4	49.3	54.8	60.3	68.3
	1.5	42.9	50.0	54.9	59.8	66.9
	2.5	44.6	50.8	55.1	59.4	65.5
	3.5	45.9	51.4	55.2	59.0	64.5
	4.5	46.9	51.9	55.3	58.8	63.7
	5.5	47.7	52.3	55.4	58.6	63.2
	6.5	48.4	52.6	55.6	58.5	62.7
	7.5	48.9	52.9	55.7	58.4	62.4
	8.5	49.3	53.1	55.8	58.4	62.2
	9.5	49.7	53.3	55.9	58.4	62.0
	10.5	50.0	53.5	55.9	58.4	61.9
	11.5	50.3	53.7	56.0	58.4	61.8
November	0.25	30.3	37.5	42.5	47.4	54.6
	0.75	31.1	37.9	42.6	47.2	54.0
	1.5	32.2	38.4	42.7	47.0	53.2
	2.5	33.4	39.0	42.9	46.8	52.4
	3.5	34.4	39.5	43.1	46.6	51.7
	4.5	35.2	40.0	43.3	46.6	51.3
	5.5	35.9	40.4	43.5	46.5	51.0
	6.5	36.5	40.7	43.6	46.5	50.8
	7.5	37.0	41.0	43.8	46.6	50.6
	8.5	37.4	41.3	44.0	46.6	50.5
	9.5	37.8	41.5	44.1	46.7	50.4
	10.5	38.1	41.8	44.3	46.8	50.4
	11.5	38.4	42.0	44.4	46.8	50.4
December	0.25	19.5	26.6	31.5	36.4	43.5
	0.75	20.2	27.0	31.6	36.3	43.0
	1.5	21.3	27.5	31.8	36.1	42.4
	2.5	22.4	28.1	32.0	36.0	41.7
	3.5	23.4	28.6	32.3	35.9	41.2
	4.5	24.2	29.1	32.5	35.9	40.8
	5.5	24.9	29.5	32.7	36.0	40.6
	6.5	25.5	29.9	33.0	36.0	40.4
	7.5	26.1	30.3	33.2	36.1	40.3
	8.5	26.5	30.6	33.4	36.2	40.3
	9.5	27.0	30.9	33.6	36.3	40.3
	10.5	27.4	31.2	33.8	36.5	40.3
	11.5	27.8	31.5	34.0	36.6	40.3

Table 10.3 Pavement temperatures for climate condition of Detroit, Michigan.

Month	Depth (inch)	Temperature (Fahrenheit) for Each Quintile				
		Quintile 1	Quintile 2	Quintile 3	Quintile 4	Quintile 5
January	0.25	16.59	24.89	30.64	36.39	44.69
	0.75	17.45	25.28	30.70	36.13	43.96
	1.5	18.63	25.82	30.80	35.78	42.97
	2.5	19.93	26.43	30.93	35.43	41.92
	3.5	21.01	26.94	31.06	35.17	41.10
	4.5	21.90	27.38	31.18	34.98	40.47
	5.5	22.67	27.77	31.31	34.85	39.95
	6.5	23.32	28.12	31.44	34.76	39.55
	7.5	23.91	28.43	31.57	34.70	39.22
	8.5	24.42	28.72	31.69	34.67	38.97
	9.5	24.88	28.98	31.82	34.66	38.76
	10.5	25.28	29.22	31.95	34.67	38.61
	11.5	25.66	29.45	32.07	34.70	38.49
February	0.25	19.25	28.26	34.50	40.75	49.76
	0.75	20.22	28.67	34.51	40.36	48.81
	1.5	21.55	29.22	34.53	39.84	47.50
	2.5	22.97	29.81	34.55	39.29	46.12
	3.5	24.11	30.29	34.57	38.86	45.04
	4.5	25.00	30.67	34.60	38.53	44.20
	5.5	25.75	31.00	34.63	38.27	43.52
	6.5	26.36	31.27	34.67	38.07	42.97
	7.5	26.88	31.50	34.70	37.90	42.52
	8.5	27.32	31.71	34.74	37.78	42.16
	9.5	27.71	31.89	34.78	37.68	41.85
	10.5	28.05	32.05	34.83	37.60	41.61
	11.5	28.35	32.21	34.88	37.55	41.40
March	0.25	28.01	38.45	45.67	52.90	63.33
	0.75	29.09	38.85	45.60	52.35	62.10
	1.5	30.55	39.37	45.49	51.60	60.42
	2.5	32.06	39.91	45.34	50.78	58.63
	3.5	33.20	40.29	45.20	50.11	57.21
	4.5	34.05	40.56	45.07	49.58	56.10
	5.5	34.72	40.76	44.95	49.14	55.18
	6.5	35.23	40.90	44.83	48.76	54.44
	7.5	35.64	41.01	44.73	48.44	53.81
	8.5	35.97	41.08	44.62	48.17	53.28
	9.5	36.23	41.13	44.53	47.93	52.83
	10.5	36.45	41.17	44.44	47.72	52.44
	11.5	36.63	41.20	44.36	47.53	52.10

Table 10.3 (cont'd).

April	0.25	40.56	51.74	59.49	67.23	78.42
	0.75	41.88	52.22	59.38	66.54	76.89
	1.5	43.67	52.86	59.22	65.59	74.78
	2.5	45.51	53.49	59.01	64.54	72.52
	3.5	46.91	53.94	58.81	63.68	70.71
	4.5	47.92	54.24	58.61	62.99	69.30
	5.5	48.70	54.45	58.42	62.40	68.14
	6.5	49.27	54.57	58.24	61.91	67.20
	7.5	49.71	54.64	58.06	61.47	66.41
	8.5	50.02	54.67	57.88	61.10	65.75
	9.5	50.26	54.66	57.72	60.77	65.17
	10.5	50.42	54.64	57.56	60.47	64.69
	11.5	50.54	54.60	57.40	60.21	64.26
May	0.25	52.43	64.46	72.79	81.12	93.14
	0.75	53.97	65.01	72.65	80.29	91.33
	1.5	56.07	65.74	72.44	79.14	88.82
	2.5	58.22	66.46	72.17	77.87	86.11
	3.5	59.85	66.97	71.90	76.83	83.94
	4.5	61.01	67.28	71.63	75.98	82.26
	5.5	61.88	67.49	71.37	75.26	80.86
	6.5	62.49	67.59	71.12	74.65	79.75
	7.5	62.93	67.62	70.87	74.12	78.81
	8.5	63.22	67.60	70.63	73.66	78.04
	9.5	63.41	67.54	70.39	73.25	77.37
	10.5	63.51	67.44	70.16	72.88	76.81
	11.5	63.55	67.32	69.94	72.55	76.32
June	0.25	61.75	74.07	82.60	91.13	103.44
	0.75	63.45	74.68	82.47	90.25	101.48
	1.5	65.77	75.52	82.27	89.01	98.76
	2.5	68.19	76.35	82.00	87.66	95.82
	3.5	70.03	76.95	81.74	86.54	93.46
	4.5	71.34	77.33	81.48	85.64	91.63
	5.5	72.34	77.59	81.23	84.87	90.12
	6.5	73.03	77.72	80.98	84.23	88.93
	7.5	73.53	77.78	80.73	83.67	87.93
	8.5	73.85	77.77	80.48	83.20	87.12
	9.5	74.05	77.71	80.24	82.77	86.42
	10.5	74.15	77.60	80.00	82.39	85.85
	11.5	74.18	77.48	79.76	82.04	85.34

Table 10.3 (cont'd).

July	0.25	66.77	78.81	87.14	95.48	107.51
	0.75	68.53	79.46	87.03	94.60	105.53
	1.5	70.96	80.35	86.86	93.37	102.77
	2.5	73.50	81.26	86.64	92.01	99.77
	3.5	75.47	81.93	86.41	90.89	97.36
	4.5	76.90	82.39	86.19	89.99	95.48
	5.5	78.02	82.71	85.96	89.21	93.91
	6.5	78.82	82.91	85.74	88.57	92.66
	7.5	79.43	83.03	85.52	88.01	91.60
	8.5	79.84	83.06	85.29	87.53	90.75
	9.5	80.13	83.05	85.07	87.09	90.01
	10.5	80.31	82.99	84.85	86.71	89.39
	11.5	80.40	82.90	84.63	86.36	88.85
August	0.25	63.91	75.90	84.21	92.52	104.51
	0.75	65.67	76.59	84.15	91.71	102.64
	1.5	68.09	77.53	84.06	90.60	100.03
	2.5	70.64	78.50	83.94	89.38	97.24
	3.5	72.61	79.23	83.81	88.40	95.01
	4.5	74.06	79.75	83.69	87.62	93.31
	5.5	75.20	80.14	83.56	86.98	91.91
	6.5	76.03	80.40	83.42	86.45	90.82
	7.5	76.67	80.58	83.29	86.00	89.90
	8.5	77.13	80.69	83.15	85.62	89.17
	9.5	77.47	80.74	83.01	85.28	88.55
	10.5	77.70	80.75	82.87	84.98	88.04
	11.5	77.86	80.73	82.72	84.71	87.59
September	0.25	53.38	65.28	73.51	81.75	93.64
	0.75	55.02	65.96	73.53	81.11	92.05
	1.5	57.25	66.89	73.56	80.24	89.88
	2.5	59.60	67.87	73.60	79.33	87.60
	3.5	61.43	68.64	73.64	78.63	85.85
	4.5	62.78	69.21	73.67	78.12	84.55
	5.5	63.86	69.67	73.69	77.71	83.52
	6.5	64.67	70.01	73.71	77.41	82.75
	7.5	65.32	70.28	73.72	77.16	82.12
	8.5	65.81	70.49	73.73	76.96	81.64
	9.5	66.22	70.65	73.73	76.80	81.24
	10.5	66.53	70.78	73.72	76.66	80.91
	11.5	66.78	70.87	73.70	76.54	80.63

Table 10.3 (cont'd).

October	0.25	43.82	53.58	60.34	67.09	76.85
	0.75	45.10	54.14	60.39	66.65	75.68
	1.5	46.86	54.90	60.47	66.04	74.09
	2.5	48.72	55.73	60.58	65.43	72.44
	3.5	50.18	56.39	60.68	64.98	71.18
	4.5	51.30	56.90	60.78	64.66	70.25
	5.5	52.21	57.33	60.87	64.41	69.53
	6.5	52.93	57.67	60.96	64.24	68.98
	7.5	53.53	57.97	61.04	64.11	68.54
	8.5	54.01	58.21	61.11	64.02	68.21
	9.5	54.42	58.42	61.18	63.95	67.94
	10.5	54.76	58.59	61.25	63.90	67.73
	11.5	55.05	58.74	61.30	63.86	67.56
November	0.25	33.41	41.89	47.76	53.64	62.12
	0.75	34.35	42.33	47.85	53.37	61.35
	1.5	35.66	42.94	47.98	53.03	60.31
	2.5	37.07	43.62	48.16	52.69	59.24
	3.5	38.22	44.19	48.32	52.45	58.42
	4.5	39.15	44.66	48.48	52.30	57.82
	5.5	39.93	45.07	48.64	52.20	57.35
	6.5	40.58	45.43	48.79	52.15	57.00
	7.5	41.14	45.74	48.93	52.12	56.72
	8.5	41.62	46.02	49.07	52.12	56.52
	9.5	42.04	46.27	49.20	52.13	56.36
	10.5	42.40	46.49	49.33	52.16	56.25
	11.5	42.73	46.70	49.45	52.20	56.17
December	0.25	21.60	30.05	35.91	41.77	50.22
	0.75	22.46	30.48	36.03	41.58	49.59
	1.5	23.66	31.07	36.21	41.34	48.75
	2.5	24.98	31.75	36.44	41.13	47.90
	3.5	26.08	32.33	36.67	41.00	47.25
	4.5	26.99	32.84	36.89	40.94	46.79
	5.5	27.78	33.29	37.11	40.92	46.43
	6.5	28.47	33.70	37.32	40.95	46.18
	7.5	29.08	34.07	37.53	40.99	45.98
	8.5	29.62	34.41	37.73	41.06	45.85
	9.5	30.10	34.73	37.93	41.14	45.76
	10.5	30.54	35.02	38.13	41.23	45.71
	11.5	30.94	35.30	38.31	41.33	45.68

Table 10.4 Pavement ME frequencies at different depths within the AC layer for all structures (depths below 6 inches).

Month	Quintile	Loading Frequencies (Hz) at Mid Depth of Each AC Sublayer						
		0.25 inch	0.75 inch	1.5 inch	2.5 inch	3.5 inch	4.5 inch	5.5 inch
January	1	120.47	84.64	58.53	41.47	32.11	26.20	21.82
	2	120.47	84.64	58.53	41.47	32.11	26.20	21.82
	3	120.47	84.64	58.53	41.47	32.11	26.20	21.82
	4	120.47	84.64	58.53	41.47	32.11	26.20	21.82
	5	120.47	84.64	58.53	41.47	32.11	26.20	21.82
February	1	120.47	84.64	58.53	41.47	32.11	26.20	21.82
	2	120.47	84.64	58.53	41.47	32.11	26.20	21.82
	3	120.47	84.64	58.53	41.47	32.11	26.20	21.82
	4	120.47	84.64	58.53	41.47	32.11	26.20	21.82
	5	120.47	84.64	58.53	41.47	32.11	26.20	21.82
March	1	120.47	84.64	58.53	41.47	32.11	26.20	21.82
	2	120.47	84.64	58.53	41.47	32.11	26.20	21.82
	3	120.47	84.64	58.53	41.47	32.11	26.20	21.82
	4	120.47	84.64	58.53	41.47	32.11	26.20	21.82
	5	120.47	84.64	58.53	41.47	32.11	26.20	21.82
April	1	120.47	84.64	58.53	41.47	32.11	26.20	21.82
	2	120.47	84.64	58.53	41.47	32.11	26.20	21.82
	3	120.47	84.64	58.53	41.47	32.11	26.20	21.82
	4	120.47	84.64	58.53	41.47	32.11	26.20	21.82
	5	120.47	84.64	58.53	41.47	32.11	26.20	21.82
May	1	120.47	84.64	58.53	41.47	32.11	26.20	21.82
	2	120.47	84.64	58.53	41.47	32.11	26.20	21.82
	3	120.47	84.64	58.53	41.47	32.11	26.20	21.82
	4	120.47	84.64	58.53	41.47	32.11	26.20	21.82
	5	120.47	84.64	58.53	41.47	32.11	26.20	21.82
June	1	120.47	84.64	58.53	41.47	32.11	26.20	21.82
	2	120.47	84.64	58.53	41.47	32.11	26.20	21.82
	3	120.47	84.64	58.53	41.47	32.11	26.20	21.82
	4	120.47	84.64	58.53	41.47	32.11	26.20	21.82
	5	120.47	84.64	58.53	41.47	32.11	26.20	21.82

Table 10.4 (cont'd).

July	1	120.47	84.64	58.53	41.47	32.11	26.20	21.82
	2	120.47	84.64	58.53	41.47	32.11	26.20	21.82
	3	120.47	84.64	58.53	41.47	32.11	26.20	21.82
	4	120.47	84.64	58.53	41.47	32.11	26.20	21.82
	5	120.47	84.64	58.53	41.47	32.11	26.20	21.82
August	1	120.47	84.64	58.53	41.47	32.11	26.20	21.82
	2	120.47	84.64	58.53	41.47	32.11	26.20	21.82
	3	120.47	84.64	58.53	41.47	32.11	26.20	21.82
	4	120.47	84.64	58.53	41.47	32.11	26.20	21.82
	5	120.47	84.64	58.53	41.47	32.11	26.20	21.82
September	1	120.47	84.64	58.53	41.47	32.11	26.20	21.82
	2	120.47	84.64	58.53	41.47	32.11	26.20	21.82
	3	120.47	84.64	58.53	41.47	32.11	26.20	21.82
	4	120.47	84.64	58.53	41.47	32.11	26.20	21.82
	5	120.47	84.64	58.53	41.47	32.11	26.20	21.82
October	1	120.47	84.64	58.53	41.47	32.11	26.20	21.82
	2	120.47	84.64	58.53	41.47	32.11	26.20	21.82
	3	120.47	84.64	58.53	41.47	32.11	26.20	21.82
	4	120.47	84.64	58.53	41.47	32.11	26.20	21.82
	5	120.47	84.64	58.53	41.47	32.11	26.20	21.82
November	1	120.47	84.64	58.53	41.47	32.11	26.20	21.82
	2	120.47	84.64	58.53	41.47	32.11	26.20	21.82
	3	120.47	84.64	58.53	41.47	32.11	26.20	21.82
	4	120.47	84.64	58.53	41.47	32.11	26.20	21.82
	5	120.47	84.64	58.53	41.47	32.11	26.20	21.82
December	1	120.47	84.64	58.53	41.47	32.11	26.20	21.82
	2	120.47	84.64	58.53	41.47	32.11	26.20	21.82
	3	120.47	84.64	58.53	41.47	32.11	26.20	21.82
	4	120.47	84.64	58.53	41.47	32.11	26.20	21.82
	5	120.47	84.64	58.53	41.47	32.11	26.20	21.82

Table 10.5 Pavement ME frequencies at different depths within the AC layer for all structures (depths greater than 6 inches).

Month	Quintile	Loading Frequencies (Hz) at Mid Depth of Each AC Sublayer					
		6.5 inch	7.5 inch	8.5 inch	9.5 inch	10.5 inch	11.5 inch
January	1	18.28	15.71	13.76	12.24	11.01	10.00
	2	18.28	15.71	13.76	12.24	11.01	10.00
	3	18.28	15.71	13.76	12.24	11.01	10.00
	4	18.28	15.71	13.76	12.24	11.01	10.00
	5	18.28	15.71	13.76	12.24	11.01	10.00
February	1	18.28	15.71	13.76	12.24	11.01	10.00
	2	18.28	15.71	13.76	12.24	11.01	10.00
	3	18.28	15.71	13.76	12.24	11.01	10.00
	4	18.28	15.71	13.76	12.24	11.01	10.00
	5	18.28	15.71	13.76	12.24	11.01	10.00
March	1	18.28	15.71	13.76	12.24	11.01	10.00
	2	18.28	15.71	13.76	12.24	11.01	10.00
	3	18.28	15.71	13.76	12.24	11.01	10.00
	4	18.28	15.71	13.76	12.24	11.01	10.00
	5	18.28	15.71	13.76	12.24	11.01	10.00
April	1	18.28	15.71	13.76	12.24	11.01	10.00
	2	18.28	15.71	13.76	12.24	11.01	10.00
	3	18.28	15.71	13.76	12.24	11.01	10.00
	4	18.28	15.71	13.76	12.24	11.01	10.00
	5	18.28	15.71	13.76	12.24	11.01	10.00
May	1	18.28	15.71	13.76	12.24	11.01	10.00
	2	18.28	15.71	13.76	12.24	11.01	10.00
	3	18.28	15.71	13.76	12.24	11.01	10.00
	4	18.28	15.71	13.76	12.24	11.01	10.00
	5	18.28	15.71	13.76	12.24	11.01	10.00
June	1	18.28	15.71	13.76	12.24	11.01	10.00
	2	18.28	15.71	13.76	12.24	11.01	10.00
	3	18.28	15.71	13.76	12.24	11.01	10.00
	4	18.28	15.71	13.76	12.24	11.01	10.00
	5	18.28	15.71	13.76	12.24	11.01	10.00

Table 10.5 (cont'd).

July	1	18.28	15.71	13.76	12.24	11.01	10.00
	2	18.28	15.71	13.76	12.24	11.01	10.00
	3	18.28	15.71	13.76	12.24	11.01	10.00
	4	18.28	15.71	13.76	12.24	11.01	10.00
	5	18.28	15.71	13.76	12.24	11.01	10.00
August	1	18.28	15.71	13.76	12.24	11.01	10.00
	2	18.28	15.71	13.76	12.24	11.01	10.00
	3	18.28	15.71	13.76	12.24	11.01	10.00
	4	18.28	15.71	13.76	12.24	11.01	10.00
	5	18.28	15.71	13.76	12.24	11.01	10.00
September	1	18.28	15.71	13.76	12.24	11.01	10.00
	2	18.28	15.71	13.76	12.24	11.01	10.00
	3	18.28	15.71	13.76	12.24	11.01	10.00
	4	18.28	15.71	13.76	12.24	11.01	10.00
	5	18.28	15.71	13.76	12.24	11.01	10.00
October	1	18.28	15.71	13.76	12.24	11.01	10.00
	2	18.28	15.71	13.76	12.24	11.01	10.00
	3	18.28	15.71	13.76	12.24	11.01	10.00
	4	18.28	15.71	13.76	12.24	11.01	10.00
	5	18.28	15.71	13.76	12.24	11.01	10.00
November	1	18.28	15.71	13.76	12.24	11.01	10.00
	2	18.28	15.71	13.76	12.24	11.01	10.00
	3	18.28	15.71	13.76	12.24	11.01	10.00
	4	18.28	15.71	13.76	12.24	11.01	10.00
	5	18.28	15.71	13.76	12.24	11.01	10.00
December	1	18.28	15.71	13.76	12.24	11.01	10.00
	2	18.28	15.71	13.76	12.24	11.01	10.00
	3	18.28	15.71	13.76	12.24	11.01	10.00
	4	18.28	15.71	13.76	12.24	11.01	10.00
	5	18.28	15.71	13.76	12.24	11.01	10.00

Table 10.6 Corrected Pavement ME frequencies at different depths within the AC layer for BL-I-94.

Month	Quintile	Loading Frequencies (Hz) at Mid Depth of Each AC Sublayer								
		0.25 inch	0.75 inch	1.5 inch	2.5 inch	3.5 inch	4.5 inch	5.5 inch	6.5 inch	7.5 inch
January	1	16.10	18.50	23.82	38.64	32.27	27.70	24.26	13.93	7.83
	2	16.15	18.55	23.87	38.64	32.27	27.70	24.26	14.08	7.97
	3	16.20	18.60	23.91	38.64	32.27	27.70	24.26	14.20	8.08
	4	16.24	18.64	23.96	38.64	32.27	27.70	24.26	14.33	8.21
	5	16.32	18.72	24.03	38.64	32.27	27.70	24.26	14.54	8.42
February	1	16.13	18.53	23.85	38.64	32.27	27.70	24.26	14.01	7.90
	2	16.19	18.59	23.90	38.64	32.27	27.70	24.26	14.18	8.06
	3	16.24	18.64	23.95	38.64	32.27	27.70	24.26	14.31	8.19
	4	16.29	18.69	24.00	38.64	32.27	27.70	24.26	14.46	8.34
	5	16.38	18.78	24.09	38.64	32.27	27.70	24.26	14.69	8.57
March	1	16.22	18.62	23.94	38.64	32.27	27.70	24.26	14.27	8.15
	2	16.31	18.71	24.02	38.64	32.27	27.70	24.26	14.51	8.39
	3	16.38	18.78	24.09	38.64	32.27	27.70	24.26	14.70	8.59
	4	16.46	18.86	24.17	38.64	32.27	27.70	24.26	14.92	8.80
	5	16.59	19.00	24.29	38.64	32.27	27.70	24.26	15.26	9.17
April	1	16.41	18.82	24.12	38.64	32.27	27.70	24.26	14.80	8.68
	2	16.53	18.94	24.24	38.64	32.27	27.70	24.26	15.11	9.01
	3	16.62	19.03	24.32	38.64	32.27	27.70	24.26	15.35	9.27
	4	16.73	19.14	24.42	38.64	32.27	27.70	24.26	15.62	9.57
	5	16.90	19.31	24.58	38.64	32.27	27.70	24.26	16.04	10.06
May	1	16.66	19.07	24.36	38.64	32.27	27.70	24.26	15.45	9.37
	2	16.81	19.23	24.50	38.64	32.27	27.70	24.26	15.84	9.82
	3	16.93	19.35	24.62	38.64	32.27	27.70	24.26	16.14	10.17
	4	17.07	19.48	24.74	38.64	32.27	27.70	24.26	16.46	10.56
	5	17.28	19.70	24.94	38.64	32.27	27.70	24.26	16.96	11.20
June	1	16.91	19.32	24.59	38.64	32.27	27.70	24.26	16.07	10.09
	2	17.08	19.50	24.76	38.64	32.27	27.70	24.26	16.51	10.62
	3	17.22	19.64	24.89	38.64	32.27	27.70	24.26	16.83	11.03
	4	17.37	19.79	25.02	38.64	32.27	27.70	24.26	17.17	11.48
	5	17.61	20.03	25.24	38.64	32.27	27.70	24.26	17.70	12.21

Table 10.6 (cont'd).

July	1	17.06	19.48	24.74	38.64	32.27	27.70	24.26	16.46	10.55
	2	17.24	19.66	24.90	38.64	32.27	27.70	24.26	16.87	11.08
	3	17.38	19.80	25.03	38.64	32.27	27.70	24.26	17.19	11.49
	4	17.52	19.94	25.16	38.64	32.27	27.70	24.26	17.51	11.94
	5	17.75	20.18	25.37	38.64	32.27	27.70	24.26	18.01	12.66
August	1	16.98	19.40	24.66	38.64	32.27	27.70	24.26	16.26	10.31
	2	17.16	19.58	24.83	38.64	32.27	27.70	24.26	16.68	10.84
	3	17.29	19.71	24.95	38.64	32.27	27.70	24.26	16.99	11.24
	4	17.44	19.86	25.09	38.64	32.27	27.70	24.26	17.32	11.68
	5	17.67	20.09	25.30	38.64	32.27	27.70	24.26	17.83	12.39
September	1	16.70	19.11	24.40	38.64	32.27	27.70	24.26	15.55	9.49
	2	16.86	19.28	24.55	38.64	32.27	27.70	24.26	15.96	9.96
	3	16.99	19.41	24.67	38.64	32.27	27.70	24.26	16.27	10.33
	4	17.13	19.55	24.80	38.64	32.27	27.70	24.26	16.61	10.74
	5	17.35	19.77	25.00	38.64	32.27	27.70	24.26	17.13	11.41
October	1	16.47	18.88	24.18	38.64	32.27	27.70	24.26	14.96	8.85
	2	16.58	18.99	24.29	38.64	32.27	27.70	24.26	15.25	9.16
	3	16.67	19.08	24.37	38.64	32.27	27.70	24.26	15.47	9.40
	4	16.76	19.18	24.46	38.64	32.27	27.70	24.26	15.71	9.67
	5	16.91	19.33	24.60	38.64	32.27	27.70	24.26	16.09	10.11
November	1	16.29	18.69	24.00	38.64	32.27	27.70	24.26	14.45	8.33
	2	16.37	18.77	24.08	38.64	32.27	27.70	24.26	14.68	8.56
	3	16.43	18.84	24.14	38.64	32.27	27.70	24.26	14.85	8.74
	4	16.50	18.91	24.21	38.64	32.27	27.70	24.26	15.04	8.93
	5	16.62	19.03	24.32	38.64	32.27	27.70	24.26	15.34	9.25
December	1	16.15	18.55	23.87	38.64	32.27	27.70	24.26	14.07	7.95
	2	16.21	18.61	23.93	38.64	32.27	27.70	24.26	14.25	8.13
	3	16.26	18.67	23.98	38.64	32.27	27.70	24.26	14.39	8.27
	4	16.32	18.72	24.03	38.64	32.27	27.70	24.26	14.54	8.42
	5	16.41	18.82	24.12	38.64	32.27	27.70	24.26	14.79	8.68

Table 10.7 Corrected Pavement ME frequencies at different depths within the AC layer for US-127.

Month	Quintile	Loading Frequencies (Hz) at Mid Depth of Each AC Sublayer								
		0.25 inch	0.75 inch	1.5 inch	2.5 inch	3.5 inch	4.5 inch	5.5 inch	6.5 inch	7.5 inch
January	1	16.16	18.56	23.88	38.64	32.27	27.70	24.26	14.11	7.99
	2	16.22	18.62	23.94	38.64	32.27	27.70	24.26	14.27	8.16
	3	16.27	18.67	23.99	38.64	32.27	27.70	24.26	14.41	8.29
	4	16.33	18.73	24.04	38.64	32.27	27.70	24.26	14.56	8.44
	5	16.42	18.82	24.13	38.64	32.27	27.70	24.26	14.81	8.69
February	1	16.19	18.59	23.91	38.64	32.27	27.70	24.26	14.19	8.07
	2	16.26	18.66	23.97	38.64	32.27	27.70	24.26	14.38	8.26
	3	16.31	18.72	24.03	38.64	32.27	27.70	24.26	14.53	8.41
	4	16.38	18.78	24.09	38.64	32.27	27.70	24.26	14.70	8.58
	5	16.48	18.89	24.19	38.64	32.27	27.70	24.26	14.98	8.87
March	1	16.28	18.68	23.99	38.64	32.27	27.70	24.26	14.42	8.30
	2	16.38	18.78	24.09	38.64	32.27	27.70	24.26	14.70	8.58
	3	16.46	18.87	24.17	38.64	32.27	27.70	24.26	14.93	8.82
	4	16.56	18.97	24.26	38.64	32.27	27.70	24.26	15.19	9.09
	5	16.73	19.14	24.42	38.64	32.27	27.70	24.26	15.62	9.56
April	1	16.48	18.89	24.19	38.64	32.27	27.70	24.26	14.98	8.87
	2	16.62	19.03	24.32	38.64	32.27	27.70	24.26	15.34	9.26
	3	16.73	19.14	24.43	38.64	32.27	27.70	24.26	15.63	9.58
	4	16.85	19.27	24.54	38.64	32.27	27.70	24.26	15.94	9.94
	5	17.06	19.48	24.73	38.64	32.27	27.70	24.26	16.44	10.54
May	1	16.73	19.14	24.42	38.64	32.27	27.70	24.26	15.61	9.56
	2	16.90	19.32	24.59	38.64	32.27	27.70	24.26	16.06	10.08
	3	17.04	19.46	24.72	38.64	32.27	27.70	24.26	16.41	10.49
	4	17.20	19.62	24.87	38.64	32.27	27.70	24.26	16.78	10.96
	5	17.45	19.88	25.10	38.64	32.27	27.70	24.26	17.36	11.73
June	1	16.97	19.39	24.65	38.64	32.27	27.70	24.26	16.23	10.28
	2	17.17	19.59	24.84	38.64	32.27	27.70	24.26	16.72	10.88
	3	17.33	19.75	24.99	38.64	32.27	27.70	24.26	17.08	11.36
	4	17.50	19.93	25.15	38.64	32.27	27.70	24.26	17.47	11.88
	5	17.78	20.20	25.40	38.64	32.27	27.70	24.26	18.07	12.74
July	1	17.13	19.55	24.80	38.64	32.27	27.70	24.26	16.61	10.74
	2	17.33	19.76	24.99	38.64	32.27	27.70	24.26	17.09	11.37
	3	17.49	19.92	25.14	38.64	32.27	27.70	24.26	17.45	11.85
	4	17.67	20.09	25.30	38.64	32.27	27.70	24.26	17.83	12.39
	5	17.94	20.37	25.55	38.64	32.27	27.70	24.26	18.40	13.25

Table 10.7 (cont'd).

July	1	17.13	19.55	24.80	38.64	32.27	27.70	24.26	16.61	10.74
	2	17.33	19.76	24.99	38.64	32.27	27.70	24.26	17.09	11.37
	3	17.49	19.92	25.14	38.64	32.27	27.70	24.26	17.45	11.85
	4	17.67	20.09	25.30	38.64	32.27	27.70	24.26	17.83	12.39
	5	17.94	20.37	25.55	38.64	32.27	27.70	24.26	18.40	13.25
August	1	17.05	19.46	24.72	38.64	32.27	27.70	24.26	16.41	10.50
	2	17.25	19.67	24.91	38.64	32.27	27.70	24.26	16.89	11.10
	3	17.40	19.83	25.05	38.64	32.27	27.70	24.26	17.25	11.58
	4	17.57	20.00	25.21	38.64	32.27	27.70	24.26	17.63	12.10
	5	17.84	20.27	25.46	38.64	32.27	27.70	24.26	18.20	12.94
September	1	16.76	19.17	24.45	38.64	32.27	27.70	24.26	15.69	9.65
	2	16.94	19.35	24.62	38.64	32.27	27.70	24.26	16.15	10.18
	3	17.08	19.50	24.76	38.64	32.27	27.70	24.26	16.50	10.61
	4	17.24	19.66	24.90	38.64	32.27	27.70	24.26	16.88	11.09
	5	17.50	19.92	25.14	38.64	32.27	27.70	24.26	17.46	11.87
October	1	16.53	18.94	24.23	38.64	32.27	27.70	24.26	15.11	9.01
	2	16.65	19.06	24.35	38.64	32.27	27.70	24.26	15.43	9.36
	3	16.75	19.16	24.45	38.64	32.27	27.70	24.26	15.68	9.64
	4	16.86	19.27	24.55	38.64	32.27	27.70	24.26	15.95	9.95
	5	17.03	19.45	24.71	38.64	32.27	27.70	24.26	16.38	10.46
November	1	16.34	18.75	24.05	38.64	32.27	27.70	24.26	14.60	8.48
	2	16.43	18.84	24.14	38.64	32.27	27.70	24.26	14.85	8.74
	3	16.51	18.91	24.21	38.64	32.27	27.70	24.26	15.04	8.94
	4	16.59	19.00	24.29	38.64	32.27	27.70	24.26	15.26	9.17
	5	16.72	19.13	24.42	38.64	32.27	27.70	24.26	15.60	9.55
December	1	16.21	18.61	23.93	38.64	32.27	27.70	24.26	14.24	8.13
	2	16.28	18.68	23.99	38.64	32.27	27.70	24.26	14.43	8.31
	3	16.34	18.74	24.05	38.64	32.27	27.70	24.26	14.58	8.46
	4	16.40	18.80	24.11	38.64	32.27	27.70	24.26	14.75	8.64
	5	16.50	18.91	24.21	38.64	32.27	27.70	24.26	15.03	8.92

Table 10.8 Corrected Pavement ME frequencies at different depths within the AC layer for US-131.

Month	Quintile	Loading Frequencies (Hz) at Mid Depth of Each AC Sublayer						
		0.25 inch	0.75 inch	1.5 inch	2.5 inch	3.5 inch	4.5 inch	5.5 inch
January	1	16.08	18.47	23.80	38.64	32.27	27.70	10.78
	2	16.13	18.52	23.84	38.64	32.27	27.70	10.95
	3	16.17	18.57	23.88	38.64	32.27	27.70	11.08
	4	16.21	18.61	23.93	38.64	32.27	27.70	11.24
	5	16.29	18.69	24.00	38.64	32.27	27.70	11.50
February	1	16.09	18.49	23.81	38.64	32.27	27.70	10.84
	2	16.15	18.55	23.87	38.64	32.27	27.70	11.03
	3	16.19	18.60	23.91	38.64	32.27	27.70	11.19
	4	16.25	18.65	23.96	38.64	32.27	27.70	11.36
	5	16.33	18.74	24.04	38.64	32.27	27.70	11.66
March	1	16.17	18.57	23.88	38.64	32.27	27.70	11.09
	2	16.25	18.65	23.97	38.64	32.27	27.70	11.38
	3	16.32	18.73	24.04	38.64	32.27	27.70	11.63
	4	16.40	18.81	24.11	38.64	32.27	27.70	11.91
	5	16.54	18.95	24.25	38.64	32.27	27.70	12.40
April	1	16.33	18.74	24.05	38.64	32.27	27.70	11.66
	2	16.46	18.86	24.16	38.64	32.27	27.70	12.09
	3	16.56	18.97	24.26	38.64	32.27	27.70	12.45
	4	16.67	19.08	24.37	38.64	32.27	27.70	12.85
	5	16.86	19.27	24.55	38.64	32.27	27.70	13.53
May	1	16.54	18.95	24.25	38.64	32.27	27.70	12.41
	2	16.71	19.12	24.41	38.64	32.27	27.70	12.99
	3	16.84	19.26	24.53	38.64	32.27	27.70	13.47
	4	16.99	19.41	24.67	38.64	32.27	27.70	14.01
	5	17.24	19.66	24.90	38.64	32.27	27.70	14.90
June	1	16.74	19.16	24.44	38.64	32.27	27.70	13.11
	2	16.93	19.35	24.61	38.64	32.27	27.70	13.79
	3	17.08	19.50	24.75	38.64	32.27	27.70	14.33
	4	17.24	19.66	24.91	38.64	32.27	27.70	14.92
	5	17.51	19.93	25.15	38.64	32.27	27.70	15.89
July	1	16.86	19.28	24.55	38.64	32.27	27.70	13.55
	2	17.07	19.49	24.74	38.64	32.27	27.70	14.29
	3	17.23	19.65	24.90	38.64	32.27	27.70	14.88
	4	17.41	19.83	25.06	38.64	32.27	27.70	15.53
	5	17.69	20.12	25.32	38.64	32.27	27.70	16.56

Table 10.8 (cont'd).

July	1	16.86	19.28	24.55	38.64	32.27	27.70	13.55
	2	17.07	19.49	24.74	38.64	32.27	27.70	14.29
	3	17.23	19.65	24.90	38.64	32.27	27.70	14.88
	4	17.41	19.83	25.06	38.64	32.27	27.70	15.53
	5	17.69	20.12	25.32	38.64	32.27	27.70	16.56
August	1	16.81	19.22	24.50	38.64	32.27	27.70	13.35
	2	17.00	19.42	24.68	38.64	32.27	27.70	14.05
	3	17.15	19.57	24.82	38.64	32.27	27.70	14.60
	4	17.32	19.74	24.98	38.64	32.27	27.70	15.20
	5	17.59	20.01	25.22	38.64	32.27	27.70	16.18
September	1	16.59	19.00	24.29	38.64	32.27	27.70	12.56
	2	16.75	19.16	24.44	38.64	32.27	27.70	13.13
	3	16.87	19.29	24.56	38.64	32.27	27.70	13.58
	4	17.01	19.43	24.69	38.64	32.27	27.70	14.08
	5	17.24	19.66	24.90	38.64	32.27	27.70	14.90
October	1	16.41	18.81	24.12	38.64	32.27	27.70	11.92
	2	16.51	18.92	24.22	38.64	32.27	27.70	12.29
	3	16.59	19.00	24.30	38.64	32.27	27.70	12.58
	4	16.68	19.10	24.38	38.64	32.27	27.70	12.90
	5	16.83	19.25	24.52	38.64	32.27	27.70	13.43
November	1	16.25	18.65	23.96	38.64	32.27	27.70	11.37
	2	16.32	18.72	24.03	38.64	32.27	27.70	11.62
	3	16.38	18.78	24.09	38.64	32.27	27.70	11.82
	4	16.44	18.85	24.15	38.64	32.27	27.70	12.04
	5	16.54	18.95	24.25	38.64	32.27	27.70	12.39
December	1	16.13	18.53	23.85	38.64	32.27	27.70	10.97
	2	16.19	18.59	23.90	38.64	32.27	27.70	11.16
	3	16.23	18.63	23.95	38.64	32.27	27.70	11.31
	4	16.28	18.68	23.99	38.64	32.27	27.70	11.48
	5	16.36	18.76	24.07	38.64	32.27	27.70	11.75

Table 10.9 Corrected Pavement ME frequencies at different depths within the AC layer for I-94 (depths below 6 inches).

Month	Quintile	Loading Frequencies (Hz) at Mid Depth of Each AC Sublayer						
		0.25 inch	0.75 inch	1.5 inch	2.5 inch	3.5 inch	4.5 inch	5.5 inch
January	1	16.13	18.53	23.85	38.64	32.27	27.70	24.26
	2	16.19	18.59	23.90	38.64	32.27	27.70	24.26
	3	16.23	18.63	23.94	38.64	32.27	27.70	24.26
	4	16.27	18.68	23.99	38.64	32.27	27.70	24.26
	5	16.35	18.76	24.06	38.64	32.27	27.70	24.26
February	1	16.16	18.56	23.88	38.64	32.27	27.70	24.26
	2	16.22	18.62	23.94	38.64	32.27	27.70	24.26
	3	16.27	18.67	23.99	38.64	32.27	27.70	24.26
	4	16.32	18.73	24.04	38.64	32.27	27.70	24.26
	5	16.41	18.82	24.12	38.64	32.27	27.70	24.26
March	1	16.27	18.67	23.98	38.64	32.27	27.70	24.26
	2	16.36	18.76	24.07	38.64	32.27	27.70	24.26
	3	16.43	18.84	24.14	38.64	32.27	27.70	24.26
	4	16.51	18.92	24.22	38.64	32.27	27.70	24.26
	5	16.64	19.05	24.34	38.64	32.27	27.70	24.26
April	1	16.50	18.91	24.21	38.64	32.27	27.70	24.26
	2	16.62	19.03	24.32	38.64	32.27	27.70	24.26
	3	16.71	19.13	24.41	38.64	32.27	27.70	24.26
	4	16.82	19.23	24.51	38.64	32.27	27.70	24.26
	5	16.98	19.40	24.66	38.64	32.27	27.70	24.26
May	1	16.80	19.21	24.49	38.64	32.27	27.70	24.26
	2	16.95	19.37	24.64	38.64	32.27	27.70	24.26
	3	17.07	19.49	24.75	38.64	32.27	27.70	24.26
	4	17.20	19.62	24.86	38.64	32.27	27.70	24.26
	5	17.40	19.82	25.05	38.64	32.27	27.70	24.26
June	1	17.11	19.53	24.78	38.64	32.27	27.70	24.26
	2	17.28	19.70	24.94	38.64	32.27	27.70	24.26
	3	17.41	19.83	25.06	38.64	32.27	27.70	24.26
	4	17.54	19.97	25.18	38.64	32.27	27.70	24.26
	5	17.76	20.19	25.38	38.64	32.27	27.70	24.26
July	1	17.31	19.73	24.96	38.64	32.27	27.70	24.26
	2	17.47	19.89	25.11	38.64	32.27	27.70	24.26
	3	17.59	20.01	25.22	38.64	32.27	27.70	24.26
	4	17.72	20.14	25.34	38.64	32.27	27.70	24.26
	5	17.92	20.34	25.52	38.64	32.27	27.70	24.26

Table 10.9 (cont'd).

July	1	17.31	19.73	24.96	38.64	32.27	27.70	24.26
	2	17.47	19.89	25.11	38.64	32.27	27.70	24.26
	3	17.59	20.01	25.22	38.64	32.27	27.70	24.26
	4	17.72	20.14	25.34	38.64	32.27	27.70	24.26
	5	17.92	20.34	25.52	38.64	32.27	27.70	24.26
August	1	17.21	19.63	24.88	38.64	32.27	27.70	24.26
	2	17.37	19.80	25.03	38.64	32.27	27.70	24.26
	3	17.50	19.92	25.14	38.64	32.27	27.70	24.26
	4	17.63	20.05	25.26	38.64	32.27	27.70	24.26
	5	17.84	20.26	25.45	38.64	32.27	27.70	24.26
September	1	16.86	19.28	24.55	38.64	32.27	27.70	24.26
	2	17.03	19.45	24.71	38.64	32.27	27.70	24.26
	3	17.15	19.57	24.82	38.64	32.27	27.70	24.26
	4	17.29	19.71	24.95	38.64	32.27	27.70	24.26
	5	17.51	19.93	25.15	38.64	32.27	27.70	24.26
October	1	16.58	18.99	24.28	38.64	32.27	27.70	24.26
	2	16.69	19.11	24.39	38.64	32.27	27.70	24.26
	3	16.78	19.19	24.47	38.64	32.27	27.70	24.26
	4	16.88	19.29	24.56	38.64	32.27	27.70	24.26
	5	17.03	19.44	24.70	38.64	32.27	27.70	24.26
November	1	16.35	18.76	24.06	38.64	32.27	27.70	24.26
	2	16.44	18.84	24.15	38.64	32.27	27.70	24.26
	3	16.51	18.91	24.21	38.64	32.27	27.70	24.26
	4	16.58	18.99	24.28	38.64	32.27	27.70	24.26
	5	16.70	19.11	24.39	38.64	32.27	27.70	24.26
December	1	16.19	18.59	23.90	38.64	32.27	27.70	24.26
	2	16.25	18.66	23.97	38.64	32.27	27.70	24.26
	3	16.31	18.71	24.02	38.64	32.27	27.70	24.26
	4	16.37	18.77	24.08	38.64	32.27	27.70	24.26
	5	16.46	18.87	24.17	38.64	32.27	27.70	24.26

Table 10.10 Corrected Pavement ME frequencies at different depths within the AC layer for I-94 (depths greater than 6 inches).

Month	Quintile	Loading Frequencies (Hz) at Mid Depth of Each AC Sublayer					
		6.5 inch	7.5 inch	8.5 inch	9.5 inch	10.5 inch	11.5 inch
January	1	21.58	19.44	17.68	11.54	7.05	5.08
	2	21.58	19.44	17.68	11.64	7.17	5.18
	3	21.58	19.44	17.68	11.72	7.26	5.26
	4	21.58	19.44	17.68	11.81	7.36	5.35
	5	21.58	19.44	17.68	11.95	7.53	5.49
February	1	21.58	19.44	17.68	11.60	7.12	5.14
	2	21.58	19.44	17.68	11.71	7.25	5.25
	3	21.58	19.44	17.68	11.80	7.35	5.34
	4	21.58	19.44	17.68	11.90	7.47	5.44
	5	21.58	19.44	17.68	12.05	7.65	5.61
March	1	21.58	19.44	17.68	11.80	7.35	5.34
	2	21.58	19.44	17.68	11.96	7.54	5.51
	3	21.58	19.44	17.68	12.09	7.70	5.65
	4	21.58	19.44	17.68	12.23	7.87	5.80
	5	21.58	19.44	17.68	12.46	8.16	6.06
April	1	21.58	19.44	17.68	12.21	7.85	5.78
	2	21.58	19.44	17.68	12.42	8.11	6.02
	3	21.58	19.44	17.68	12.58	8.31	6.21
	4	21.58	19.44	17.68	12.75	8.54	6.42
	5	21.58	19.44	17.68	13.01	8.90	6.76
May	1	21.58	19.44	17.68	12.72	8.50	6.39
	2	21.58	19.44	17.68	12.97	8.84	6.71
	3	21.58	19.44	17.68	13.15	9.10	6.96
	4	21.58	19.44	17.68	13.34	9.38	7.23
	5	21.58	19.44	17.68	13.64	9.83	7.68
June	1	21.58	19.44	17.68	13.20	9.18	7.03
	2	21.58	19.44	17.68	13.46	9.55	7.40
	3	21.58	19.44	17.68	13.64	9.84	7.69
	4	21.58	19.44	17.68	13.83	10.14	8.00
	5	21.58	19.44	17.68	14.12	10.62	8.51
July	1	21.58	19.44	17.68	13.50	9.61	7.47
	2	21.58	19.44	17.68	13.73	9.97	7.83
	3	21.58	19.44	17.68	13.89	10.23	8.10
	4	21.58	19.44	17.68	14.06	10.52	8.40
	5	21.58	19.44	17.68	14.32	10.96	8.88

Table 10.10 (cont'd).

July	1	21.58	19.44	17.68	13.50	9.61	7.47
	2	21.58	19.44	17.68	13.73	9.97	7.83
	3	21.58	19.44	17.68	13.89	10.23	8.10
	4	21.58	19.44	17.68	14.06	10.52	8.40
	5	21.58	19.44	17.68	14.32	10.96	8.88
August	1	21.58	19.44	17.68	13.36	9.41	7.26
	2	21.58	19.44	17.68	13.60	9.77	7.62
	3	21.58	19.44	17.68	13.77	10.04	7.90
	4	21.58	19.44	17.68	13.95	10.33	8.20
	5	21.58	19.44	17.68	14.22	10.78	8.68
September	1	21.58	19.44	17.68	12.82	8.64	6.52
	2	21.58	19.44	17.68	13.08	9.01	6.87
	3	21.58	19.44	17.68	13.28	9.28	7.14
	4	21.58	19.44	17.68	13.48	9.58	7.44
	5	21.58	19.44	17.68	13.78	10.06	7.92
October	1	21.58	19.44	17.68	12.35	8.02	5.94
	2	21.58	19.44	17.68	12.54	8.27	6.17
	3	21.58	19.44	17.68	12.69	8.46	6.35
	4	21.58	19.44	17.68	12.84	8.67	6.54
	5	21.58	19.44	17.68	13.08	9.00	6.86
November	1	21.58	19.44	17.68	11.95	7.53	5.49
	2	21.58	19.44	17.68	12.10	7.71	5.66
	3	21.58	19.44	17.68	12.22	7.86	5.79
	4	21.58	19.44	17.68	12.35	8.02	5.94
	5	21.58	19.44	17.68	12.55	8.27	6.17
December	1	21.58	19.44	17.68	11.64	7.17	5.18
	2	21.58	19.44	17.68	11.77	7.32	5.31
	3	21.58	19.44	17.68	11.87	7.43	5.41
	4	21.58	19.44	17.68	11.98	7.56	5.52
	5	21.58	19.44	17.68	12.15	7.77	5.71